UNIVERSITÀ DEGLI STUDI DI MILANO

Scuola di Dottorato in Scienze Farmacologiche
XXVIII ciclo

ROLE OF MUTANT VAPB IN THE PATHOGENESIS OF AMYOTROPHIC LATERAL SCLEROSIS: GAIN OR LOSS OF FUNCTION?

Coordinatore: Prof. Alberto CORSINI
Tutor: Dr.ssa Mariaelvina SALA
Co-Tutor: Dr.ssa Francesca NAVONE

Tesi di Dottorato di:
Paola GENEVINI
Matricola: R10122

Anno Accademico 2014-2015

Abstract

Amyotrophic Lateral Sclerosis is a fatal neurodegenerative disease that leads to progressive paralysis due to motorneuron degeneration and eventually death due to respiratory failure. No effective treatments are currently available and, even though several cellular pathways are altered during the disease course, the initiating event that triggers motorneuron degeneration is still unclear. The majority of ALS cases are sporadic, however approximately 10% are familial and several disease-linked genes have been identified. Ten years ago a mutation in the gene encoding for VAPB was associated with a dominantly inherited form of ALS (termed ALS8). Moreover, sporadic ALS patients have reduced levels of the endogenous protein. VAPB belongs, along with its homologue VAPA, to the VAP protein family: ER resident tail anchored proteins that, thanks to their binding partners, are involved in several cellular functions like lipid transport, ER stress and membrane contact site formation. The ALS-associated mutation P56S dramatically alters VAPB structure, thus preventing the binding to its physiological interactors and causing its aggregation. However, is has been unclear whether ALS8 is due to a gain or loss of function mechanism: P56S-generated inclusions could be directly toxic or reduced levels of the endogenous protein might underlie its pathogenicity.

To understand the pathogenic mechanism of this mutant I used two complementary approaches: I analyzed cellular models that either express moderate levels of P56S-VAPB or have reduced levels of the endogenous protein. As already observed in epithelial cells, under basal conditions the mutant protein can be easily degraded by the proteasome in motorneuronal cells. However, following autophagy stimulation it can became a substrate also of this pathway. Moreover, the presence of P56S-VAPB doesn't interfere with general proteostasis or protein transport. These results prompted us to investigate VAPB-downregulated motorneuronal cells. In this model, we saw an increase in the phosphoinositide PI4P in the Golgi and a reduction in neurite extension following differentiation.

The results indicate that P56S-VAPB inclusions are not toxic, while reduced levels of the endogenous VAPB can alter motorneuronal homeostasis. Therefore, these findings suggest that ALS8 pathogenicity is not due to toxic gain of function of the mutant but rather to a loss of function of the endogenous protein. This finding is relevant not only for ALS8, but also for forms of sporadic ALS, in which VAPB levels are reduced.

List of Abbreviations

Abbreviation	Full name
ADP	Adenosinediphosphate
ALS	Amyotrophic Lateral Sclerosis
ATF6	Activating Transcription Factor 6
ATP	Adenosine tri phosphate
BSA	Bovine Serum Albumine
CERT	Ceramide Transfer Protein
ChAT	Choline Acetyl Transferase
CHX	Cycloheximide
CNS	Central Nervous System
DAG	DiacylGlycerol
DMEM	Dulbecco Modified Eagle Medium
DMEM/F12	Dulbecco Modified Eagle Medium/F12
DMSO	Dimethylsulfoxide
DNA	Deoxyribonucleic acid
DRP	Dipeptide Repeat Proteins
EBSS	Earle's Buffered Salt Solution
Eph	Ephrine
ER	Endoplasmic Reticulum
ERAD	ER-Associated Degradation
ERGIC	ER-Golgi intermediate compartment
fALS	Familial Amyotrophic Lateral Sclerosis
FFAT	Two Fenilalanies in an Acidic Tract
FTD	Fronto Temporal Dementia
FUS	Fused in Sarcoma
GA	Glutaraldheyde
GAP43	Growth Associated Protein 43
GDP	Guanosine diphosphate
GEF	GDP/GTP Exchange Factor
GFP	Green Fluorescent Protein
GM130	Golgi Matrix protein of 130 KDa
GSL	GlycoSphingoLipid
GTP	Guanosine-5'-triphosphate
HDAC	Hystone Deacetylase
IF	Immunofluorescence
IRE1	Inositol Requiring enzyme 1
LAMP1	Lysosome Associated Membrane Protein 1
LE	Late Endosome
LTP	Lipid Transfer Protein
MAM	Mitocontrial Associated Membrane
MCS	Membrane Contact Site

Miro-1	Mitochondrial Rho GTPase-1
MN	Motor Neuron
MND	Motor Neuron Disease
MOM	Mitochondrial Outer Membrane
MSP	Major Sperm Protein
NEAA	Non Essential Amino Acids
OD	Optical Density
OSER	Organized Smooth ER
P/S	Penicillin/Streptomycin
PAGE	PolyAcrilamide Gel Electrophoresis
PBS	Phosphate Buffered Saline
PERK	Protein kinase RNA-like Endoplasmic Reticulum Kinase
PH	Pleckstrin Homology
PI	Phosphatidil Inosytol
PI4K	phosphatidylinositol 4-kinase
PI4P	Phospahtidil Inositol 4 monophosphate
PLS	Primary Lateral Sclerosis
PMA	Progressive Muscular Atrophy
RAN	Repeat-Associated Non-ATG translation
RNA	Ribonucleic acid
RT	Room Temperature
Sac1	Suppressor of Actin 1
sALS	Sporadic Amyotrophic Lateral Sclerosis
SDS	Sodium Dodecyl Sulphate
shRNA	short haipin RNA
siRNA	silencing RNA
SM	Sphingomyelin
SMA	Spinal Muscular Atrophy
SOD1	Superoxide Dismutase 1
SpMN	Spinal Motor Neuron
SR	Serine Repeat
START	Steroidogenic Acute Regulatory protein (StAR)-Related lipid Transfer
TBS	Tris Buffered Saline
TDP43	TAR DNA-binding protein 43
TRAK	Trafficking Kinesin Protein-1
UPR	Unfolded Protein Response
UPS	Ubiquitin Proteasome System
VAPA	(Vesicle-associated membrane protein)-Associated Protein A
VAPB	(Vesicle-associated membrane protein)-Associated Protein B
VSVG	Vesicular Stomatitis Virus G glycoprotein
WB	Western Blot

Table of Contents

1. Introduction

1.1. Motor Neuron Diseases

Motor Neuron Diseases (MND) are a heterogeneous group of neurodegenerative disorders characterized by progressive and selective injury and death of motor neurons (MNs). At present, unfortunately, there are no effective drugs to alter the course of these diseases, which are widespread and of fatal outcome.

MNs are neuronal cells located in the central nervous system (CNS). There are two main types of MNs: upper MNs and lower MNs. Upper MN cell bodies are located in the pre-motor and primary motor region of the cerebral cortex, also known as the "motor strip". They make glutammatergic synaptic connections with lower MNs, whose cell bodies are located in the brainstem and in the-ventral horn of the spinal cord. Lower MNs make cholinergic connections with their target muscles. Spinal motor neurons (SpMNs) are located in the ventral horn of the spinal cord and control effector muscles in the periphery. In mammals, their axons can extend through several meters, making them the longest known cell type.

Due to their highly polarized morphological features, topological constraints and post-mitotic nature, MNs are uniquely vulnerable to pathogenic stimuli and dependent on the maintenance of a balanced cellular homeostasis, thus playing an irreplaceable function in the nervous system. For this reason, MNDs such as amyotrophic lateral sclerosis (ALS), progressive muscular atrophy (PMA), spinal muscular atrophy (SMA) and primary lateral sclerosis (PLS) are rapidly and irreversibly debilitating. Understanding the molecular mechanisms underlying MN diversity and susceptibility to degeneration is among the fundamental steps required to develop successful regenerative therapies in the future (Stifani, 2014).

1.2. ALS: Amyotrophic Lateral Sclerosis

Amyotrophic Lateral Sclerosis (ALS) is a MND affecting both upper and lower motor neurons. It is characterized by weakness and muscular atrophy, leading to a progressive paralysis due to muscle denervation following motor neuron degeneration. The first symptoms can arise in the limbs (spinal form) or as dysarthria/dysphagia (bulbar form). After the focal initiation, symptoms spread to other regions over time and some evidence suggests that the spread may be mediated by non-cell autonomous propagation or "prion-like propagation" (Leblond et al., 2014). Progressive paralysis leads to death due to respiratory failure on average 3 years after the onset of the first symptoms, although a proportion of patients have a

slower disease course. The mean age of onset is approximately 55-60 years, incidence is 2 new cases per year every 100 000 people, with a slight male prevalence (M:F ratio 1,5:1) (Wijesekera and Leigh, 2009).

Even though ALS has traditionally been considered a pathology affecting only MNs, recent findings in some patients have shown that sensory and spinocerebellar pathways may also be involved (Ferraiuolo et al., 2011). Moreover, neurons of the prefrontal and temporal cortex are also affected in ALS and degeneration of such neurons results in frontal executive dysfunction in many patients. Indeed, several observations have suggested that there is a link between ALS and Fronto Temporal Dementia (FTD). FTD is the second most common cause of early onset dementia, resulting in the degeneration of the frontal and temporal lobes of the brain. It occurs with an incidence of 3.5–4.1/100 000 per year in individuals under 65. Motor dysfunctions have been described in 15% of FTD patients and FTD is present in 15–18% of patients with ALS. There is also emerging evidence that these disorders share mutual pathological and genetic features, suggesting that they can be considered at the opposite ends of a same spectrum of diseases (Lattante et al., 2015; Robberecht and Philips, 2013)

The majority of ALS cases are sporadic (sALS), although 5-10% of cases are familial (fALS), when the patient has a first or second-degree relative affected, and usually of autosomal dominant inheritance (Byrne et al., 2011). fALS is a genetically heterogeneous pathology with approximately 20 disease-linked genes so far identified (Peters et al., 2015). Table 1 shows a comprehensive list of the genes whose mutations have been found in association with ALS.

Mutations in the gene encoding the enzyme [Cu/Zn] superoxide desmutase SOD1 are responsible for 20% of inherited ALS cases, while those in the RNA/DNA-binding proteins TDP-43 and FUS cause a small fraction (~5%) of FALS each. Hexanucleotide repeat expansions in *C9ORF72* are the most common (40-50%) genetic cause of ALS and their identification established the molecular link between ALS and FTD. Several other genes have been identified as genetic causes of ALS and collectively today over 60% of fALS can be explained by known mutations. A small fraction of apparently sporadic patients present mutations in the genes known to cause fALS, thus revealing an unexpected clinico-pathological link between sALS and fALS.

Gene	% of fALS	Locus	Encoded Protein	Inheritance	Clinical phenotype
Repeat expansion					
C9ORF72	40-50	9p21.3	C9ORF72	Dominant	ALS, ALS+FTD
ATXN2	1-2	12q24	Ataxin2	Dominant	ALS; ALS+FTD; PMA
Enzyme					
SOD1	20-25	21q22	SOD1	Dominant	ALS, PMA
Proteostasis					
OPTN	2-3	10p13	Optineurin	Dominant	ALS; ALS+FTD
VCP	1-2	9 p13	VCP/p97	Dominant	ALS; ALS+FTD;

Gene	% of fALS	Locus	Encoded Protein	Inheritance	Clinical phenotype FTD
SQSTM1	<1	5q35	p62/Sequestosome 1	Dominant	ALS; ALS+FTD; FTD
CHMP2B	<1	3p11	CHMPB2	Dominant	ALS; PMA;FTD
FIG4	<1	6q21	Phosphatidylinositol 3,5-bisphosphate 5-phosphatase	Dominant	ALS;PLS
UBQLN2	<1	Xp11	Ubiquilin2	X-linked dominant	ALS, ALS+FTD
ALS2	<1	2q33.1	Alsin	Recessive	ALS;PLS
Cytoskeleton/ protein/lipid transport deficit					
PFN1	1 2	17p13	Profilin-1	Dominant	ALS
TUBA4A	1	2q35	Tubulin α4A	Unknown	ALS, ALS+FTD
VAPB	<1	20q13	VAPB	Dominant	ALS;PMA;PLS
DCTN1	<1	2p13	Dynactin	Dominant	ALS
NEFH	<1	22q12.2	Neurofilament Heavy Chain	Dominant	ALS
PRPH	Unknown	12q13.2	Peripherin	Sporadic	ALS
RNA processing					
TARDBP	4-5	1p36.2	TDP-43	Dominant	ALS; ALS+FTD;FTD;
FUS	4-5	16p11.2	FUS (FUS/TLS)	Dominant	ALS; ALS+FTD; FTD
ANG	1-2	14q11.2	Angiogenin	Dominant	ALS, ALS+FTD
TAF15	<1	17q11	TAF15	Unknown	ALS
EWSR1	<1	22q12.2	EWSR1	Unknown	ALS
hnRNPA1	<1	12q13	hnRNPA1	Dominant	ALS+FTD
hnRNPA2B1	<1	7p15	hnRNPA2/B1	Dominant	ALS, ALS+FTD
SEXT	<1	9q34.13	Senataxin	Dominant	ALS
Excitotoxicity					
DAO	<1	12q24	D-amino-acid oxidase	Dominant	ALS
Uncertain					
CREST	<1	20q13.3	SS18L1	Unknown	ALS
MATR3	<1	5q31.2	Matrin3	Unknown	ALS
SIGMAR1	<1	9p13.3	SIGMAR1	Unknown	ALS; ALS+FTD; FTD
SPG11	<1	15q21.1	Spatascin	Recessive	ALS; HSP

Table 1: Genetic causes of ALS. ALS: Amyotrophic Lateral Sclerosis; PMA: Primary Muscular Atrophy; PLS: Primary Lateral Sclerosis; FTD: Fronto Temporal Dementia; HSP: Hereditary Spastic Paraplegia (Peters et al., 2015) (Robberecht and Philips, 2013)

Several studies have reported ALS/FTD cases with mutations in more than one ALS gene in the same individual, and the emerging idea is that the co-occurrence of mutations can modify the phenotype or influence the clinical features of the disease, such as age of onset and survival rate (Lattante et al., 2015). Since the *C9ORF72* repeat expansion is the most common cause of fALS, most co-

occurrences have been observed to involve a *C9ORF72* expansion alongside another mutation such as, for example, mutations in the *TARDBP*, *OPTN*, *UBQLN2*, *VAPB*, *SOD1* and *FUS* genes (Leblond et al., 2014).

Genetic factors can trigger disease pathogenesis through the alteration of one or more pathways converging on different aspects of cellular physiology. Cellular dysfunctions observed in ALS include, for example, oxidative stress, altered RNA metabolism, dysregulated endosome trafficking and cell signalling, glutamate excitotoxicity, mitochondrial dysfunction, endoplasmic reticulum (ER) stress, altered protein degradation as well as cytoskeleton disorganization and impaired axonal trafficking (Robberecht and Philips, 2013) (Ferraiuolo et al., 2011).

The initiating events contributing to progressive MN loss observed in both sALS and fALS remain controversial and not fully determined. Given its complexity and multifactorial etiology, including both genetic and environmental factors, and the concomitant involvement of different intracellular pathways, ALS pathogenic mechanisms are likely to be linked, so that a defect in one cellular pathway will have a domino effect leading to multiple stresses on the cell. The clinical and pathological similarity between sporadic and familial forms suggests at least some common pathogenetic pathways. Therefore, unraveling the disease mechanisms of fALS-linked genes is important to understand the pathogenesis of the much more frequent sporadic forms (Robberecht and Philips, 2013).

In the following sections, I will discuss in more detail some of the pathogenic mechanisms by which mutant proteins may induce disease.

1.2.1. Pathogenic mechanisms underlying ALS.

(i). Aggregate formation

Different fALS-associated genes give rise to misfolded and aggregate-prone mutant proteins. Therefore, the presence of intracellular aggregates is a pathological hallmark of ALS, as for other neurodegenerative diseases. It is still unclear whether these aggregates are protective, by sequestering dangerous oligomeric species, or toxic. The toxic role of aggregates might be exerted either by causing "traffic jams" and inducing axonal transport impairment and mitochondria disorganization/dysfunction, or by interfering with the two major intracellular protein degradation pathways, the ubiquitin proteasome system (UPS) and autophagy (Navone et al., 2015). Deposits of misfolded mutant proteins may disturb the cellular degradative pathways on their own, via a gain of toxic function, or by sequestering functional proteins important for these processes. Moreover, intracellular inclusions formed by fALS-linked mutants proteins may sequester both their wild type counterparts and their endogenous binding partners, or even whole interactomes that could prove to be essential for neuronal physiology, leading to a loss of function of several pathways (Blokhuis et al., 2013).

SOD1 was the first gene and protein whose mutations were demonstrated to cause ALS. It is an enzyme composed of 153 amino acids and is involved in free radical scavenging. Mutant SOD1 is misfolded and targeted for degradation through ubiquitylation, however, it seems to escape this regulatory process in the cell. Mutant SOD1 accumulates as oligomers with a high propensity to form aggregates, thus leading to a cellular stress response. Eventually, cellular stress gives rise to axonal retraction and ultimately cell death (Robberecht and Philips, 2013) (see below).

Mutations in *TARDBP*, which encodes the RNA and DNA-binding protein TDP43, are a rare cause of dominant fALS. This gene was investigated as a candidate gene for ALS because in most cases of sALS, fALS, and FTD the hyperphosphorylated, cleaved form of TDP-43 has been shown to accumulate diffusely in the cytoplasm of neurons and glia, where it assembles into round and thread-like inclusions. Under physiological conditions, TDP43 is localized in the nucleus, where it is involved in different aspects of RNA processing. Upon stress, it leaves the nucleus and accumulates in stress granules in the cytoplasm. If stress resolves, TDP43 is released from these sites and re-enters the nucleus. Mutations favor TDP43 leaving the nucleus and its irreversible accumulation in stress granules. Other proteins may be sequestered in the TDP43 accumulations (Andersen and Al-Chalabi, 2011) (Ince et al., 2011).

Mutant *FUS*, an RNA-processing protein that shares some similarities with TDP43, is also detected in diverse types of intracellular inclusions like mutant SOD1 and TDP-43. In contrast with TDP-43 aggregates, the frequency of FUS-positive inclusion bodies in sALS is low (Robberecht and Philips, 2013) (Peters et al., 2015).

The most frequent ALS-associated gene is *C9ORF72*. This gene encodes a protein of approximately 54.3 kDa (481 amino acids) whose function remains unknown, but recent studies suggest that it is structurally related to a GDP/GTP exchange factor (GEF) that activates Rab-GTPases and that may be important for endosomal trafficking (Peters et al., 2015). The genetic alteration consists in the expansion of a GGGGCC hexanucleotide repeat in an intronic region. Healthy controls have 2-20 repeats, while affected patients typically carry hundreds or thousands of repeats (Rohrer et al., 2015). The GGGGCC expansion produces both nuclear RNA foci and cytoplasmic protein inclusions generated by Repeat-Associated Non-ATG (RAN) translation from the expanded GGGGCC repeat (Ash et al., 2013). The mechanism underlying RAN translation is not completely understood, but probably relies on a particular conformational structure adopted by the expanded region (Zu et al., 2011).

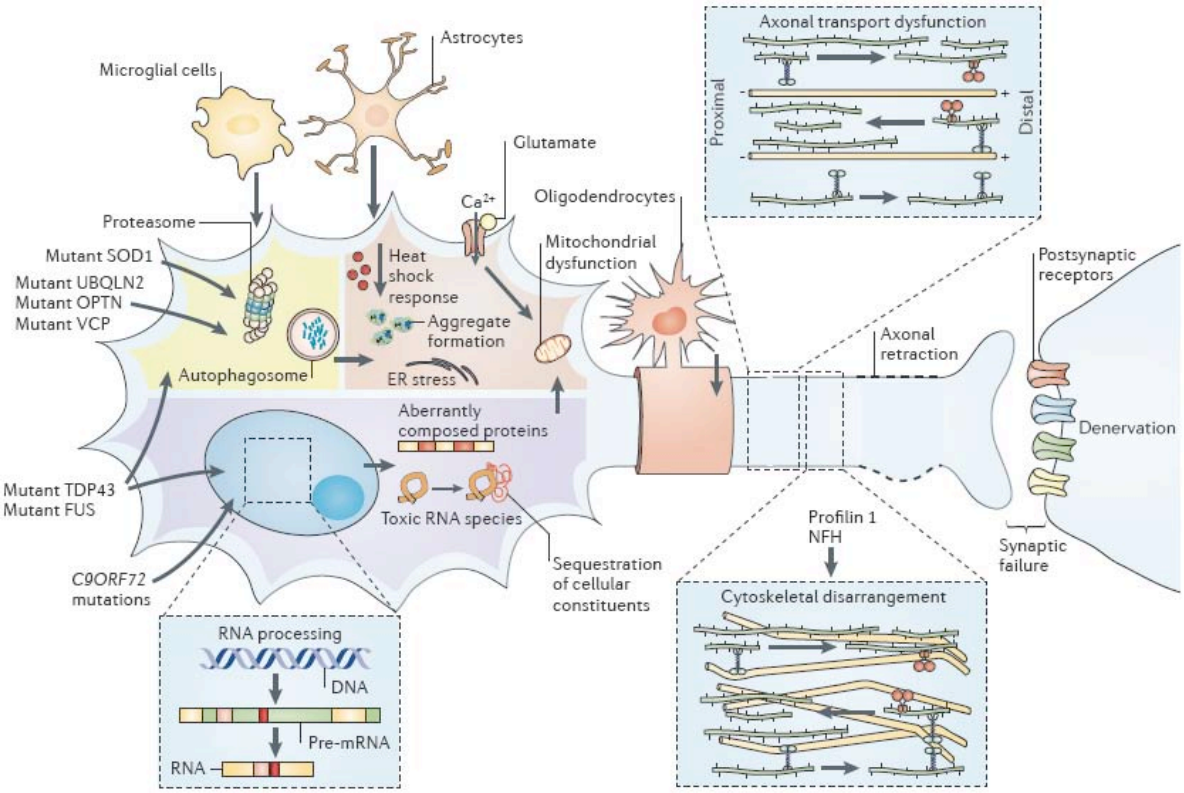

Figure 1.1: Overview of events implicated in the pathogenesis of ALS. From (Robberecht and Philips, 2013). See text for a more detailed description.

(ii). Failure of proteostasis

As described in the previous section, the presence of cytoplasmic inclusions or protein aggregates in affected motor neurons is a pathological hallmark of ALS, suggesting that impairment of protein degradation plays a role in the disease process. Unlike mitotic cells, which are able to clear aggregates of intracellular proteins through their dilution or asymmetric distribution during cell division, postmitotic neurons rely on two major pathways of protein degradation for aggregate removal: the UPS and autophagy-associated lysosomal degradation (Navone et al., 2015).

The UPS regulates the turnover of many proteins and eliminates the unfolded ones. During ubiquitination, ubiquitin is covalently bound to a lysine in the target protein. Other ubiquitin molecules are subsequently conjugated to the first one and polyubiquitinated proteins are recognized and brought to the proteasome, where they are degraded (Lehman, 2009). With this mechanism, one protein at a time is degraded.

During autophagy, double membranes form vesicles called autophagosomes that surround cytoplasmic components and later on fuse with lysosomes, where degradation occurs. Although this pathway has long been considered as a non-selective process responsible for the bulk elimination of cytosolic material, it is now clear that selective autophagy can remove aggregated proteins, damaged organelles as well as big complexes (Navone et al., 2015). Molecular chaperones, the UPS and the

autophagy-lysosome system function together to monitor protein quality and protect cells from dysfunctional, misfolded or denatured proteins. The presence of ubiquitin, p62 (an autophagy receptor) and molecular chaperones in ALS aggregates implicates a role for all these three systems in ALS pathophysiology.

Evidences from fALS causative genes support the hypothesis of a dysfunctional proteostasis as a pathogenic mechanism in ALS. For example, mutant SOD1 seems to have toxic effects on the cellular degradation machinery, impairing both the proteasome and the autophagy pathways. Further evidence for a failure of ubiquitin-dependent protein degradation in ALS comes from the discovery of some fALS-linked mutations affecting proteins that are directly involved in proteostasis. For example, ubiquilin 2 (UBQLN2) delivers ubiquitylated proteins to the proteasomal degradation machinery and mutations in this gene cause X-linked fALS or fALS-FTD. Mutations in SQSTM1 (p62) were found in patients with fALS and in individuals with sALS, but this gene was originally linked to neurodegeneration due to its presence in ubiquitin-positive cytoplasmic aggregates of misfolded proteins. Other genes involved in protein degradation and associated with ALS are those that encode autophagy receptors, such as Optineurin, the ER-Associated Degradation (ERAD, see below) protein p97, the endosomal ESCRTIII-complex subunit CHMP2B and the phosphatidylinositol 3,5-bisphosphate 5-phosphatase FIG4 (Robberecht and Philips, 2013) (Navone et al., 2015).

(iii). RNA processing

Numerous ALS-linked proteins are directly or indirectly involved in RNA processing. The most common are TDP-43 and FUS, but other less common genes have been found (see Table 1). TDP-43 and FUS function in almost every aspect of DNA and RNA processing, including transcription, splicing, RNA transport, miRNA processing, and translation. The mutant, ALS-associated variant proteins are mislocalized to the cytoplasm, often leaving the nucleus entirely depleted of the affected protein. It is unclear whether the primary pathology is loss of function in the nucleus or an acquired cytotoxic effect of the mutant protein (Robberecht and Philips, 2013).

The association of mutant *C9ORF72* with ALS shows another aspect of altered RNA biology in ALS. In patients with *C9ORF72* mutations, the expanded hexanucleotide repeat forms nuclear RNA foci in neurons in the frontal cortex and spinal cord (DeJesus-Hernandez et al., 2011). Both sense and antisense RNA transcripts are present in these intranuclear foci. How repeat expansions in *C9ORF72* cause ALS remains to be elucidated. One possibility is that they may cause abnormal recruitment of splice factors, thus resulting in aberrant splicing of a whole range of genes. Such mechanism is suggested by studies in myotonic dystrophy type 1, where RNA foci transcribed from CTG expansions sequester the transcriptional splice factor Musclebind-like 1 (MBNL-1), depleting the pool of the protein in the nucleus. Besides sequestering transcription factors, the expanded GGGGCC sequence and/or the foci might reduce expression of the normal C9ORF72 protein, with deleterious effects on MN viability (Robberecht and Philips, 2013) (Peters et al., 2015). Finally, the expansion may generate insoluble and

potentially toxic dipeptide repeat proteins (DPR) proteins through the previously mentioned RAN translation (Ash et al., 2013).

(iv). Alterations in the secretory pathway and impairment of axonal transport

Recent studies suggest that dysfunctions in protein traffic and axonal transport constitute a common denominator in neurodegenerative diseases, including MND. The secretory pathway consists in a series of subsequent steps that cells use to move proteins between different organelles and finally deliver them to their proper destination. It starts in the endoplasmic reticulum (ER), which is recognized as the site of synthesis and folding of secreted, membrane-bound, and some organelle-targeted proteins. It then moves to the Golgi apparatus, where proteins can be modified, and from where they are sorted from the Trans Golgi Network (TGN) to reach their final destination. As the secretory pathway involves different steps, alterations in any of the organelles involved may contribute to dysfunctions in the whole system. The correct function of this process is critical: the MN cell body is the primary site of metabolic function, and must continuously supply newly synthesized proteins to dendritic and axonal processes. In this context, a common feature of both fALS and sALS is Golgi fragmentation, meaning loss of the normal ribbon-like configuration, which is replaced by disconnected vesicular pattern. However, whether Golgi complex disorganization in sALS is an indicator of pathogenesis or rather a secondary consequence remains to be determined (Nassif et al., 2010). In addition to anterograde transport from the cell body to dendrites and the axon, retrograde transport in the opposite direction must also be considered. This process is essential for the degradation of misfolded or aggregated proteins, as the cell body is the primary site for degradative functions (Chevalier-Larsen and Holzbaur, 2006).

Axonal pathology is a key feature of ALS and is thought to have a crucial role in the pathophysiology of the disease. Since MNs are highly polarized cells with long axons, active transport from cell center to cell periphery, and from the periphery back to the cell body, is required for delivery of essential components, such as RNA, proteins and organelles to their proper destinations and to maintain the overall metabolic balance of the cell. Golgi-derived vesicles travel along microtubules to reach their final destination. Mutations in the motors that drive axonal transport are clearly sufficient to cause MN degeneration. Patients with missense mutations in the microtubule motors (like dynein or kinesin) develop neuropathies. As previously noted, cells carrying mutant SOD1show defects in axonal transport that contribute to the pathology (Chevalier-Larsen and Holzbaur, 2006). Cytoskeletal architecture and dynamics have a major role in ALS pathogenesis, as shown by the identification of mutations in several cytoskeletal components such as in the neuronfilament heavy chain, α-tubulin and profilin-1, a protein essential for actin polimerization (Robberecht and Philips, 2013) (Smith et al., 2014). TDP43 could indirectly affect cytoskeletal dynamics, as it has a role in the processing of mRNA coding for intermediate filaments (Millecamps and Julien, 2013).

(v). ER stress response

As described earlier, neurodegenerative diseases like ALS are characterized by accumulation of misfolded proteins. This leads to ER stress and activation of the Unfolded Protein Response (UPR), a series of cellular reactions aiming at re-establishing homeostasis in the presence of perturbations that compromise the protein folding capacity of the ER. At first, UPR activation initiates a signaling pathway leading to a reduction of protein load in the ER through a general inhibition of protein translation. Secondly, the folding capacity of the organelle is increased by upregulating the production of chaperone proteins. Finally, there is an upregulation of the ERAD pathway (ER-Associated Degradation), a system involved in the degradation of misfolded ER proteins via their retrotranslocation to the cytosol and delivery to the proteasome. Should these mechanisms fail, chronic ER stress will lead to irreversible alterations of the organelle and eventually trigger apoptosis (Hetz and Mollereau, 2014) (Ron and Walter, 2007).

Three different UPR transducers have been identified, which are devoted to sensing the presence of abnormal amounts of unfolded proteins and activating downstream pathways: IRE1 (Inositol Requiring enzyme1), ATF6 (Activating Transcription Factor 6) and PERK (Protein kinase RNA-like Endoplasmic Reticulum Kinase) (Ron and Walter, 2007).

Recent studies suggest that cellular toxicity caused by UPR could be a relevant pathogenic mechanism in ALS. Both in sALS and fALS the presence of ER stress has been detected: several UPR transducers are upregulated in spinal cords of sALS patients and of mouse models carrying mutations in SOD1, TDP43, VAPB, FUS and Ataxin2 (Matus et al., 2013). Additional evidence in favor of an involvement of this pathway came from detailed studies on mutant SOD1 mice: in this model, ER stress is a very early alteration that precedes axonal damage, as it is already detectable in vulnerable MNs at a presymptomatic stage (Saxena et al., 2009). Moreover, genetic and pharmacological modulations of UPR alter disease progression of fALS models. In mutant SOD1 mice, treatment with Salubrinal, an ER stress–inhibitor drug, attenuates symptoms and delays progression, whereas chronic enhancement of ER stress promotes the disease (Saxena et al., 2009). Genetic inactivation of one PERK allele accelerates disease onset and progression in mutant SOD1 mice, highlighting a protective activity of PERK in fALS pathogenesis (Wang et al., 2011). In contrast, deficiency of XBP-1 (the effector of IRE1) in the nervous system increases life span and MNs survival of mutant SOD1 transgenic mice and concomitantly enhances autophagy and diminishes levels of SOD1 aggregation (Hetz et al., 2009). These data suggest that different UPR effectors could play distinct roles in the cellular responses to mutant SOD1 protein misfolding.

(vi). Mitochondrial Dysfunction

Mitochondria are cellular compartments essential for energy production, maintenance of Ca^{2+} homeostasis and regulation of apoptosis. In ALS, several alterations in the mitochondrial compartment have been observed.

Analysis of biopsies from sALS and fALS patients shows that in skeletal muscle and MNs mitochondrial morphology and localization are altered. More evidence regarding mitochondrial dysfunctions came from the analysis of mutant SOD1 mice. In this model, mitochondrial vacuolation is already present in a presymptomatic stage, suggesting that this is an early event in ALS pathogenesis (Ferraiuolo et al., 2011). In the same model, defects in the activity of respiratory chain complexes have also been detected (Lin and Beal, 2006). In addition, in a motorneuronal cell line overexpressing mutant SOD1, the mitochondrial network was severely fragmented (Raimondi et al., 2006). Interestingly no effect on mitochondria was observed in epithelial cells similarly overexpressing mutant SOD1, highlighting the particular sensitivity of motor neurons to mutant SOD1.

Even though SOD1 is a cytoplasmic protein, in affected tissues small amounts of the mutant can be recruited onto the external surface of the mitochondria and also be imported into the inter-membrane space (Lin and Beal, 2006). Alteration in mitochondrial axonal transport has also been reported, which could influence energy production at the synapse (Millecamps and Julien, 2013). Finally, as ER and mitochondria are involved together in the regulation of intracellular Ca^{2+} levels, an imbalance in the first compartment due to ER stress could indirectly damage also the second one (Ferraiuolo et al., 2011).

1.3. ALS8

ALS8 is a slow onset form of fALS caused by a mutation in the *VAPB* gene situated at genomic locus 20q13.3. The link with the *VAPB* gene was initially identified in a large Brazilian family with Portuguese ancestry. Four generations of affected patients were observed and the mutation consists in a transition from C to T in exon 2 of the *VAPB* gene, resulting in the substitution of a proline at position 56 with a serine residue in the mature protein (P56S-VAPB). The same variation was subsequently observed in six other Brazilian families, all but one with Caucasian ancestry (the remaining one has an African background) (Nishimura et al., 2004). Linkage analysis suggested that the distribution of this mutation in the affected families is due to a founder effect that occurred 23 generations before and that its origin dates back to the mid 15th century in Portugal, from where it was brought to Brazil during the first colonial period (Nishimura et al., 2005). In Europe, only one German family with the *VAPB* mutation has been identified, which is affected by late onset SMA and other dominant MND. These patients' haplotype is different from the Brazilian one, suggesting that this mutation is not linked to the Brazilian founder. Three additional mutations of *VAPB* have since been identified in fALS patients (Chen et al., 2010) (Kabashi et al., 2013) (van Blitterswijk et al., 2012), however, in these cases, the segregation of the

mutation with the disease has not been demonstrated.

In addition to its involvement in ALS8, the P56S-VAPB has been linked to two additional MNDs: typical severe ALS with rapid progression and late-onset SMA (Spinal Muscular Atrophy) (Nishimura et al., 2004). The latter is a neurodegenerative disease characterized by selective death of SpMNs, muscular atrophy and generalized weakness (Lunn and Wang, 2008). This observation highlights once more the relatedness of different MNDs, which are part of a more general spectrum of pathologies.

1.3.1 The VAPB Protein

VAPB belongs to the VAP [Vesicle-associated membrane protein (VAMP)- Associated Protein] protein family. The VAMP-associated protein of 33 kD (VAP- 33) was first identified in *A. californica* (Skehel et al., 1995). This protein is highly conserved in different species, with homologues in yeast (SCS2), fly (DVAP-33), mouse, rat and human (VAPA and VAPB) (Lev et al., 2008). The two isoforms VAPA and VAPB share a high sequence homology (63%), while VAPC is a splicing variant of VAPB, which includes the first 70 aminoacids of VAPB followed by a unique sequence of 29 residues.

The VAPB protein has three structural domains: the first 150 residues constitute a MSP domain conserved between all VAP family members and so called because of its 22% homology with the *C.Elegans* Major Sperm Protein (Lev et al., 2008). The central region of the protein contains a helical structure and is predicted to form a coiled/coil protein-protein interaction motif; finally, a hydrophobic carboxy terminus acts as a membrane anchor and contains a GXXXG dimerization domain. Given the presence of the single transmembrane domain followed by the short C-terminal tail, VAPs are integral membrane proteins denominated ER-resident, tail-anchored proteins. Thanks to this sequence and the coiled/coil domain, VAPB can make homo and heterodimers (with VAPA) (Kim et al., 2010). Moreover, VAP proteins from different species have a highly conserved sequence of 16 aminoacids inside the MSP (the VAP consensus sequence) (see Fig. 1.2). This region is also involved in the process of VAPB dimerization. Importantly, the MSP domain contains several positively charged aminoacids essential for the binding to proteins carrying the FFAT domain, two phenylalanines in an acidic tract (the complete sequence is EFFDAXE, where X is any aminoacid) (Kanekura et al., 2006).

VAPA and VAPB are both ubiquitously expressed, however their expression varies among different tissues (Teuling et al., 2007). They are localized in the ER, even though they do not perfectly localize to all regions of this cellular compartment, suggesting that they may play preferential roles in distinct functional areas of the ER (Gkogkas et al., 2008).

1.3.2. VAPB functions

VAPs are considered to be adaptor proteins that recruit to the ER numerous and diverse interacting partners, which have in common the possession of a FFAT motif capable of binding to VAP's MSP domain. These proteins have been implicated in a variety of physiological functions, including membrane trafficking, lipid transport and metabolism, membrane contact site formation, Ca^{2+} homeostasis, ER-cytoskeleton interactions, participation in the unfolded protein response, neurotransmitter release and neurite extension (Lev et al., 2008). So far, no functions exclusive to VAPA or VAPB have been identified.

Below, I will describe some of the functions of VAP proteins before analyzing the characteristics of the ALS-associated mutant VAPB.

(i). ER stress response

An important aspect of VAPB function is in the ER stress response, although a role of VAP proteins in the regulation of the UPR has not been well defined, yet. Among the three previously described UPR transducers, IRE1, ATF6, and PERK (see section 1.2.1), both VAPA and VAPB can directly interact with ATF6. More specifically, VAPB has an inhibitory effect on this transducer: when VAPB levels rise in the cell, ATF6 signaling decreases, while VAPB downregulation is followed by an increase in ATF6-dependent transcription. Since increased VAPB levels alter membrane trafficking, this could indirectly influence ATF6 activity by modifying its mobility from ER to the Golgi, a necessary step for ATF6 activation (Gkogkas et al., 2008).

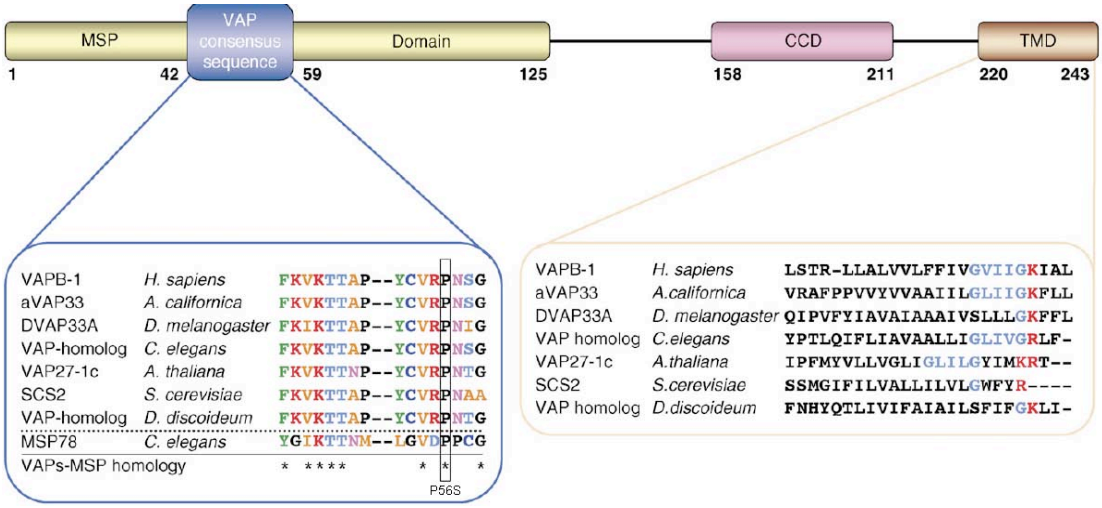

Figure 1.2: Schematic structure of VAP proteins (adapted from Lev et al., 2008), showing MSP domain (with VAP consensus sequence), Coiled-Coil Domain and Transmembrane domain. The lower part compares the VAP consensus sequences and the dimerization motifs from different species to show that they are evolutionary conserved.

VAPB has also been implicated in the IRE1 pathway: its overexpression activates UPR through this pathway, while its downregulation attenuates IRE1 signaling (Kanekura et al., 2006).

In summary, VAP proteins could regulate the UPR either by facilitating its activation via the classical transmembrane kinase IRE1, or, in contrast, by negatively modulating the activity of the UPR-related transcription factor ATF6.

(ii) Lipid transport at ER-Golgi Membrane Contact Sites (MCS)

Although VAP proteins have been implicated in many processes, perhaps the best documented function and the one most relevant to neurodegeneration is their role in recruiting lipid exchange proteins to the ER membrane (Peretti et al., 2008). This depends on VAPs' ability to interact with the FFAT motif of proteins able to sense, bind or transfer lipids; among these lipid transfer proteins (LTPs) are CERT (Ceramide Transfer Protein), OSBP (Oxysterol Binding Protein) and Nir2 (PI/PC transport protein) (Lev et al., 2008). The transfer of lipids is thought to occur at ER regions in close contact to the Golgi membrane, known as membrane contact sites (MCS). Indeed, VAPs have been implicated in the genesis of MCS between the ER and other organelles, including the plasma membrane, endosomes, the yeast vacuole and the trans-Golgi network (Raiborg et al., 2015b).

CERT transports ceramide from the ER to the Golgi. Ceramide is the precursor for all sphingolipids (SL), a class of lipids containing a sphingoid base. After *de novo* synthesis on the ER, ceramide needs to be transported to the Golgi to be further metabolized. At least two pathways exist for ceramide transport: a vesicular and a non-vesicular one. Vesicular transport is thought to be the major pathway of ceramide delivery for the synthesis of Glucosyl Ceramide (GlcCer), the common precursor of Glycospingolipids (GSL). The non-vesicular pathway is predominantly used for Sphingomyelin (SM) biosynthesis and relies on CERT. SM is synthesized through the transfer of the phosphocholine head group of phosphatidylcholine (PC) to ceramide (ceramide+PC➔SM+diacylglycerol), a reaction catalyzed by SM synthase 1 and 2 (SMS1 and 2) in the *trans* Golgi. The CERT molecule contains several structural domains and aminoacid motifs, as illustrated in Fig. 1.3b: the N-terminal pleckstrin homology (PH) domain (≈100 amino acids), the C-terminal Steroidogenic Acute Regulatory protein (StAR)-Related lipid Transfer (START) domain (≈230 amino acids) and the two phenylalanines (FF) in an acidic tract (FFAT) motif at the N-terminal side of the START domain.

The START domain is responsible for ceramide transfer. The PH and FFAT domains are necessary for the correct targeting of CERT at MCS between ER and Golgi. The PH domain binds to phosphatidylinositol 4-monophosphate (PI4P), which is highly abundant in the Golgi, especially at the *trans* Golgi cisternae and at the TGN, while the FFAT motif binds to VAP proteins (Yamaji and Hanada, 2015).

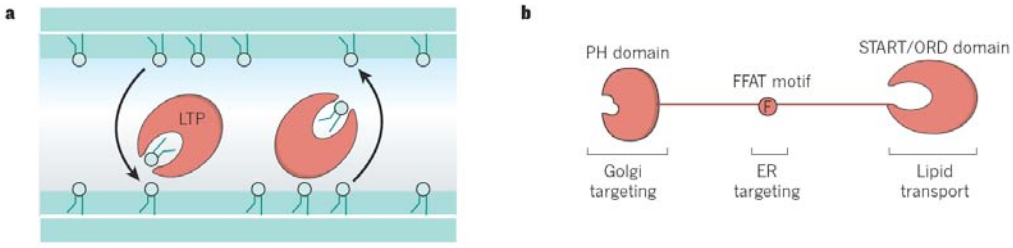

Figure 1.3.: general representation of a LTP that shuttles lipids between two compartments. b: structure of CERT and OSBP that carry dual membrane tethering domains (PH domain and FFAT motif) and a lipid transfer domain. From (Holthuis and Menon, 2014).

OSBP transports cholesterol from the ER to the Golgi and back transfers PI4P to the ER, where it is quickly hydrolyzed to phosphatidylinositol (PI) by the phosphatase Sac1. The energy provided by PI4P hydrolysis drives sterol transfer (Mesmin et al., 2013). Similarly to CERT, the structural organization of OSBP shows a N-terminal domain PH domain that binds to PI4P, as well as a central FFAT motif that interacts with VAP proteins and a C-terminal lipid transport domain called OSBP-related domain (ORD) (see Fig. 1.3b for a schematic representation).

Phosphoinositides are a class of lipids generated by phosphorylation of the precursor Phosphatidylinositol (PI) and are concentrated at the cytosolic surface of membranes. Reversible phosphorylation of the PI inositol ring, performed by different kinases and phosphatases at positions 3, 4 and 5 results in the generation of seven phosphoinositide species. Each of the seven phosphoinositides has a unique subcellular distribution with a predominant localization in a subset of membranes. This spatial restriction and steady-state levels are determined primarily by the concerted action of phosphoinositide kinases and phosphatases, whose localization is tightly controlled (Balla, 2013) (Di Paolo and De Camilli, 2006).

PI4P is the predominant phosphoinositide in the Golgi complex and a deficiency of this lipid affects its structure and function. PI4P synthesis is catalyzed by the activity of different PI4K (phosphatidylinositol 4-kinase). Spatial restriction of PI4P to the Golgi complex is ensured by phosphatases, which removes the phosphate group of PI4P in locations other than the Golgi, to obtain PI. Very interestingly, the phosphatase Sac1 is localized in the ER and binds VAP proteins via their transmembrane domain, thus revealing an important role of the VAPs not only in lipid transport, but also in their metabolism (Fig. 1.4): indeed in *Drosophila* models, downregulation of either Sac1 or DVAP (the homologue of VAP proteins) increases levels of PI4P (Forrest et al., 2013). PI4P is known to function in the recruitment of cytosolic proteins onto TGN membranes (Di Paolo and De Camilli, 2006) and, as explained above, it is involved in tethering both CERT and OSBP at MCS between Golgi and ER thanks to the PH domain of these proteins.

Finally, the last LTP is Nir2, which transfers PI from the ER to the Golgi and Phosphatidyl Choline (PC) from the Golgi to the ER. The transported PI is subsequently phosphorylated into PI4P, thus enhancing the recruitment of OSBP and CERT to the Golgi (Lev, 2010) (Fig. 1.5).

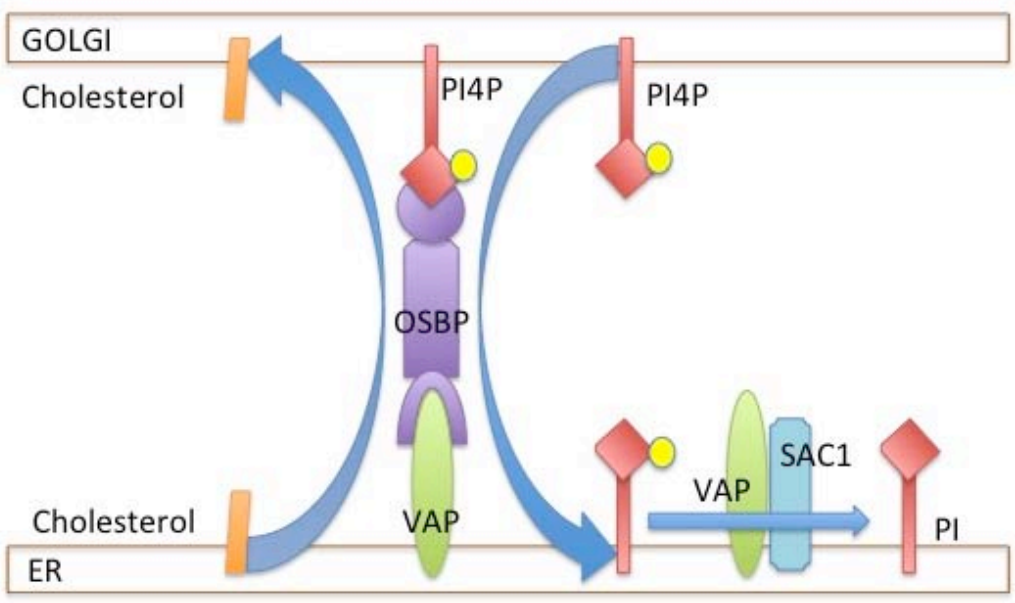

Figure 1.4: Schematic representation of PI4P transport from Golgi to ER and subsequent dephosphorylation by Sac1.

In conclusion, LTPs work in a coordinate way at ER-Golgi MCS. Most likely, Nir2 exchanges PC in the Golgi with PI in the ER; next, PI is phosphorylated by PI4K, thus generating PI4P that recruits OSBP and CERT through their PH domain. This allows non-vesicular ceramide transport and subsequent production of SM and DAG. Moreover, lipid traffic between the ER and the Golgi mediated by LTP is tightly linked to the turnover of PI4P, present at different concentrations on both partner membranes, and its regulation involves the PI4P dephosphorylating enzyme Sac1. Silencing of both VAPA and B isoforms causes mislocalization of CERT, OSBP and Nir2 and an alteration in their lipid transport function. As a consequence, lipid composition in the Golgi membranes is altered. Since a correct lipid composition is essential for organelle homeostasis, and especially for vesicular transport, in VAP-depleted cells both Golgi to plasma membrane and to endosome/lysosome transport and Golgi to ER transport are inhibited (Peretti et al., 2008). Nonetheless, the effects of the downregulation of the sole VAPB on lipid transport have not been elucidated yet.

(iii). Role of the VAPs in other MCS

MCS between ER and the mitochondrial outer membrane (MOM) occur in a region termed MAMs (mitochondrial associated membranes). These sites of close membrane apposition, that involve from 5 to 20% of the outer mitochondrial membrane, have been implicated in a variety of processes, including Ca^{2+} and phospholipid exchange, ATP production, autophagy, protein folding in the ER, mitochondrial biogenesis and transport and apoptosis (Stoica et al., 2014).

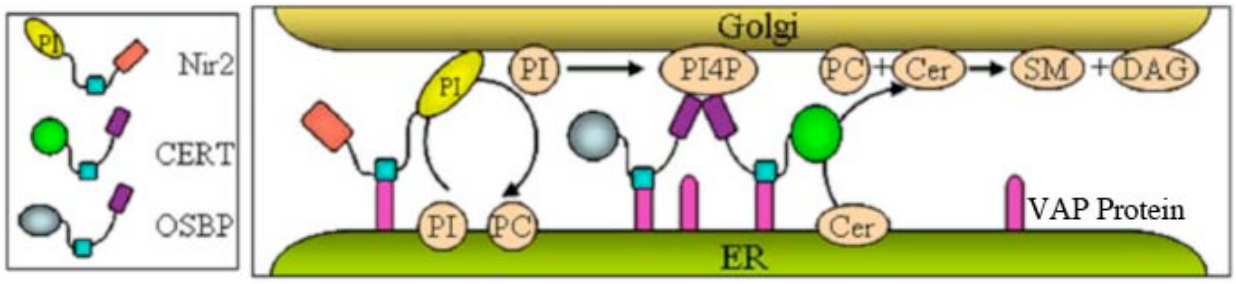

Figure 1.5: Schematic representation of lipid transport mediated by LTP at ER-Golgi MCS. Adapted from (Peretti et al., 2008).

Several studies have linked defective ER-mitochondria interaction to neurodegenerative diseases. A recent paper showed that VAPB interacts with the mitochondrial protein PTPIP51 (protein tyrosine phosphatase-interacting protein 51), thereby regulating ER-mitochondria association (Stoica et al., 2014) and loss of one of these two proteins is sufficient to alter calcium absorption and buffering by mitochondria (De Vos et al., 2012). Moreover, the expression of the ALS-linked protein TDP43 seems to influence this binding: the expression of either the wt of mutant TDP43 alters VAPB-PTPIP51 binding and MAM formation (Stoica et al., 2014).

Other important MCS are formed between ER and Late Endosomes (LE), where they have a role in cholesterol transfer, receptor dephosphorylation, endosome positioning and fission. Distinct types of contacts sites have been identified, which are mediated by different molecular bridges. VAPs proteins have been involved in triggering several of them (Raiborg et al., 2015b). They are for example involved in STARD3 (START domain-3) and STARD3NL (STARD3 N-terminal like)-dependent MCS formation. These proteins are localized on LE and carry a START domain, that can bind and transfer cholesterol, and the FFAT domain, that can bind both VAP isoforms and trigger MCS formation (Alpy et al., 2013). In another paper, authors showed that VAPs interacts with the LE cholesterol-binding protein ORP1L. In conditions of reduced levels of free cholesterol on LE membranes, ORP1L is not bound to this lipid and assumes a conformation that allows the interaction of its FFAT motif with VAPs localized on the ER (Rocha et al., 2009). Despite both STARD3/ STARD3NL and ORP1L can sense cholesterol levels, their direct role in cholesterol transfer has not been demonstrated. More likely, they sense levels of this lipid and trigger MCS formation where other machineries are responsible for cholesterol transfer (Raiborg et al., 2015b). Moreover, as better described in the neurite extension section, VAPs are involved in the formation of ER-LE contacts mediated by protrudin, a process that allows the loading of LE from ER to microtubules and their subsequent movement (Raiborg et al., 2015b).

(iv) Early secretory pathway

The role of VAPB in the early secretory pathway was first suggested by observations obtained using the model protein VSVG to study intracellular transport. While downregulation of both VAPs has

been shown to inhibit the transport of VSVG from the TGN to the plasma membrane (Peretti et al., 2008), upregulation of VAPB was reported to enhance its transport (Rao et al., 2012). More recently, it has been shown that VAPB binds the ER-Golgi trafficking protein YIFIA, which is predominantly localized in the ER-Golgi intermediate compartment (ERGIC) and recycles between the ER and the Golgi in hippocampal neurons (Kuijpers et al., 2013b). In this cellular model, VAPB–YIF1A interaction controls the shuttling of YIF1A between the ERGIC and the ER and plays an important role in early secretory events in neurons, promoting membrane trafficking and normal dendritic growth and morphology.

(v) Neurite extension

Neurons are highly specialized and polarized cells characterized by long protrusions. The molecular mechanisms that underlie neurite formation include both cytoskeletal remodeling and membrane trafficking. In particular, extension and maintenance of neuronal processes relies on the directional transport of membrane components, which are conveyed in a vectorial manner within the cell by a membrane recycling system, resulting in expansion of the neurite surface area.

Recently, several reports have highlighted the importance of protrudin as a key regulator of Rab11-dependent vesicular trafficking during neurite extension. The GTPase Rab11 regulates membrane recycling and is thought to contribute to neurite formation through modulation of directional membrane transport. Protrudin is an ER-resident protein containing a Rab11-binding domain (RBD), three hydrophobic domains (HP-1, HP-2, and HP-3), a FFAT domain, a coiled-coil domain, and a FYVE (Fab1, YOTB, Vac1, and EEA1) domain for the binding to phosphatidyl inositol 3-monophospate (PI3P). Due to its many binding sites, protrudin engages in complex relations with several proteins, including spastin, the molecular motor KIF5 (a member of the kinesin-1 family which mediates the microtubule-dependent anterograde vesicular transport of neurons), RAB7, PI3P (Matsuzaki et al., 2011) and both VAP A and B proteins, thus playing key roles in several aspects of neuronal function.

Two splicing isoforms of protrudin are known: the ubiquitous one, called protrudin-S, and a novel form generated by the inclusion of a mini exon in the mature protrudin mRNA near the FFAT domain (protrudin-L). The expression of the latter isoform is mostly restricted to the central nervous system, where it is present in neurons and astrocytes. In contrast, oligodendrocytes express only the S form. The insertion of a seven-aminoacid sequence in the L form promotes the association of protrudin with both VAPA and VAPB, thereby increasing the stimulatory effect of protrudin on polarized neurite extension (Ohnishi et al., 2014). It appears that VAP proteins are important to determine both the subcellular localization of protrudin and its ability to stimulate neurite outgrowth. In particular, downregulation of VAPA in PC12 (a cell line derived from rat pheocromocytoma) strongly inhibits neurite extension (Saita et al., 2009).

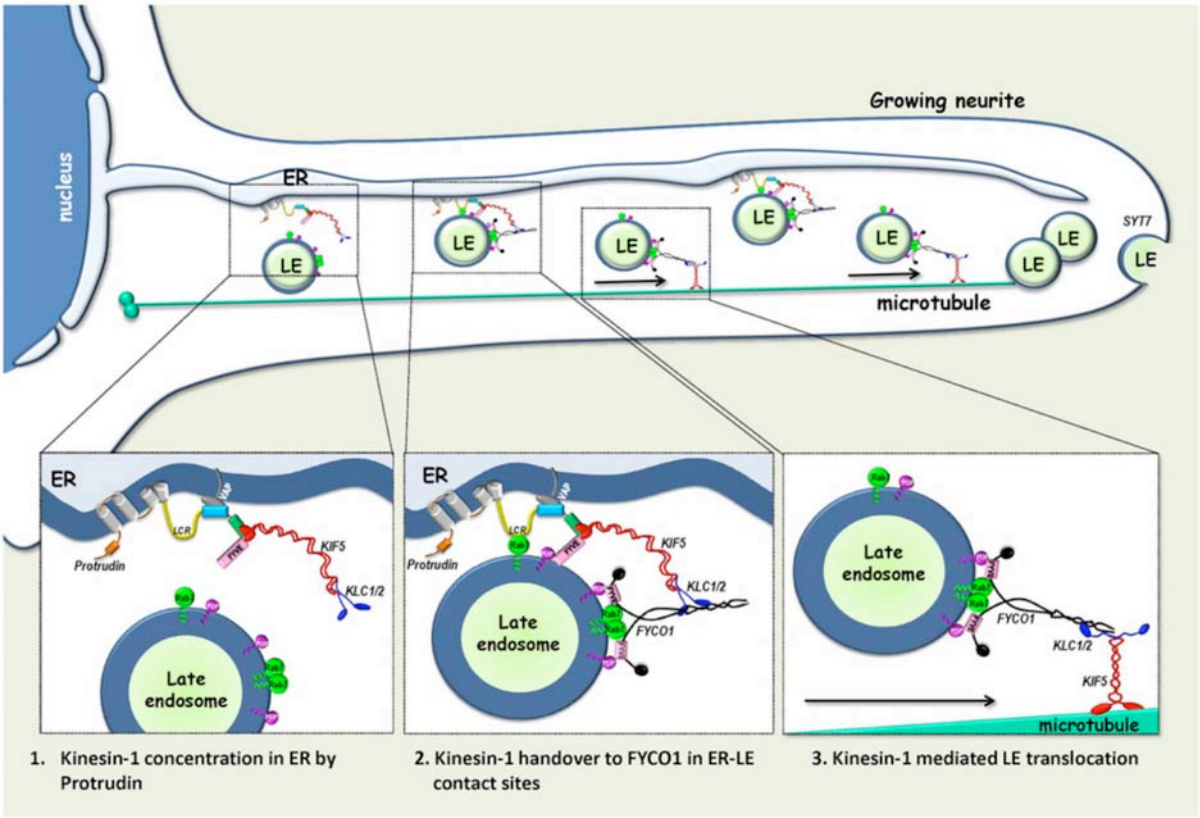

Figure 1.6: schematic representation of protrudin-dependent neurite extension. From (Raiborg et al., 2015a).

The most recently proposed model suggests that the role of protrudin in neurite outgrowth is based on the promotion of contact sites formation between ER and late endosome (LE) through its interaction with RAB7 and PI3P. These contact sites mediate transfer of the microtubule motor kinesin 1 from protrudin to the motor adaptor FYCO1 on LE. Kinesin-loaded LE can therefore move on microtubules. Repeated LE-ER contacts promote microtubule-dependent translocation of LE to the cell periphery and their subsequent fusion with the plasma membrane (Fig. 1.6) (Raiborg et al., 2015a).

(vi). Paracrine role

Experiments in model animals like *Caenorabditis Elegans* (where the VAP homologue is VPR-1) and *Drosophila Melanogaster* (where VAP is known as VAP33 or dVAP) provided evidence for a paracrine role of VAPB. In particular, the N-terminal MSP domain of VAP proteins has been reported to be cleaved from the transmembrane domain and function as a secreted ligand by binding to receptors of the ephrin axonal repellent system (Peters et al., 2015; Tsuda et al., 2008).

Ephrine (Eph) receptors are a well-conserved family of tyrosine kinase receptors. Their physiological ligands are ephrines, which are bound to the extracellular leaflet of the plasma membrane. Besides being found on oocytes (where they were originally identified), some of these receptors (such as EphA4 and A7) are expressed in the nervous system and adult skeletal muscle. Eph receptors have been

shown to function in regulating MNs survival *in vitro* in culture and influence proliferation/apoptosis in the central nervous system of mammals (Magal et al., 1996) (Ricard et al., 2006). Moreover, they appear to interact with glutamate-NMDA receptors (Dalva et al., 2000), which suggests a possible link with the excitotoxicity observed in ALS.

Both *Drosophila* and nematode MSP are thought to be secreted in the extracellular environment and to compete with ephrins for receptor binding (Tsuda et al., 2008) The mechanism of cleavage and secretion of VAP protein MSP domain is still unknown: given its localization on the cytosolic face of the ER membrane opposite to the lumen of the secretory compartment, its mechanism of secretion must require a still unidentified pathway, possibly similar to the unconventional one followed by other proteins, such as the Nef protein of HIV and interleukin1 β (Nickel, 2010).

When *Drosophila* and *Caenorabditis*, which have only one VAP gene, do not produce the protein, they show strong destabilization of mitochondria networks in muscle cells, which reflects alterations in cytoskeletal organization as a consequence of altered signaling between neurons and muscle cells. Indeed, when dVAP is selectively expressed in neurons, animals show a normal phenotype, while this doesn't happen when it is selectively expressed in muscles. In *Drosophila*, it has been demonstrated that the secreted vMSP domain interacts with two muscular receptors, Sax-3 Robo and CLR-Lar. Most likely, Robo facilitates binding of vMSP to Lar or Robo/Lar complexes, reducing Lar signaling to the Arp2/3 complex, which is necessary for actin polymerization (see Fig. 1.7 for a schematic representation of VAP paracrine function). Lack of this modulation by vMSP affects mitochondria morphology and distribution (Han et al., 2012).

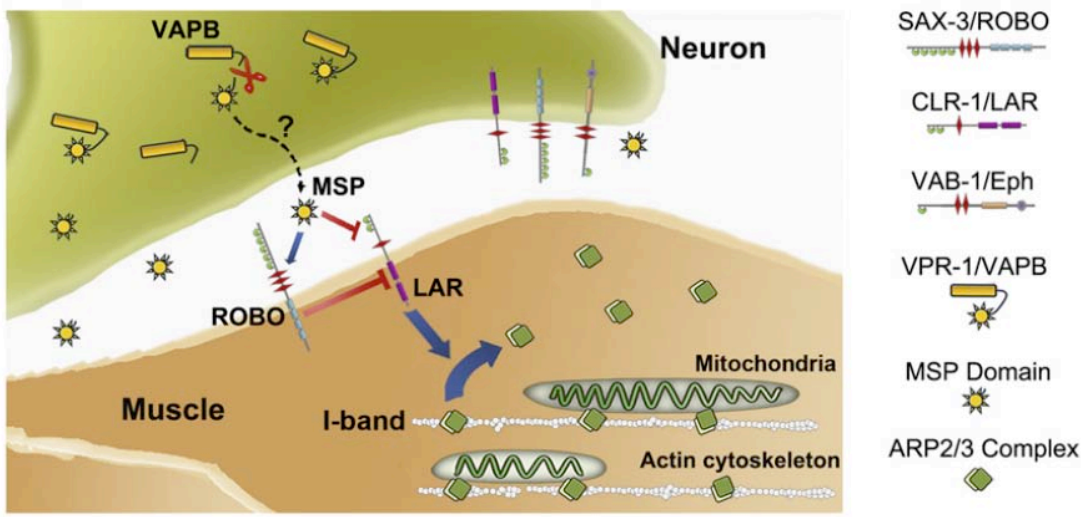

Figure 1.7: Schematic representation of VAPB-MSP domain secretion and its effects on muscle cells. From (Han et al., 2012).

Recently, an additional role of VAP has been observed in muscle metabolism. In *C. elegans*, VPR-1 causes triacylglycerol (TAG) accumulation in striated body wall muscle. Similarly, in VAPB KO mice, VAPB downregulation increases the resistance of muscle lipid stores to fasting-induced mobilization. Whether the putative metabolic changes in mouse muscle are due to secreted vMSPs is not yet clear (Han et al., 2013).

1.3.3. Mutant P56S-VAPB

The P56S mutation of VAPB is located in the VAP consensus sequence and involves a highly conserved proline residue (see Fig. 1.2). This substitution dramatically alters the MSP domain structure, which, in physiological conditions and based on crystallography data, appears to be arranged in a seven filament beta sheet domain, similarly to immunoglobulins. In particular, whereas the proline residue makes an unusual *cis* peptide bond necessary to maintain the characteristic loop of this region, the serine present in the mutant makes a conventional *trans* peptide bond, causing the disgregation of the MSP domain, which becomes insoluble and aggregate-prone (Shi et al., 2010). Despite these structural alterations, work from our laboratory has shown that mutant VAPB can still correctly insert into ER membranes (Fasana et al., 2010). However, loss of the correct folding induces metabolic instability of the protein (Genevini et al., 2014; Papiani et al., 2012), and alterations in the MSP domain compromise the ability to bind the FFAT sequence, thus preventing VAPB association with its physiological interactors (Kanekura et al., 2006) (Teuling et al., 2007). Wt VAPs interact with the P56S mutant, so that both wt VAPB and, to a lesser extent, VAPA have been shown to become sequestered in intracellular cytoplasmic insoluble aggregates in P56S- expressing cells (Suzuki et al., 2009) (Teuling et al., 2007).

Given the multiple functions in which VAP proteins are known to be involved, there are several ways by which mutant VAPB could trigger pathogenicity, as suggested by several experimental studies performed in different *in vitro* models. One possibility is that P56S-VAPB may interfere with protein trafficking and lipid homeostasis (see previous chapter on VAPB functions). In this regard, an important feature of P56S-expressing cells is Golgi fragmentation, in agreement with the notion that altered intracellular transport and lipid metabolism cause disassembly of the Golgi apparatus (Teuling et al., 2007).

As for the ER stress response, both UPR branches where VAPB is implicated appear to be altered: although the mutant protein can still bind ATF6, it has been shown to exert a stronger inhibitory effect compared to the wt protein (Gkogkas et al., 2008). Moreover, it looses its ability to activate IRE1 (Suzuki et al., 2009). A general malfunctioning of VAPB-mediated UPR could lead to an accumulation of unfolded proteins in the ER, which could contribute to MNs death (Suzuki et al., 2009).

Besides damage in the ER, ALS is characterized by alterations in mitochondria and calcium homeostasis, as described in a previous section. As recent data implicate VAPB in calcium uptake by

mitochondria (De Vos et al., 2012), an impairment of VAPB function could play a role in this aspect of the pathology. Another feature regarding mitochondria is their mobility. Mitochondria transport along axons is a vital process for neurons. In addition to producing ATP, these organelles are essential to maintain calcium concentration at the synaptic terminal, which is necessary for a correct vesicle exocytosis. Mitochondria are moved to the periphery by microtubule-mediated anterograde transport. On the outer mitochondrial membrane the integral membrane protein Miro-1 (mitochondrial Rho GTPase-1) binds the adaptor protein TRAK (trafficking kinesin protein-1) which, in turn, binds the motor protein kinesin-1, thus promoting the anterograde transport of the whole complex along microtubules. The presence of P56S-VAPB interferes with anterograde (but not retrograde) transport of mitochondria, reducing speed, movement frequency and persistence. These alterations could be the consequence of altered calcium homeostasis caused by the expression of the mutant (Morotz et al., 2012).

Finally, regarding the paracrine function of VAPB, the P58S mutation of *Drosophila* VAP33 has been reported to cause a decrease in MSP-VAP secretion, thus interfering with neuron-muscle cross-talk at the neuromuscular junction. This mechanism could alter the target cell and, synergistically with the cell autonomous damage of P58S, could contribute to ALS pathology (Tsuda et al., 2008). Indeed, the reduction in vMSP secretion and consequent alteration in Robo/Lar signaling causes defects in muscle cells of P58S-carrying organisms.

Characteristics of P56S-generated aggregates

Like in many neurodegenerative diseases, which share the common feature of accumulating mutant proteins, P56S-VAPB transiently expressed in a variety of cultured cells forms perinuclear cytoplasmic inclusions that can be observed at the optical microscope. Ultrastructural analysis, however, revealed dramatic differences between P56S-VAPB inclusions and other inclusion bodies linked to neurodegenerative disorders. In particular, mutant VAPB inclusions correspond to profoundly restructured ER domains and not to a cytosolic protein aggregate, as is generally the case. They correspond to a novel form of OSER (Organized Smooth ER), consisting of two or three juxtaposed ER cisternae separated by a 30 nm electron-dense cytosolic layer (see Fig. 1.7). The electron-dense layer between two tubules is in continuity with the cytoplasm and is enriched in mutant VAPB. Pairing of two cisternae is most likely mediated by *trans* interaction of VAPB mutated cytosolic domains (Fasana et al., 2010) (Papiani et al., 2012). Immunofluorescence studies revealed that many ER markers are present within the inclusions, while FRAP experiments showed that these aggregates are in continuity with the rest of the ER (Fasana et al., 2010). Finally, formation, clustering and localization of P56S-VAPB inclusions to the juxtanuclear region was shown not to depend on the microtubule cytoskeleton, in contrast with inclusions observed in other neurodegenerative diseases (Papiani et al., 2012).

Recent evidence from our laboratory showed that in newly formed inclusions, P56S-VAPB is ubiquitinated and that mutant protein is cleared from cells faster than the wt one. Using drugs that specifically inhibit either the proteasome or autophagy (MG132 and 3-Methyladenine, respectively), we

demonstrated that P56S-VAPB degradation is blocked with the first, but not the second treatment, indicating that mutant VAPB is eliminated by the proteasome. Moreover, in immunofluorescence experiments no colocalization could be detected between P56S inclusions and the autophagic receptor p62, a protein that binds ubiquitinated proteins and selectively shuttles them to the nascent autophagosome for subsequent degradation (Papiani et al., 2012). This result was unexpected, since the elimination of inclusion bodies observed in other neurodegenerative diseases (like Huntington and Parkinson) is usually autophagy-dependent (Ravikumar et al., 2002).

Given that proteasome-mediated degradation proceeds by eliminating one protein molecule at a time, P56S-VAPB has to be extracted from aggregates where it is tightly packed before being eliminated. Since it is an ER transmembrane protein, its delivery to the proteasome must involve extraction, not only from the aggregate, but also from the ER membrane. For this reason, the involvement of ERAD (ER Associated Degradation) in the degradation of mutant VAPB was investigated. An important ERAD factor is the AAA-ATPase p97/VCP, which utilizes the energy derived from ATP hydrolysis to extract substrates from the ER to the cytosol. By using a dominant negative mutant of p97 we demonstrated that this protein has an important role in P56S degradation. p97 could be involved in the extraction of VAP proteins from the lipid bilayer and at the same time dissolve protein-protein interactions responsible for the aggregation (Papiani et al., 2012).

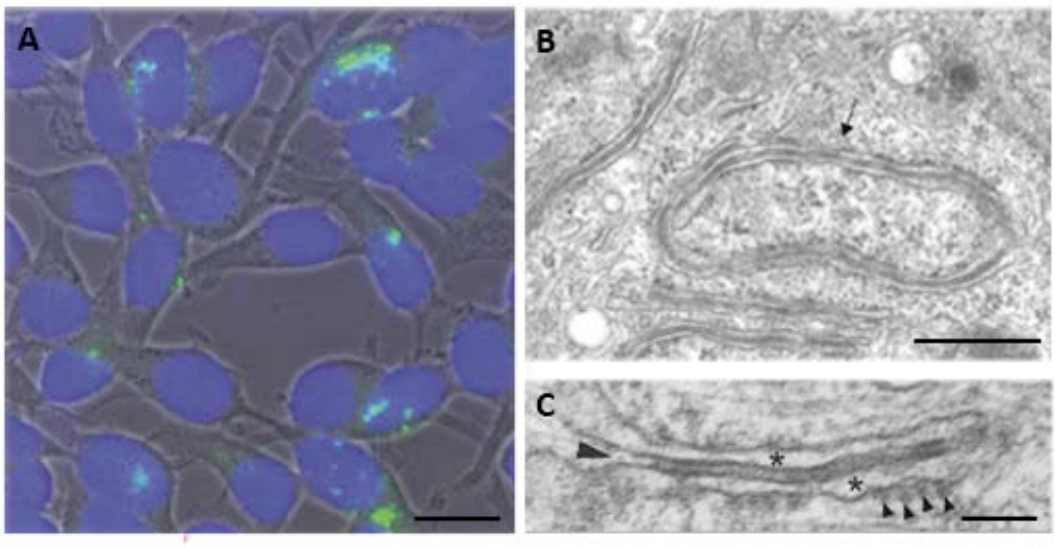

Figure 1.8. P56S-VAPB aggregates. A: immunofluorescence image showing intracellular localization of P56S-VAPB. Blue: DAPI, green: P56S-VAPB inclusions, gray: phase contrast. B: electron microscopy showing altered ER structure following P56S-VAPB expression. C: electron microscopy at higher magnification Asterisks indicate ER cisternae, arrowheads ribosomes. Scale bars: A: 10 μm, B: 500 nm, C: 200 nm. Adapted from (Papiani et al., 2012).

1.3.4. Possible pathogenic mechanisms of mutant VAPB

ALS8 is a dominantly inherited pathology: the presence of only one mutated allele is sufficient to trigger the development of the disease. In general, dominant inheritance can be explained by either a gain or loss of function of the mutant protein, even though intermediate situations where both mechanisms contribute are possible. In the gain of function hypothesis, the mutant protein has an enhanced or a completely new function that is toxic for cells, while in the loss of function situation, levels of the normal protein are not sufficient to support cellular homeostasis. This might be due either to pure haploinsufficiency, when the mutant protein is completely inert, or dominant negative activity of the altered protein that binds and sequesters the native one, thus further reducing its levels inside the cell.

The pathogenic mechanism of P56S-VAPB is still unclear, and in the literature there is evidence supporting both a gain and a loss of function hypothesis.

Supporting the first hypothesis, as previously described, transient *in vitro* transfection of the mutant protein has been shown to alter several cellular pathways in which VAPB is involved. However, several studies with mouse models question whether unregulated P56S-VAPB expression and aggregate formation are able to trigger ALS *in vivo*. As a matter of fact, even though P56S-VAPB expressed *in vivo* forms cytoplasmic aggregates similar to those observed *in vitro*, several studies with transgenic mice models failed to show defects in motor performances (Kuijpers et al., 2013a) (Qiu et al., 2013) (Tudor et al., 2010). Only one model, which specifically overexpressed P56S-VAPB in neurons, with a 7-fold increase compared to endogenous VAPB (the highest so far described in mice), showed motor defects in aged mice (Aliaga et al., 2013), along with an increase in UPR activation and selective degeneration of cortico-spinal MNs. A more in depth analysis of the above cited works suggests that a dose dependent mechanism is probably responsible for the development of motor abnormalities following P56S-VAPB overexpression. For example, Tudor, whose mutant mouse had a moderate overexpression of the transgenic protein in the nervous system, only saw a subtle cytoplasmic TDP-43 accumulation in old mice. In contrast, Qiu, whose model only had a 2-fold ubiquitous overexpression of P56S-VAPB, failed to see any difference compared to wt mice, leading the authors to suggest that MNs can tolerate the presence of mutant VAPB aggregates without degenerating.

Taken together, the studies described above indicate that, at least in the mouse, toxicity of mutant VAPB cannot, by itself, explain its dominant inheritance. Most of the mouse models carrying the mutation showed visible inclusions however, they did not develop motor deficits, a sign that MNs can cope with the presence of the aggregates. It is also a matter of debate whether ALS8 patients have inclusions. Since there are no autoptic data, the closest available model are iPSCs differentiated into MNs derived from affected patients (Mitne-Neto et al., 2011). These cells do not develop visible inclusions, however, they show reduced VAPB levels, up to half compared to controls.

To analyze mechanisms alternative to aggregate toxicity, it is useful to compare the results of two recent studies, one reporting on either heterozygous or homozygous VAPB-knock-out mice (Kabashi et

al., 2013), the other on a knock-in mouse that expresses the mutant protein in its correct genetic locus, and has physiological levels of the mutant protein (Larroquette et al., 2015). Both these models showed mild motor defect, which were slightly more severe in the knock-in model. These results suggest that the loss-of-function caused by the lack of the product of one VAPB allele may be aggravated by the production of the mutant protein. Since the aggregates themselves do not appear to be toxic (as discussed above), the effect of the mutant protein could be due to a dominant negative effect; indeed wt VAPB and, to a lesser extent, VAPA are recruited into P56S-VAPB-generated inclusions (Teuling et al., 2007). The dominant negative effect would become harmful only in the context of already reduced levels of wt VAPB. It should, however, be kept in mind, that P56S-VAPB is unstable, so that one would not expect it to accumulate in neurons that express it at normal levels. Therefore, the difference in the knock-in and knock-out model may simply reflect differences in the genetic background of the mice used in these studies.

In summary, the mouse model studies suggest that the dominant inheritance of VAPB cannot be explained solely by a toxic effect of the aggregates, as pathological effects in transgenic mice with two normal VAPB alleles were observed only under conditions of unphysiological overexpression of the mutant protein. In contrast, normal levels of expression of the mutant in a genetic background with only one normal allele did produce mild motor deficit, suggesting that at least partial loss of VAPB function is required for pathogenicity.

2. Aims of the thesis

ALS is a fatal neurodegenerative disease characterized by degeneration of MNs leading to progressive paralysis and eventually death due to respiratory failure. So far, no effective treatments are available for this devastating disease. Interestingly, genetic forms of ALS show the same pathological alterations observed in the most frequent sporadic cases. For this reason, studying the role of single disease causing mutations is important to gain insight into the pathophysiological events that lead to disease development.

VAPB is one of the less investigated genes linked to fALS. However, because of the reduction of VAPB levels observed also in sporadic ALS, elucidating its pathogenic mechanism may be important not only for the rare fALS form that it underlies, but also for a more general understanding of the pathogenic factors triggering sALS

As described in the introduction, the cellular and molecular mechanisms underlying pathogenicity of mutant VAPB are still poorly understood. It is still unclear whether P56S-VAPB-generated inclusions exert a direct toxic function or whether reduced levels of the wt protein are sufficient to trigger the disease. An intermediate situation, where both mechanisms contribute to ALS development, could also be possible.

The aim of my thesis is to analyze the contribution of mutant VAPB gain or loss of function in the development of ALS. To reach this goal, I investigated whether P56S-VAPB could interfere with physiological protein degradation and trafficking pathways and, in parallel, whether downregulation of wt VAPB produced detrimental effects on motorneuronal cell viability. To address these questions, I used two complementary experimental approaches. First, because previous cellular studies were carried out with heavily overexpressed mutant VAPB, I used epithelial and motorneuronal cellular models expressing only moderate levels of the protein to analyze a possible toxic action in a context more closely resembling the diseased organism. Second, I developed stable VAPB-downregulated motorneuronal cell lines to examine if partial or near complete lack of this protein could have any deleterious effect. The cell line I used (NSC34) was derived from primary murine MN and is the best available one to study motorneuronal diseases.

By integrating the results obtained with the two approaches I expect to broaden our knowledge on mutant VAPB pathogenic mechanisms.

3. Materials and Methods

3.1. Plasmid construction

3.1.1. Bacterial transformation with plasmid DNA

The following media were used to grow bacteria:

LB (500 ml autoclaved) - brought to pH 7.2 with NaOH		SOB (1L autoclaved) brought to pH 7.2 with NaOH		FSB (sterile filtered) brought to pH 6.8 with 0.1 N HCl	
Tryptone	5g	Tryptone	20 g	$MnCl_2$	45 mM
Yeast extract	2.5g	Yeast extract	5 g	$CaCl_2$	10 mM
NaCl	5g	NaCl	0.5 g	KCl	100 mM
+Agar for petri dish	7,5g	KCl	0.18 g	Glycerol	10%
				Hexamine cobalt chloride	3 mM
				Potassium acetate	10 mM

To prepare bacteria competent to incorporate exogenous DNA, the method developed by (Hanahan, 1983) was followed with slight modifications.

The DH5α strain of *E.Coli* was used since it is optimized to amplify plasmid DNA. Two colonies of non competent bacteria grown overnight (o/n) at 37°C on a LB+agar petri dish were inoculated in 100 ml SOB medium supplemented with 20 mM $MgSO_4$. The culture was grown at 37°C with shaking until it reached 0,1 OD (optical density) at 600 nm (this corresponds to the beginning of the log phase of growth). The culture was split into two 50 ml tubes and centrifuged for 10 minutes at 4000 rpm at 4°C, then each pellet was resuspended in 20 ml cold FSB (see the table above). After 10 minutes of incubation on ice, the bacteria were centrifuged again and resuspended in 4 ml of cold FSB. After adding 140 µl of dimethylsulfoxide (DMSO), the bacterial suspension was incubated for 15 minutes on ice. Finally, after adding an additional 140 µl DMSO aliquot, the bacteria were transferred into single-use cryogenic vials, immediately frozen in liquid nitrogen, and stored at -80° until use.

Competent bacteria were thawed and kept on ice for 10 minutes. In the meantime, 2-20 ng of plasmid DNA were diluted in 10 µl of water in transformation tubes. 100 µl of bacteria were added to the DNA solution and left on ice for 30 minutes. Next, they were subjected to a heat shock step for 90

seconds at 42°C, thus allowing the DNA to enter the cells. After a quick cooling step on ice, 800 µl of SOC medium (SOB supplemented with 20mM glucose and 10 mM $MgCl_2$) were added and the bacteria were incubated for 1h at 37°C with shaking to allow recovery. Finally, they were plated on a LB+agar petri dish supplemented with the appropriate selection antibiotic and allowed to grow o/n (overnight) at 37°C.

3.1.2. DNA extraction (MINI and MIDI preparation)

Following transformation, MINI preparations were used to screen bacterial colonies carrying the plasmid of interest and MIDI preps to obtain DNA for sequencing and transfection. While MIDIs were performed using the Plasmid MIDI kit from Qiagen, MINIs were prepared according to the procedure described in (Sambrook and Russel, 2001), as outlined below.

Briefly, each colony was inoculated into 2 ml of LB supplemented with the appropriate selection antibiotic and incubated o/n at 37°C with shaking. 500 µl of the resulting bacterial suspension was stored at 4°C, while the rest was subjected to DNA purification. The solution was centrifuged for 2 minutes at 12 000 rpm at 4°C and the bacterial pellet resuspended in 100 µl of resuspension buffer (50 mM Tris-HCl pH 8.0, 10 mM EDTA, 100 µg/ml RNase A). 200 µl of lysis buffer (1% SDS, 0,2 N NaOH) was added to lyse cells and denature DNA. After briefly shacking the sample, 150 µl of neutralization buffer (3 M K^+ acetate, pH 5.5) was added to neutralize the effects of the lysis buffer and to generate a K^+-SDS precipitate. Under these conditions, the small plasmid DNA is renatured, while the large chromosomal DNA co-precipitates with the K^+-SDS. After a 5 minute incubation on ice, the sample was centrifuged at 13 000 rpm at 4°C for 15 minutes to eliminate genomic DNA and cell debris. Two volumes of 100% ethanol were added to the supernatant to precipitate plasmid DNA. After a 30 min incubation at RT, the sample was centrifuged at 13 000 rpm at 4°C for 15 minutes and the DNA pellet was washed with 30 µl of 70% ethanol and centrifuged again for 10 minutes. Once dried, the DNA was resuspended in water and stored at -20°C.

3.1.3. Construction of recombinant plasmids

(i). Plasmid for siRNA silencing

shRNAs are small RNA molecules composed of a sense and antisense sequences separated by an hairpin loop. Following transcription, sense and antisense (red and blue in Fig. 3.1) anneal, thus forming a tight hairpin turn. shRNAs are processed by the cellular machinery into mature and active siRNAs (Brummelkamp et al., 2002).

Figure 3.1: structure of the two oligonucleotides used for preparation of pSuper.neo.GFP plasmid targeting VAPB

To create stable cell lines silenced for VAPB expression, I used the pSuper.neo.gfp vector (OligoEngine). As shown in Fig. 3.2, this plasmid carries the sequences for expression of ampicillin for bacterial resistance, neomycin (G418) for mammalian cells resistance and soluble EGFP. The restriction sites used for insertion of the shRNA sequence (BglII and HindIII) are indicated. To drive the expression of endogenous the shRNA, the vector uses the H1 RNA polymerase III promoter (Brummelkamp et al., 2002).

The two DNA oligonucleotides targeting VAPB mRNA (shown in Fig. 3.1) were obtained from Sigma (PAGE purification) and were annealed to obtain a double stranded DNA. Briefly, the two oligonucleotides (500 pmol each) were mixed in 50 µl of TE buffer (10 mM TrisHCl, pH 7.5, 1 mM EDTA), heated for 5 minutes at 95°C, and allowed to cool to room temperature (RT) on the bench. Next, the annealed oligonucleotides were 5' phosphorylated with Polynucleotide Kinase (NEB). In parallel, the vector was double digested with BglII and HindIII (NEB), purified (Nucleospin Extract II, Macherey-Nagel), de-phosphorylated with Shrimp Alkaline Phospatase (NEB) and purified again. The annealed oligos were ligated into the digested dephosphorylated pSuper.neo.GFP, using T4 DNA ligase (Promega), and the ligation mixture was used to transform competent *E.Coli* DH5α. Plasmid DNA miniprepes were prepared from antibiotic-resistant colonies.

The insertion of the annealed oligo into the p.Super.neo.GFP disrupts the BglII restriction site. Therefore, the loss of this restriction site was used to screen the purified DNA by BglII digestion. Positive clones were expanded, and the plasmid DNA was sequenced by MWG Eurofins.

(ii) Other plasmids

pCINeoHACD3δ was used to analyze proteasome function and was generously provided by A.M. Weissman (National Institutes of Health, Bethesda, MD). pCDM8.1-ts045VSVG-EGFP was used to study protein transport and was a kind gift of J. Lippincott-Schwartz (National Institutes of Health, Bethesda, MD. The pTre-Tight vectors (Clontech), coding either for myc-wt-VAPB or myc-P56S-VAPB were used to generate stable inducible NSC34 Tet-Off cell lines and were already available in our laboratory (Fasana et al., 2010). pEGFP-N1 (Clontech) was cotransfected with pCINeoHACD3δ and used to check transfection efficiency; pTK-hygro (Clonthech) was cotransfected with pTre-Tight vectors and used to grant hygromycin resistance to mammalian cells.

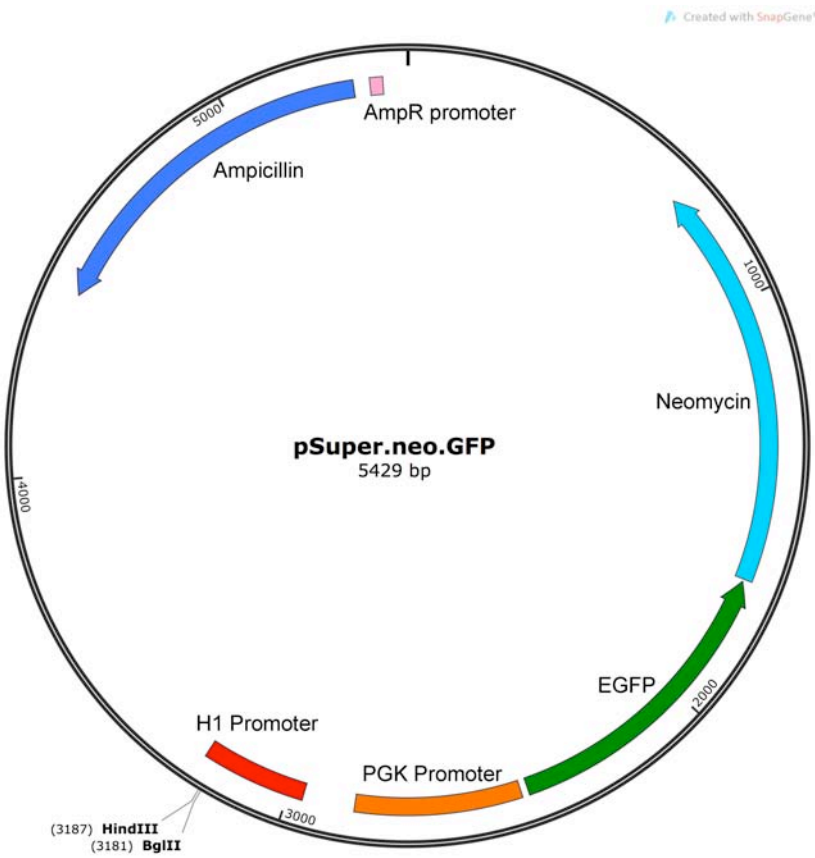

Figure 3.2: pSuper.neo.GFP (OligoEngine) sequence map**.**

3.2. Cell Culture

3.2.1. Hela Tet-Off cell lines

HeLa (an epithelial cell line derived from cervical cancer) Tet-Off cell lines inducibly expressing a myc-tagged version of either wild type-VAPB or mutant P56S-VAPB had been previously generated in the laboratory (Fasana et al., 2010). Thanks to the stable insertion of the Tet-Off plasmid (Clontech), these cells express the transgenic product only in the absence of doxycycline (Dox) (see Fig. 3.3).

Cells were grown in DMEM supplemented with 10% FBS Tet-free (purchased from Clontech or Euroclone), 1% Penicillin/Streptomycin, 1% L-glutamine at 37°C with 5% CO_2. At the first passage after thawing, 100 µg/ml G418 and 100 µg/ml hygromycin were added to the culture medium to maintain stable insertion of the Tet-Off and pTreTight plasmid respectively. Cells were grown in the presence of 500 ng/ml Dox to repress the expression of the transgenic product. To induce expression of the transgene, Dox was removed from the medium and cells were grown for 6 days in the absence of the antibiotic (Papiani et al., 2012).

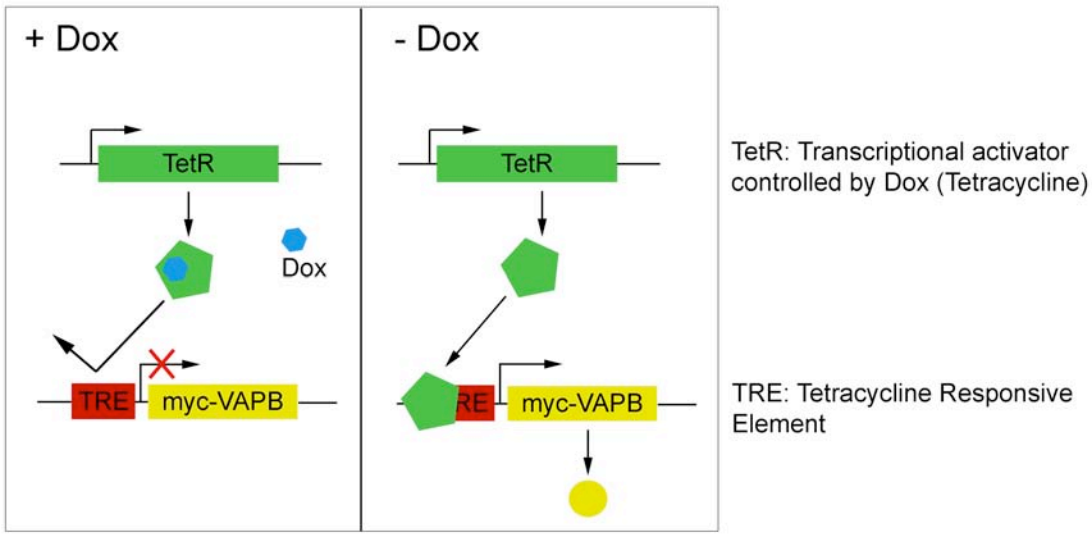

Figure 3.3: Schematic representation of Tet-Off system. In absence of Dox in culture medium, TetR is free to bind to TRE and activate the transcription of the downstream transgene.

3.2.2. NSC34 cells

Neuroblastoma Spinal Cord (NSC34) is a mouse cell line created by fusion of a neuroblastoma line with spinal cord primary motor neurons, and currently represents the best characterized available cell line with motorneuronal characteristics. These cells express ChAT (Choline Acetyl Transferase), the key enzyme for acetylcholine synthesis, make neurite-like protrusions, support action potentials and express neurofilament proteins. Moreover, NSC34 cells make contacts with co-cultured myotubes, and induce contraction and clustering of acetylcholine receptors (Cashman et al., 1992).

NSC34 were maintained in DMEM supplemented with 10% FBS, 1% penicillin/streptomycin, 1% L-glutamine and 1% Na^+ pyruvate at 37°C with 5% CO_2.

These cells will be called NSC34 wild-type (wt).

Differentiation of NSC34

For differentiation, cells were plated onto Matrigel (BD Bioscience)-coated plates and grown with differentiating media, consisting of DMEM/F12 supplemented with 1% FBS, 1% penicillin/streptomycin, 1% L-glutamine, 1% Na^+ Pyruvate, 1% Non Essential Amino Acids (NEAA) and 1 µg/ml *all-trans* retinoic acid (Sigma, 10 mg/ml stock solution diluted in ethanol) (Maier et al., 2013). Since retinoic acid is unstable in culture, the media was changed every 2 days. Unless otherwise stated, cells were grown in differentiation medium for six days and then either fixed for immunofluorescence or collected to make a cell lysate and analyzed by Western blot. Neurite length of the cells at various stages of differentiation was determined on images of tubulin-stained cells acquired with a 10x magnification lens (see section on microscopy and legend to Fig 4.17 for details)

3.2.3. NSC34 tTA40

NSC34 tTA40 are an NSC34-derived stable cell line that expresses TetR (see Fig 3.3). This allows them to inducibly express a transgenic protein, encoded in a pTre-Tight plasmid, after Dox removal. These cells were generated in the laboratory of Dr. Cantoni (Babetto et al., 2005) and maintained in DMEM supplemented with 10% FBS, 1% P/S, 1% L-Glutamine, 1% Na^+ pyruvate and 250 μg/ml G418.

3.3. Transfection

3.3.1. Transient siRNA transfection

The transfecting reagent (Lipofectamine) and siRNAs were obtained from Invitrogen. Cells were plated in penicillin/streptomycin-depleted media 24 h before silencing in 12 multiwell (mw) plates and allowed to grow to 40% confluence. Prior to the experiment, the medium was removed and 800 μl of fresh medium was added. For each well, two solutions were prepared: the first one containing the appropriate siRNA mixture, the other one 2 μl of Lipofectamine; both were diluted in 100 μl of Optimem. After mixing, the siRNA solution was added to the one containing the Lipofectamine. This mixture was stored at RT for 20 minutes and finally added to cells. The final concentration of siRNAs in the well was 10nM. After 6h, the medium was removed, the cells were washed and returned to the incubator with complete, penicillin/streptomycin containing media.

The following siRNAs, retrieved from the Invitrogen catalogue, were used to downregulate VAPB (for each oligonucleotide pair, only the sense strand is shown):

siRNA 1 (MSS285791) 5’ UGGCCCUGGUGGUUCUGUUCUUUAU 3’

siRNA 2 (MSS285792) 5’ CAUUAUAGGGAAGAUUGCCUUGUAG 3’

siRNA 3 (MSS244288) 5’ GCAGCUCAAGGAAGAAGACGGACUU 3’

3.3.2. Transient DNA transfection

All transfections were performed with JetPEI (Polyplus Transfection). Hela and NSC34 tTA40 cells were transfected according to the manufacturer's instructions. Briefly, cells were plated 24h before transfection in 6 mw plates to allow growth to 50% confluence. Prior to transfection, the medium was changed to remove cell debris. For each well, two solutions were prepared: the first one containing 3 μg of DNA, the second one 6 μl of JetPEI; both were diluted in 100 μl of 150 mM NaCl. After mixing, the JetPEI solution was added to the one containing the DNA. This mixture was stored at RT for 20 minutes and then added to cells.

The protocol described above for Hela and NSC34 tTA40 cell lines lead to massive death of wt NSC34 cells. Therefore, the manufacturer's protocol was adapted for the latter cell line and both the amount of DNA and JetPEI used were reduced: for transfection in 12mw plates, the reaction was performed with 750 ng of DNA and 1,5 µl of JetPEI.

3.3.3. Stable DNA transfection and selection of cell lines

To obtain stable VAPB downregulated cell lines, wt NSC34 were transfected with either the empty pSuper.neo.GFP vector or the one coding for a VAPB-targeted shRNA (see section 3.1.3) designed after choosing the target sequence with transient VAPB downregulation with siRNAs (see Fig. 4.11).

To generate NSC34 Tet-Off VAPB clones, NSC34 tTA40 cells were co-transfected with pTK-hygro and pTre-tight vectors coding either for myc-wt-VAPB or myc-P56S-VAPB. The transfection was performed in presence of Dox to inhibit the expression of the transgene.

One day after transfection, cells were diluted 1:10 and plated in 10 cm petri dish. After two more days, selection was initiated on the basis of growth in 500 µg/ml G418 for the pSuper vectors and 150 µg/ml hygromycin for pTre-tight plasmids. The media were changed every 3-4 days to remove dead cells and maintain antibiotic concentration.

After 3-4 weeks visible colonies were collected with cloning cylinders (Sigma), amplified and frozen. One aliquot of each clone was used for screening by western blot analysis. VAPB downregulated cell lines were screened by assessing the expression levels of the endogenous VAPB. Tet-Off clones were induced to express the transgene by growth in the absence of Dox for 4–5 days. Enhancement of gene expression was obtained by addition of 10 mM Na^+Butyrate for 12 h. Positive clones were identified by the presence of the myc-VAPB band on Western Blots.

3.4. Drug treatments and starvation

Lactacystine and Torin 1 were from Cayman Chemical; MG132 was from Calbiochem. Other drugs were from Sigma. 3-Methyladenine (3-MA) and Cycloheximide (CHX) were dissolved in water and used at a final concentration of 10 mM and 50 mg/ml, respectively. Na^+ Butyrate was dissolved in complete medium and used at 10 mM final concentration. The following drugs were dissolved in DMSO and used at the final concentrations indicated between brackets: Bafilomycin (200 nM), MG132 (10 µM), Lactacystin (10 µM) and Torin1 (250 nM). Control cells received equal volumes of the vector.

Cells were starved by replacing the culture medium with EBSS (Earle's Balanced Salt Solution), a medium that lacks both serum and aminoacids.

3.5. Biochemical analysis

3.5.1. Cell collection and lysis

Confluent monolayers were washed twice with PBS and mechanically detached from the culture well with pipette tips in the presence of SDS-lysis buffer (50 mM Tris HCl pH 6.8, 2% SDS) supplemented with protease inhibitors (Roche). Complete lysis was obtaining by boiling the samples at 95°C for 2 minutes. DNA released by the lysis was fragmented by repeated passages through an insulin needle.

Protein concentration was assessed with BCA Protein assay kit (from Thermo Scientific or Euroclone).

3.5.2. SDS-PAGE and Western Blot

Polypeptides were separated with the Tris-glycine system using a vertical electrophoretic device. Before loading, samples were heated to 60°C for 2 minutes after adding 1/3 of volume of Denaturation Buffer (DB) 4X (8% β mercaptoethanol, 34% glycerol, 0,04% bromophenol blue).

Following separation by SDS-PAGE, proteins were transferred onto 0,45 μm nitrocellulose membrane (either from Biorad or Perkin Elmer). When lipidated proteins, like LC3, levels were assessed, a PVDF membrane (Biorad) was used. After checking the quality of the SDS-PAGE run and of the protein transfer by Ponceau S staining (Euroclone), membranes were incubated o/n in blocking buffer (Tris-buffered saline (TBS) with 0,1% Tween and 5% dried skim milk) under agitation at 4°C. Blots were then returned to RT, and probed with primary antibodies diluted in the same solution. After 3 washes with blocking buffer, blots where incubated with secondary antibodies. Unbound antibodies were finally removed by washing the blots three times with TBS + 0,3% Tween, then three times with TBS + 0,1% Tween and finally with TBS alone. Peroxidase-conjugated secondary antibodies were revealed by chemioluminescence using the ECL system (Perkin Elmer). The films were digitized, and band intensities were determined with ImageJ software (National Institutes of Health) after calibration with the optical density calibration step table (Stouffer Graphics Arts). Alternatively, Infrared dye-conjugated secondary antibodies were used. In this case, blots were scanned with the Odyssey CLx Infrared Imaging System (LI-COR Biosciences), and band intensities were determined with Image Studio software (LI-COR Biosciences).

3.5.3. P56S-VAPB expression analysis

To analyze the degradation of mutant VAPB, we took advantage of the Tet-Off system. Tet-Off clones were first allowed to express and accumulate the mutant protein for 5–6 days in the absence of Dox; then, to stop synthesis of the transgene, the antibiotic was reintroduced into the medium, and the levels of P56S-VAPB were subsequently analyzed during a chase period (Papiani et al., 2012).

Briefly, four days after removal of Dox, equal amounts of cells were seeded onto 35 mm Petri dishes containing a coverslip, and incubation in the absence of Dox was continued for another two days. At this time, the coverslips were fixed and stained with DAPI; nuclei from random fields were counted to assess that each dish contained an equal number of cells. Degradation of VAPB was followed after readdition of Dox to the medium and cells were collected after treatment with the indicated drugs and at the time intervals indicated in the figures. The collected cells were lysed with SDS-lysis buffer (see "Cell collection and lysis") and all samples were brought to the same volume. Equal aliquots were then analyzed by SDS-PAGE-Immunoblotting. The levels of VAPB were normalized for minor variations in the number of plated cells using DAPI staining.

3.6. Microscopy

3.6.1. Equipment

Confocal images were acquired either with the Zeiss LSM 510 Meta confocal system or with the Perkin Elmer Ultraview spinning disk acquisition system (Yokogawa CSUX1-A3).

The Zeiss system was equipped with a 405/488/543/ 633 dichroic (Carl Zeiss, Oberkochen, Germany) and with 10xPlanNeofluar, 20xECPlanNeofluar, 40xPlanNeofluar or 63xPlanApo lens. Alexa Fluor 488, GFP and Bodipy were acquired using the 488 line of the Argon/2 laser, and a 505–550 band pass emission filter. For Alexa Fluor 568, DyLight 549 and Rhodamine, the 544 line of the He/Ne laser was used in combination with a 560–615 band pass emission filter. For DyLight 633, the 633 line of the He/Ne laser was used in combination with a 650 long pass emission filter. DAPI was imaged using the 405 diode laser and a 420–480 band pass emission filter. Low magnification DIC images were acquired with 20x objective and Nomarsky disk.

The Perkin Elmer spinning disk system was attached to a Zeiss Axiovert 200M microscope, and used to acquire Cholera toxin and Lamp1 staining. The system was equipped with a 405/488/561/640 dichroic and a 63x objective PlanApo objective was used.

Wide-field images were acquired with an Axioplan (Carl Zeiss, Oberkochen, Germany), or a Nikon E600 microscope, both equipped with an AxioCam HRm digital camera (Zeiss).

3.6.2. Sample preparation, image acquisition and image analysis

All the image analyses described in the following sections were performed with ImageJ software.

(i). Standard immunofluorescence

HeLa cells were plated on untreated coverslips, while in the case of NSC34 cells, coverslips were pre-coated with Matrigel (BD Biosciences). After washing with PBS, cells were fixed with 4% Paraformaldehyde (PFA) containing 4% sucrose for 20 minutes at 37°C. PFA was removed by rinsing four times with PBS. After two washes with HS-PBS (see below), cells were incubated for 20 minutes with blocking buffer with Triton to block non-specific binding sites and permeabilize membranes. Next, they were incubated with primary antibodies diluted in blocking buffer for 1h 30', washed four times with HS-PBS and incubated with secondary antibody diluted in the same buffer for 1h. Cells were washed four times with HS-PBS, three with PBS and once with water and finally mounted with Mowiol (Sigma). DAPI was diluted in the last PBS wash to counterstain nuclei.

Buffer compositions were as follows:

2x Blocking buffer	NaCl 0.9 M, Na^+ Phosphate Buffer pH 7.4 40 mM, Goat serum 33%, (+ Triton X100 0.6% when used for the permeabilization step)
HS-PBS	NaCl 500 mM, Na^+Phosphate Buffer pH 7,4 20 mM
PFA	PFA 4%, Sucrose 4%, Na^+ Phosphate Buffer pH 7.4 120 mM

(ii). PI4P Immunofluorescence

To stain PI4P, we followed the protocol described by (Hammond et al., 2009). In this paper, the authors show that to prevent the extraction of lipids (like PI4P) from the Golgi compartment, cells need to be fixed with 2% PFA, permeabilized with Digitonin and all steps performed at RT.

Briefly, cells were fixed for 15 minutes at RT with 2% PFA, obtained by directly adding an equal volume of PFA 4% to the medium in the culture well. After rinsing four times with PBS+50 mM NH_4Cl, cells were permeabilized with 20 µM digitonin diluted in Buffer A (20 mM Pipes pH 6,8, 137 mM NaCl, 2,7 mM KCl) for 5 minutes. The permeabilizing agent was removed by three rinses with buffer A, followed by 45 minutes incubation with blocking buffer (buffer A supplemented with 50 mM NH_4Cl and 5% goat serum). Next, cells were incubated with PI4P and Giantin primary antibodies (diluted in buffer A + 5% goat serum) for 1h 30 min, rinsed three times with buffer A and incubated with secondary antibodies for 1h. After three washes with buffer A, cells were post-fixed for 5 minutes with 2% PFA diluted in PBS, rinsed four times with PBS+NH_4Cl (DAPI was added to the last wash), once with water and finally mounted.

To quantify the amount of PI4P in the Golgi region, 1.6 µm thick (0.4 µm interval) z-stacks

(approximately 30 cells for each sample) were acquired centered around the plane with maximum Giantin staining (x–y sections). For each section, a ROI corresponding to Giantin staining was outlined; the integrated PI4P fluorescence intensity of this region was determined, and summed over the entire stack. To avoid artifacts due to differing efficacy of digitonin permeabilization of different cells, this value was normalized to that of the Giantin staining summed over the entire stack.

Images were acquired with identical parameters, taking care to remain below saturation in the PI4P and Giantin channels.

(iii). Ganglioside GM1 fluorescence staining

To stain the ganglioside GM1, we used fluorescent (488 conjugated) cholera toxin (Invitrogen) (Eidels et al., 1983). The staining procedure was the same as described in the standard immunofluorescence section, with the exception that PBS was used for all washes and instead of using the indicated blocking buffer, blocking and antibody incubations were performed with PBS supplemented with 0.5% BSA, 0.05% saponin, 50 mM NH_4Cl. Note that also in this case a mild detergent at low concentration was used, in order to avoid extraction of the ganglioside.

(iv). Mask analysis of LAMP1 positive GM1 vesicles

To assess the percentage of GM1 vesicles positive also for LAMP1 staining, fixed cells were subjected to double staining with fluorescent cholera toxin and anti-LAMP1 antibody as described in the previous paragraph. To perform quantification, Z-stacks (approximately 30 cells for each condition) comprising the total height of the cells were acquired (X–Y sections at 0.4 μm intervals) to measure Cholera and anti-LAMP1 fluorescence. A single confocal plane, corresponding to the medial cellular plane, was used for quantification for each cell using ImageJ software. Briefly, a threshold was fixed to convert cholera toxin and LAMP1 staining into binary masks. Small and big elements were excluded from the analysis by creating a second mask that took into account only particles with dimensions between 20-200 pixels. Elements remaining in this secondary mask were automatically counted. Lastly, the "AND function" was applied to secondary masks of cholera toxin and LAMP1 to visualize those elements positive for both stainings that were automatically counted. This number was divided to that of total Cholera toxin positive elements to obtain the percentage of GM1 vesicles positive also for LAMP1 staining.

(v). VSVG transport assay

Hela cells induced or not induced to express P56S-VAPB were transfected with ts045VSVG-EGFP. This is a temperature-sensitive mutant of VSVG that at 39°C is misfolded and ER retained, while at the permissive temperature of 32°C is correctly folded and can travel trough the secretory pathway (Bergmann, 1989). Immediately after transfection, cells were held at 39.3°C. After 24 h, they were brought to 32°C in the presence of CHX and incubated for the times indicated in the figures.

To evaluate the amount of VSVG in the Golgi area at each time point, coverslips were fixed and processed for immunofluorescence with anti-Giantin and anti-myc (to visualize myc-P56S-VAPB) antibodies. 1.2 μm thick z-stacks (approximately 20 cells for each condition and time point) were acquired centered on the plane with maximum Giantin staining (x–y sections). For each section, a ROI corresponding to Giantin staining was outlined; the integrated EGFP fluorescence intensity (corresponding to VSVG staining) of this region was determined, and summed over the entire stack. This value was normalized to that of the entire cell, determined in each section in ROIs drawn around the periphery of the cell.

For determination of surface VSVG, cells were placed on ice, medium was replaced with pre-chilled PBS++ (PBS supplemented with 0,5 mM $CaCl_2$ and 1 mM $MgCl_2$), and the samples were then transferred to the cold room. After two washes, cells were blocked with 0.1% BSA in the same buffer, and then incubated with anti-VSVG primary antibody diluted in blocking buffer for 1 h. Cells were washed 3 times, fixed with chilled PFA first at 4° for 10 min, then at RT for an additional 10 min. After blocking with 17% goat serum, the non-permeabilized cells were exposed to secondary anti-mouse antibody for 50 min at room temperature. After 5 washes, the cells were fixed again for 5 min with PFA, permeabilized with Triton-X100 and processed for immunofluorescence with polyclonal anti-VAPB and secondary anti-rabbit antibodies as described in the standard immunofluorescence section. To perform quantification, Z-stacks (15–30 cells for each condition and time point) comprising the total height of the cells were acquired (X–Y sections at 0.5 μm intervals) to measure EGFP and anti-VSVG fluorescence.

For both the Golgi and the surface quantification of VSVG, images were acquired with identical parameters, taking care to remain below saturation in the EGFP and anti-VSVG channels.

(vi). Ceramide transport assay

Ceramide transport was assessed by incubating cells with Bodipy-FL-Ceramide (Thermo Fisher) (Toth et al., 2006). Unless otherwise stated, all steps were performed on ice with chilled buffers.

To remove serum, cells were washed twice with FBS-free medium. Next, they were incubated with 0.5 μM Bodipy-FL-Ceramide diluted in the same buffer for 20 minutes. The excess of Bodipy-FL-Ceramide was removed by 3 washes with FBS-free medium. The sample corresponding to time zero (T0) was immediately fixed for 5 minutes with PFA + Glutaraldheyde (GA) containing DAPI, washed twice with PBS+ 50 mM NH_4Cl and mounted. Warm complete medium was added to the other samples and cells were placed at 37°C for the indicated time points. At the end of the incubation, the cells were fixed and mounted as indicated for T0. Images were acquired immediately after mounting.

Media and fixatives were as follows:

FBS-free medium	DMEM supplemented with P/S, L-glutamine, 20 mM Hepes-Na pH 7.3,
Complete medium	DMEM supplemented with P/S, L-glutamine, 20 mM Hepes-Na pH 7.3, 10% FBS
PFA + GA	PFA 4%, glutaraldehyde 0.05%, 0.2 M Hepes-Na pH 7.3

3.7 Statistical analysis

The statistical analysis performed in each experiment is indicated in the figure legends along with p values. In general, either unpaired two-tailed Student's t-test (Excel) or two-way ANOVA followed by Bonferroni's post test (GraphPad Prism) were used.

3.8 Antibodies

The primary and secondary antibodies used in this study are described in the following two tables.

3.8.1 Primary antibodies

Antigen	Species	Origin	Working Dilution	Application
Actin	Mouse	Sigma	1:1000	WB
ChAT	Goat	Millipore	1:500	WB
GAP43	Mouse	Sigma	1:2000	WB
GAPDH	Rabbit	Santa Cruz	1:4000	WB
GFP	Rabbit	MBL	1:500	WB
Giantin	Rabbit	Gift from Dr. Dr. M. Renz (Institute of Immunology and Molecular Genetics, Karlsruhe)	1:800	IF
Giantin	Rabbit	Synaptic Systems	1:500	IF
GM130	Rabbit	Gift from Dr. A. De Matteis (TIGEM, Naples)	1:2000	IF
HA (71550)	Rabbit	Invitrogen	1:1000/ 1:400	WB/IF
HA (SC805)	Rabbit	Santa Cruz	1:200	WB/IF
Lamp (ab24170)	Rabbit	Abcam	1:1000	IF
LC3 (L8918)	Rabbit	Sigma	1:750	WB
Myc (9E10)	Mouse	Santa Cruz	1:500	WB
Myc (9E10)	Mouse	Sigma	1:1000	IF

Antigen	Species	Origin	Working Dilution	Application
NF200 (N52)	Mouse	Sigma	1:2000	WB
NF68	Rabbit	Chemicon	1:300	WB
nKHC	Rabbit	Gift from Dr. R.D. Vale (UCSF, San Francisco, CA, USA)	1:800	WB
p62 (ab91526)	Rabbit	Abcam	1:5000	WB
PI4P	Mouse IgM	Echelon	1:300	IF
Synaptobrevin	Mouse	Synaptic Systems	1:1000	IF
Tubulin (B-5-1-2)	Mouse	Sigma	1:80000/ 1:1400	WB/IF
VAPA	Rabbit	Gift from Dr. C.C. Hoogenraad (Utrecht University)(Teuling et al., 2007)	1:2500	WB
VAPB	Rabbit	Produced in this study (Genevini et al., 2014)	1:1000/ 1:200	WB/IF
VSVG (IE9F9)	Mouse	Kerafast	1:500	IF

3.8.2 Secondary antibodies

Species reactivity	Conjugation	Dilution	Origin	Application
Rabbit	Peroxidase	1:150 000	Sigma	WB
Rabbit	IRDye 800CW	1:15 000	Licor	WB
Mouse	Peroxidase	1:150 000	Sigma	WB
Mouse	IRDye 680RD	1:15 000	Licor	WB
Goat	Biotin	1: 2 000	Sigma	WB
Streptavidin	Peroxidase	1: 1 000	Jackson	WB
Rabbit	Alexa Fluor 488	1: 300	Life Technologies	IF
Rabbit	Dylight 549	1: 400	Jackson	IF
Rabbit	Alexa Fluor 633	1: 400	Life Technologies	IF
Mouse	Alexa Fluor 568	1: 300	Life Technologies	IF
Mouse (IgM)	Rhodamine	1: 300	Santa Cruz	IF
Mouse	Dylight 549	1: 400	Jackson	IF
Mouse	Alexa Fluor 633	1: 400	Life Technologies	IF

4. Results

The aim of my thesis is to dissect the contribution of mutant VAPB gain and loss of function in the development of ALS. To investigate a possible gain of toxic function, I used cellular models expressing moderate levels of P56S-VAPB. To investigate the consequences of loss of VAPB function, I generated NSC34 clones silenced for VAPB expression, and analyzed their capacity to differentiate as well as possible alterations in lipid metabolism. The results of these two lines of research are presented in sections 4.1 and 4.2 of this chapter.

4.1. Effect of P56S-VAPB on proteostasis and intracellular transport

In this section, I will describe the results obtained with cells expressing moderate levels of mutant VAPB. First, I will analyze the degradation and stability of the mutant protein; second, I will show experiments aimed at unrevealing toxic effects of P56S-VAPB on general proteostasis and vesicular transport. All the results presented in this section have been recently published (Genevini et al., 2014).

4.1.1. P56S-VAPB is cleared exclusively by the proteasome under basal conditions, but can be degraded by stimulated autophagy.

To investigate the mechanism of P56S-VAPB degradation, we used the HeLa Tet-Off cell line that was already available and characterized in our laboratory (Fasana et al., 2010) (Papiani et al., 2012). In this cell line, expression of mutant, myc-tagged, VAPB is repressed by the presence of Dox, and induced by removal of the antibiotic from the medium. As already shown in my laboratory, mutant VAPB in these cells is expressed at levels close to those of the endogenous protein (Fasana et al., 2010) (Papiani et al., 2012).

To analyze P56S-VAPB clearance, cells were grown in induction medium for 6 days to allow the production and accumulation of the mutant protein and were shifted to Dox-containing medium on the day of the experiment to block the expression of the transgene. Within nine-ten hours, approximately 2/3 of P56S-VAPB was degraded (Fig. 4.1A,B). To assess whether the degradation was mediated by autophagy or the proteasome, we treated cells with drugs that selectively inhibit each of these pathways. Autophagy was blocked by treatment with either 3-MA or the proton pump blocker Bafilomycin, while the proteasome either by MG132, used in our previous study (Papiani et al., 2012), or lactacystin. As shown in Fig. 4.1A and B, P56S-VAPB degradation was prevented by both proteasomal inhibitors, while the autophagy blockers were without effect.

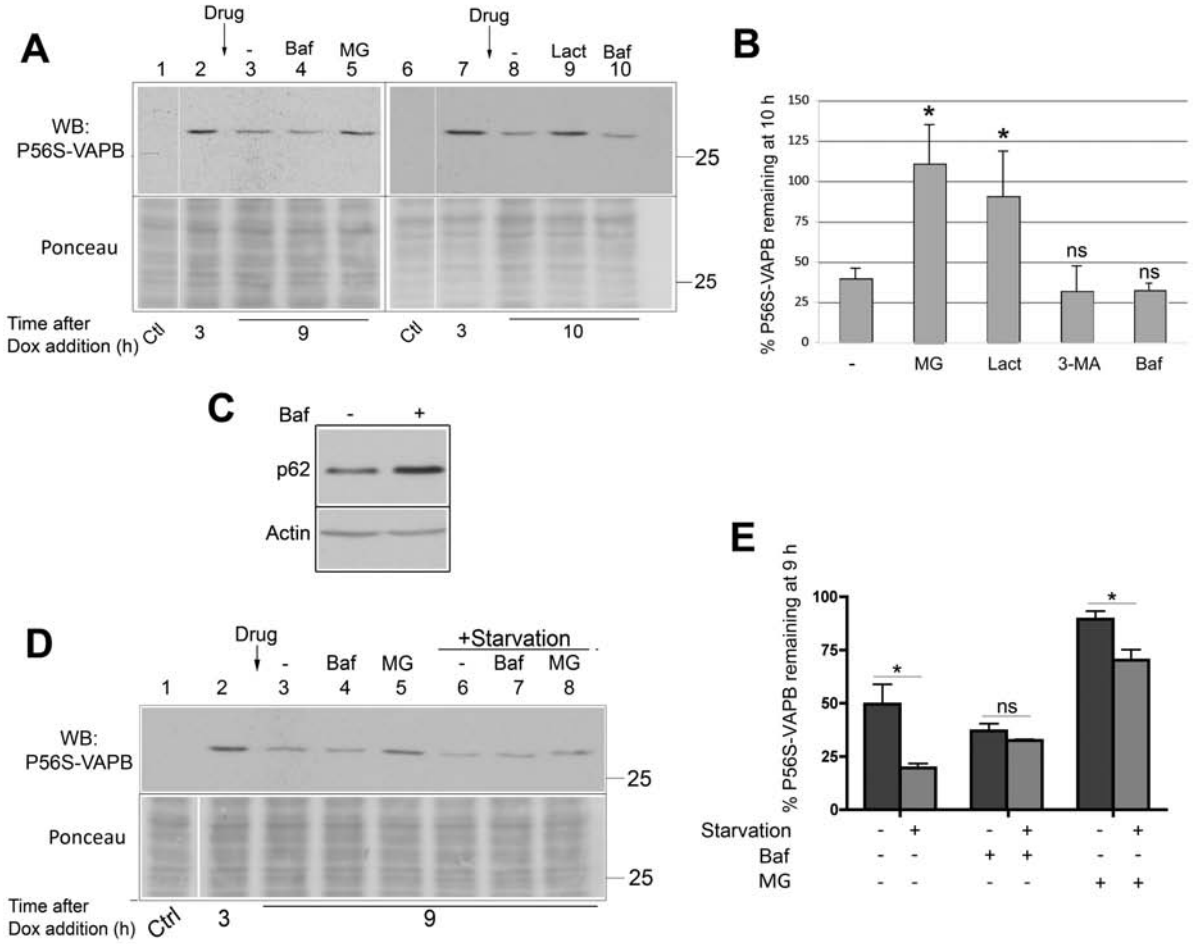

Figure 4.1: P56S-VAPB is degraded by the proteasome and by activated, but not basal, autophagy.
A: Immunoblotting analysis of degradation of P56S-VAPB in the presence or absence of proteasome or autophagy inhibitors. 3 h after the inhibition of transcription of the P56SVAPB transgene by addition of Dox to the media (lanes 2 and 7), cells were either left untreated (lanes 3 and 8), treated with the autophagy inhibitor Bafilomycin (Baf) or with the proteasome inhibitors MG132 (MG) or Lactacystin (Lact) for 6–7 h, as indicated. Control (Ctl) cells were grown in the presence of Dox. Equal aliquots of each sample were loaded (see Methods). The lower panel shows Ponceau staining of the blotted gel region, as loading control. The vertical white line (here and in panel D) juxtaposes lanes deriving from the same blot exposure. The position of the 25 kDa size marker is indicated. B: Quantification (means from 2–5 experiments +SEM) of P56S-VAPB remaining at 10 h after Dox addition in the presence or absence of drugs, as indicated, compared to levels measured at 3 h *: p = 0.013 and 0.025 for MG132 and lactacystin treated samples vs untreated by Student's t test. respectively. The difference between 3-MA or bafilomycin-treated samples and untreated was non-significant (ns). C: Equal amounts of protein of the samples of lanes 3 and 4 of panel A were analyzed for p62 by immunoblotting, to control for inhibition of autophagy by bafilomycin. Actin was probed as loading control. D: Effect of starvation on clearance of P56S-VAPB. 3 h after addition of Dox to the media (lane 2), cells were either left untreated (lane 3), or treated with bafilomycin (Baf) or MG132 (MG), as indicated, for 6 h; the samples of lanes 6–8 were also starved during the incubation with or without the drugs. Control (Ctl) cells were cultured in presence of Dox. Ponceau staining of the blotted region is shown in the lower panel. E: Quantification of three experiments (means +S.E.M.) of P56S-VAPB remaining 9 h after Dox addition under the indicated conditions compared to levels measured before drug treatment and/or starvation at 3 h after Dox addition. *: p = 0.036 by Student's t test; ns, non significant (Genevini et al., 2014).

Failure of autophagy blocking drugs to inhibit P56S degradation could be due to inactivity of these compounds. To evaluate the activity of Bafilomycin, we assessed levels of the autophagy receptor p62/SQSTM1 (to which we refer here as p62). p62 is degraded in autolysosomes and its levels increase under conditions of autophagy inhibition (Klionsky et al., 2012). As shown in Fig. 4.1C, p62 levels were higher in Bafilomycin-treated cells compared to controls, confirming that this drug is effective. The results illustrated in Fig. 4.1A–C confirm and extend our previous results that indicated that under basal conditions P56S-VAPB is degraded exclusively by the proteasomal pathway, and that autophagy is not involved (Papiani et al., 2012).

We then asked whether the inclusions could become substrate for induced autophagy. To this end, we compared the rate of degradation of P56S-VAPB under normal or starvation conditions, a treatment that enhance autophaghy (Fig. 4.1D,E). Starvation was performed by replacing the normal culture medium with the serum and aminoacid-free medium EBSS. This stimulates cells to activate autophagy to degrade proteins in order to obtain new aminoacids. As described previously, we let cells accumulate the mutant protein for six days before adding Dox and analyzing P56S-VAPB levels. Nine hours after Dox addition, the amount of the mutant protein in starved cells were reduced to less than one half those of non-starved cells (Fig. 4.1D and E). Under starvation conditions, the inhibition of P56S-VAPB degradation by MG132 was less effective than under basal conditions, suggesting that the enhanced degradation was due to autophagy. This was confirmed by the observation that Bafilomycin rescued the excess degradation observed in starved cells, so that Bafilomycin-treated starved cells had P56S-VAPB levels similar to non-starved cells.

Thus, whereas degradation of the P56S-VAPB is exclusively by the proteasomal pathway under basal conditions, the mutant protein may become an autophagosomal substrate under conditions that activate autophagy.

4.1.2. Neither proteasome-mediated degradation nor autophagic flux are altered by P56S-VAPB inclusions.

Alterations in proteostasis represent an important mechanism of proteotoxicity of pathogenic aggregates in ALS (Powers et al., 2009). Furthermore, interference with both these mechanisms by P56S-VAPB overexpressing cells has been reported both in *in vitro* and *in vivo* models (Moumen et al., 2011) (Aliaga et al., 2013). We therefore investigated whether induction of the expression of P56S-VAPB inclusions in the HeLa Tet-Off cell line interferes with one or both of these pathways.

To investigate a possible interference with the proteasome, we analyzed the clearance of a substrate of ER associated degradation (ERAD), a pathway involved in the extraction of substrates from the ER, followed by their ubiquitination and delivery to the proteasome (Bernasconi and Molinari, 2011). The substrate we chose to analyze is the CD3 complex δ chain (CD3δ), a subunit of the T-cell receptor.

This protein, when expressed in the absence of the other members of the complex, is recognized by the quality control system of the ER and degraded by ERAD (Yang et al., 1998). HA-tagged CD3δ was co-transfected for 24 hours with soluble EGFP in cells expressing or not P56S-VAPB. Since not all induced cells have detectable P56S-VAPB inclusions, soluble EGFP was used to check by immunofluorescence that inclusion-positive and negative cells were comparably transfected. We quantified the distribution of P56S-VAPB inclusions in transfected and non-transfected cells (Fig. 4.2 C). In two separate experiments, inclusions were detected in 52 and 44% of total cells and in 64 and 47% of EGFP-positive cells (approximately 300 cells from random fields analyzed in each experiment), suggesting that inclusion positive and negative cells are equally transfected. To analyze CD3δ degradation, cells were treated with cycloheximide (CHX) for three hours to block translation and selectively look at the degradation of the target substrate. This treatment did not affect levels of EGFP nor tubulin (Fig. 4.2A), but strongly reduced CD3δ levels (Fig. 4.2A,B). Importantly, after CHX treatment, CD3δ levels were comparable in cells induced or not induced to express P56S-VAPB, suggesting that the mutant protein does not interfere with ERAD.

To investigate autophagosomal flux, we analyzed the behavior of two autophagosome markers (p62 and LC3) after induction of autophagy either by starvation with EBSS (described in the previous section) of by pharmacologically inhibiting mTOR (mammalian Target Of Rapamycin) with Torin1 (Thoreen et al., 2009). mTOR is a kinase involved in cellular metabolism, growth, proliferation and most importantly is a major negative regulator of autophagy, so its inhibition results in a strong activation of this degradative pathway. As mentioned before, endogenous p62 decrease following autophagy stimulation. We measured its levels in cells grown in the absence or presence of Dox and treated with EBSS or Torin1. Levels of remaining p62 are comparable between cells induced or not to express P56S-VAPB with both autophagy-stimulating treatments (Fig. 4.2 D, top). Therefore, induction of P56S-VAPB expression did not interfere with p62 degradation. In similarly treated cells, we examined the generation of the lipidated form of LC3 (LC3-II), a reaction that occurs when LC3 is recruited to nascent autophagosomes (Kabeya et al., 2000). In our HeLa Tet-Off cell line, the lipidated (LC3-II) form predominated already under basal conditions (Fig. 4.2D, lanes 1 and 4); the non-lipidated form (LC3-I) decreased after both Torin 1 treatment and starvation and differences between the ratio of the two forms were not detected between cells grown in the presence or absence of Dox (Fig. 4.2E).

From these experiments we can conclude that presence of moderate levels of P56S-VAPB does not interfere with general proteostasis.

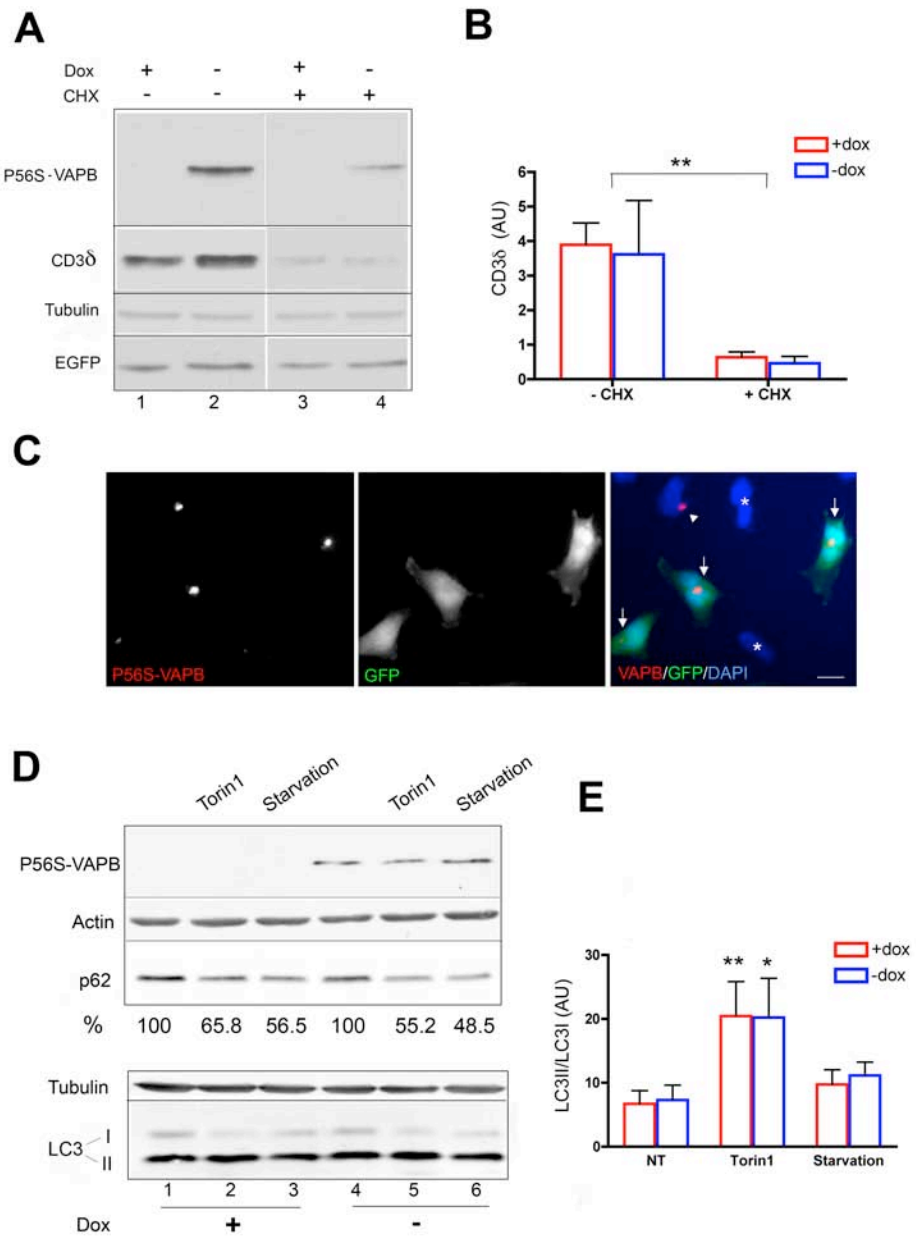

Figure 4.2: Lack of interference of P56S-VAPB inclusions with general proteostasis.
A: Immunoblotting analysis of the degradation of the ERAD substrate CD3δ. Induced or not induced cells, co-transfected with plasmids specifying HA-CD3δ and EGFP, were treated with CHX for 3 h as indicated. Equal amounts of protein (30 mg) were loaded. B: Quantification of three experiments (means+SEM) of CD3d remaining 3 h after CHX addition compared to untreated samples. Values were normalized to EGFP. By two-way Anova, the presence of Dox had no significant effect on CD3δ, while the effect of CHX was very significant ($p = 0.0014$). C: Immunofluorescence analysis of induced P56S-VAPB-Tet-Off cells co-transfected with HACD3d and EGFP. The arrows in the merge panel indicate EGFP positive cells containing P56S-VAPB inclusions, revealed with anti-myc antibodies (left panel). Approximately equal proportions of cells with or without detectable inclusions were transfected (see text). The arrowhead indicates a nontransfected cell positive for P56S-VAPB. Asterisks indicate non-transfected cells negative also for VAPB. Nuclei were stained with DAPI (blue). Scale bar, 10 μm. D: Immunoblotting analysis of the effect of P56S-VAPB inclusions on autophagic flux. Cells expressing or not expressing P56S-VAPB where either left untreated or treated for 3 h with Torin1 or starvation medium (EBSS), as indicated. The levels of p62, as percentage of the values in untreated cells are indicated below the lanes. Values were normalized to actin content. E: Quantification of three experiments (means+SEM) of LC3II/ LC3I ratio of cells treated either with Torin 1 or with starvation medium, in comparison to untreated cells. Two-way Anova analysis reported that the source of variation between samples was due to autophagocytosis induction (non-treated vs Torin 1: p,0.01 and ,0.05 for non-induced and induced cells, respectively) and not to P56S-VAPB expression (Genevini et al., 2014).

4.1.3. In a model motoneuronal cell line, P56S-VAPB inclusions are degraded by the proteasome and not by basal autophagocytosis

The results regarding the degradation of P56S-VAPB were obtained in HeLa cells, but ALS is a pathology that primary affects MNs. Therefore, we wanted to check if MNs are able to degrade the mutant protein like epithelial cells. For this purpose, we created NSC34 cell lines stably expressing wild-type or P56S-VAPB under the tetracycline-repressible promoter. As described in the Material and Methods chapter, these are the best available cell line to study motorneuronal diseases.

As shown in Fig. 4.3A, wt myc-VAPB was distributed throughout the cytoplasm, in a dense reticular network, as expected for an ER protein, whereas the P56S mutant formed inclusions similar to those observed in HeLa cells and in transiently transfected NSC34 cells (Fasana et al., 2010) (Suzuki et al., 2009).

We then investigated the mechanism of degradation of mutant VAPB as done for the HeLa cell line. After inducing cells to express the mutant protein for four days in Dox-free medium, we additionally treated them for twelve hours with Na^+Butyrate to enhance the expression of the transgene. Na^+Butyrate is an inhibitor of histone deacetylases (HDAC) and general enhancer of gene expression (Kruh, 1982). To perform the experiment, medium was replaced with one containing Dox and, as indicated in Fig. 4.3B, drugs that inhibit either the proteasome (MG132) or autophagy (Bafilomycin). As shown in Fig. 4.3B, levels of P56S-VAPB decrease between three and ten hours after exposure to Dox, indicating that this cell line can effectively degrade P56S-VAPB. The degradation of the mutant protein was nearly completely reversed by MG132, while Bafilomycin was without effect. The efficacy of Bafilomycin treatment was confirmed by the increase of p62 content as previously performed for HeLa cells.

We also analyzed the degradation of the mutant protein by immunofluorescence. After Dox addition, we saw a decrease in VAPB-positive aggregates. The inclusions were stabilized by treatment with MG132, but not with Bafilomycin (Fig. 4.3C), in agreement with the results obtained by western blot.

Thus, under basal conditions, P56S-VAPB inclusions in NSC34 cells are cleared by the same proteasome-mediated mechanism as observed in HeLa cells.

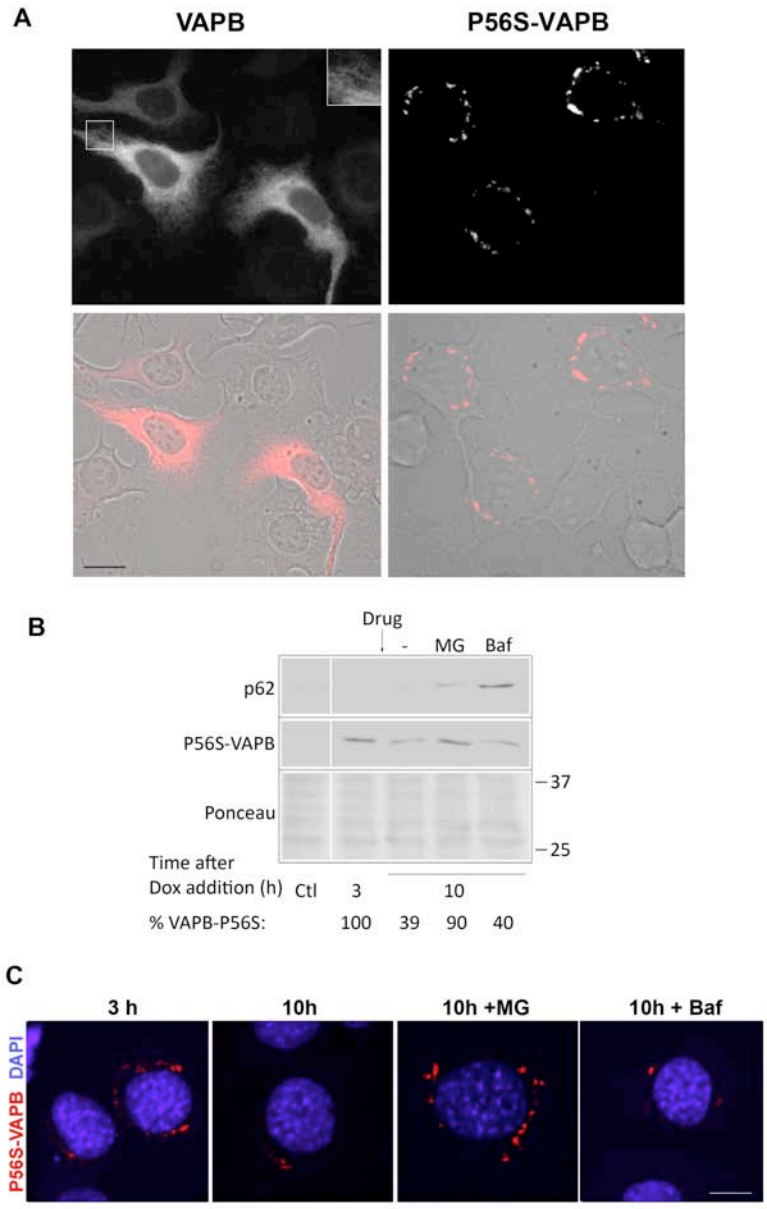

Figure 4.3: P56S-VAPB inclusions in a model motoneuronal cell line are degraded by the proteasome.
A: Immunofluorescence analysis of NSC34 Tet-Off cells induced to express myc-wt-VAPB (left) or myc-P56S-VAPB (right). The upper panel shows anti-myc immunofluorescence, the lower one the superposition of myc staining with phase contrast. The inset of the upper left panel shows a 2 fold enlargement of the boxed area, and illustrates the web-like distribution of wt VAPB typical of an ER protein. Scale bar: 15 µm. B: Degradation of P56S-VAPB stably expressed in NSC34 cells. Induced cells were supplemented with Dox; 3 h thereafter the cells were either left untreated or treated with MG132 (MG) or Bafilomycin (Baf) for 7 h. Control (Ctl) cells were grown in the presence of Dox. Equal aliquots of each sample were loaded. The lower panel shows Ponceau staining of the blotted gel region; the positions of the 25 and 37 kDa size marker are indicated. The vertical white line indicates removal of irrelevant lanes form the image. The levels of P56S-VAPB, as percentage of values in untreated cells at 3 h after Dox addition, are indicated below the lanes. p62 immunoblotting was performed to check the efficacy of bafilomycin to inhibit autophagy (upper). C: Confocal analysis (single sections are shown) of P56S-VAPB inclusions stained with anti-myc antibody (red) at 3 h after Dox addition (left) and 7 h later in the presence or absence of the indicated drugs. Nuclei were stained with DAPI. The number and size of the inclusions decreased in the absence of drugs or in the presence of Bafilomycin, but remained similar to the 3 h cells when MG132 was present. Scale bar, 10 µm (Genevini et al., 2014).

4.1.4. Close relationship between P56S-VAPB inclusions and the Golgi Complex

In most cases P56S-VAPB inclusions are localized close to the nucleus, in a position similar to that of the Golgi apparatus. Since disruption of the Golgi in neurons is a hallmark of many neurodegenerative diseases, including ALS (Gonatas et al., 2006) (van Dis et al., 2014), we wanted to investigate by immunofluorescence the relationship of the inclusions with the Golgi.

For this purpose, we compared the distribution of P56S-VAPB in our HeLa Tet-Off cells with that of two different Golgi markers: GM130 (Golgi Matrix protein of 130 KDa), which is preferentially localized to the *cis* face of the Golgi ribbon, and giantin, which is present on Golgi vesicles. With both stainings, the inclusions appeared to be embedded within the Golgi complex (Fig. 4.4), suggesting a possible interference of the aggregates with Golgi functions.

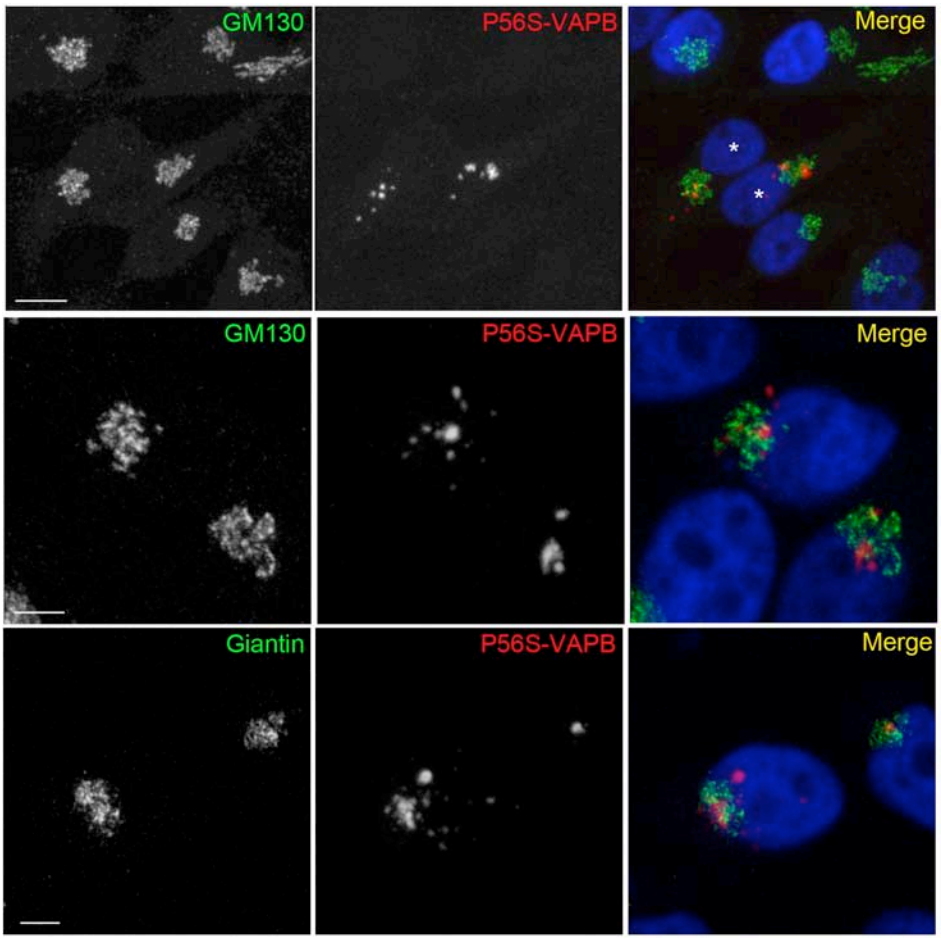

Figure 4.4. Close relationship between P56S-VAPB inclusions and the Golgi Complex.
Induced HeLa Tet-Off cells were doubly immunostained with anti-myc antibodies, to reveal P56S-VAPB, and antibodies against the Golgi proteins GM130 or giantin, as indicated. Nuclei, stained with DAPI, are shown in the merge panel. Shown are maximum intensity projections of z-stacks. Scale bars: upper row, 10 μm; middle and lower row 5 μm (Genevini et al., 2014).

4.1.5. P56S-VAPB inclusions do not interfere with the intracellular transport of Vesicular Stomatitis Virus Glycoprotein (VSVG)

The observation of the previous section suggested that the tight relationship between P56S-VAPB inclusions and the Golgi complex might underlie interference of the aggregates with transport through the secretory pathway, as reported in cells transiently transfected with mutant VAPB (Prosser et al., 2008).

To investigate the functionality of the secretory pathway in cells expressing moderate levels of P56S-VAPB, we allowed HeLa Tet-Off to accumulate the mutant protein (as described in the first section) and then transfected them with cDNA coding for the ts045 version of the secretory membrane protein VSVG coupled to GFP. This is a temperature sensitive transmembrane protein that at 39°C is misfolded and accumulates in the ER. By shifting the temperature to 32°C, VSVG is correctly folded and can travel through the secretory pathway until the plasma membrane. Because of these characteristics, ts045-VSVG-GFP has been widely used to study protein transport (Bergmann, 1989).

We first compared the time course of accumulation in the Golgi of transfected VSVG. After growth for five days in induction medium, cells were transfected placed at 39°C for 24 hours to allow expression and accumulation of VSVG-GFP. Next, they were treated with CHX and placed at 32°C for the time indicated in Fig. 4.5. After processing for immunofluorescence, random cells were imaged and Golgi localization of VSVG was evaluated by superposition on the giantin-positive area of the cells. In the case of the induced sample, we did not consider cells lacking visible inclusions. As shown in Fig. 4.5, VSVG accumulated rapidly in the Golgi, with maximum accumulation at 30 min after release of the temperature block, with similar time course in induced and non-induced cells. At later times, Golgi fluorescence decreased, with concomitant appearance of surface staining. The experiment of Fig. 4.5 indicates that transport of VSVG from the ER to the Golgi is not impaired by the presence of mutant VAPB inclusions.

To quantify transport to the cell surface, I transfected and incubated cells in the same way as in the experiment of Fig. 4.5, but at the indicated time points (Fig. 4.6) the non-permeabilized cells were exposed to an antibody that recognizes the lumenal/extracellular domain of VSVG (see Materials and Methods). Cell surface fluorescence was determined at various times after release of the temperature block. As shown in Fig. 4.6, arrival of VSVG at the cell surface was not delayed in the induced, compared to the non-induced cells, indicating that the intracellular transport of this model glycoprotein is not affected by the presence of P56S-VAPB inclusions in tight association with the Golgi complex.

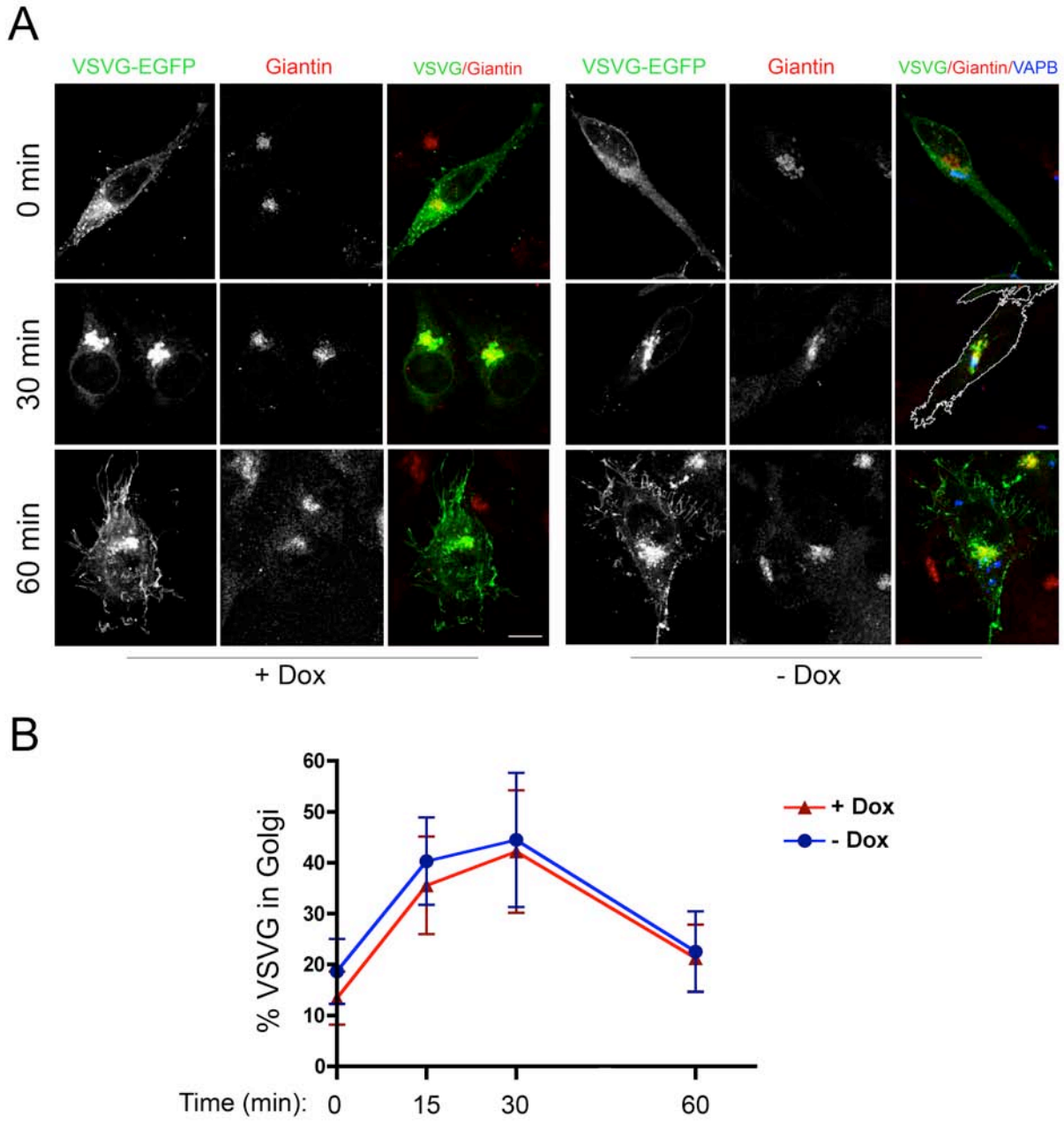

Figure 4.5. Transport of VSVG to the Golgi Complex occurs normally in cells expressing P56S-VAPB inclusions.
A: HeLa-TetOff cells, induced (-Dox, right) or not induced (+Dox, left) to express myc-P56S-VAPB, were transfected with VSVG-GFP at 39.3°C. After 24 h, one coverslip of each sample was fixed (0 min), while the others were shifted to 32°C and fixed after incubation for the indicated times. Cells were stained with anti- Giantin (red) and anti-myc (blue) antibodies. Maximum intensity projections of z-stacks are shown. The cell boundaries at the 30 min time point are indicated by the white line in the merge panel. Acquisition parameters were the same in all images. Scale bar, 10 μm. B: Time course (means ± SD) of VSVG transport through the Golgi. Significant differences between induced or non-induced samples were not detected by Student's t-test (Genevini et al., 2014).

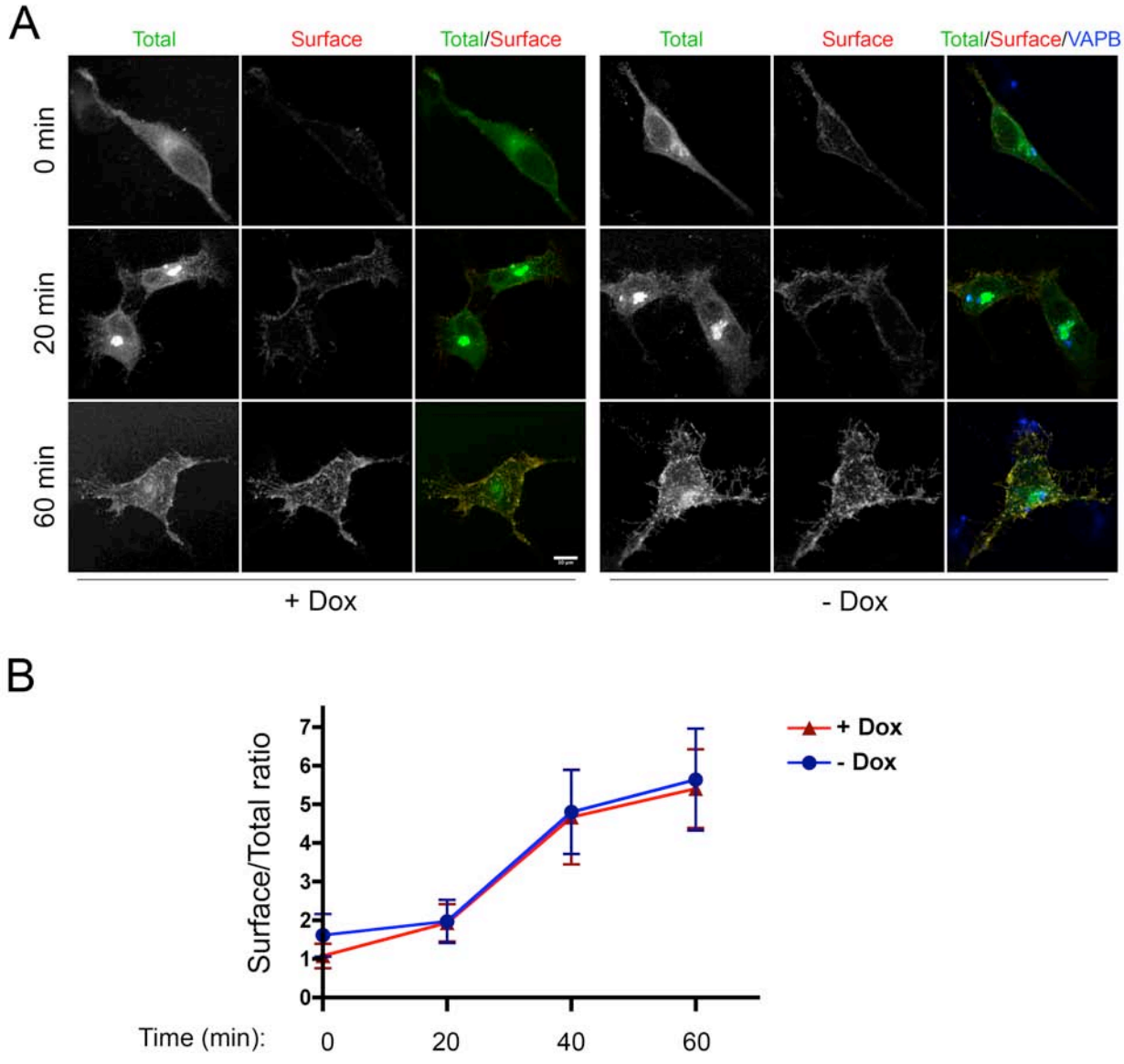

Figure 4.6. Transport of VSVG to the cell surface occurs normally in cells expressing P56S-VAPB inclusions. A: HeLa-TetOff cells, induced (-Dox) or not induced (+Dox) to express myc-P56S-VAPB, were transfected with VSVG-GFP at 39.3°C. After 24 h, cells were shifted to 32°C. At the indicated times, the cells were chilled and incubated with anti-lumenal domain of VSVG under non- permeabilizing conditions (red). The cells were then permeabilized and stained with anti-VAPB antibodies (blue in merge panel - see Methods). Total VSVG (intracellular+surface) was revealed by GFP fluorescence (green). Maximum intensity projections of z-stacks are shown. The acquisition parameters were the same in all images. Scale bar, 10 μm. B: Time course (means ± SD) of VSVG surface labeling normalized to total GFP fluorescence. Significant differences between induced or non-induced samples were not detected by Student's t-test (Genevini et al., 2014).

4.1.6. Summary of the results obtained with cellular models expressing moderate levels of P56S-VAPB.

In this section I described the results obtained with P56S-VAPB expressing cell lines. I confirmed that under basal conditions mutant VAPB is quickly cleared from cells through the proteasome, without any apparent involvement of autophagy. This result was extended also to the motorneuronal cell line NSC34. The situation is different after autophagy stimulation: in these conditions, P56S-VAPB becomes a substrate also for autophagic degradation. We next analyzed whether the presence of mutant P56S-VAPB could interfere with protein degradation pathways, as this is has been suggested as a pathogenic mechanism of ALS. However, we didn't detect any alterations nor in the proteasome nor in autophagy. We next assessed that inclusions are in close relationship with the Golgi apparatus, suggesting a possible negative effect on the secretory pathway. However, we saw no alterations in the transport of the model protein VSVG, suggesting that the presence of moderate levels of P56S-VAPB doesn't alter protein transport.

4.2. Effect of VAPB silencing on the NSC34 motor neuronal cell line.

Most of the results of the previous section were obtained with Hela cells. However, ALS is a pathology that primarily affects motor neurons. Therefore, we decided to continue our work using exclusively NSC34 cells. As already described, NSC34 is a hybrid cell line produced by fusing motorneuronal-enriched spinal cord derived cells with neuroblastoma, thus obtaining an immortalized cell line with motorneuronal characteristics.

As the aim of this work is to dissect the different contribution of mutant VAPB gain and loss of function in the pathogenesis of ALS, we developed stable VAPB-silenced NSC34 cell lines to analyze the effects of VAPB downregulation in a motorneuronal background. First, I will describe our characterization of the differentiation process of NSC34 cells (section 4.2.1), then the generation and characterization of silenced NSC34 cell lines (section 4.2.2), and finally their use in experiments regarding lipid metabolism and neurite extension (section 4.2.3), as VAPB has a role in both these phenomena.

4.2.1. Differentiation of wt NSC34 cells.

Different protocols have been described in literature to allow the differentiation of NSC34 cells into a more motorneuronal phenotype. The common strategy is to reduce serum content in the culture media. A new recent protocol improves this strategy by addition to the culture media of *all-trans* retinoic acid, a drug with known impact on morphology and biochemical differentiation of neuronal precursor cells (Maier et al., 2013). As the aim of this work is to study models of Amyotrophic Lateral Sclerosis, we applied the protocol described by Maier in order to be able work with more motorneuronal-like cells. In this section I will describe the characterization of differentiated NSC34 that we carried out.

(i). Morphological analysis

To perform these experiments, cells were left in differentiating medium (see Materials and Methods) for six days. As can be appreciated by the phase contrast picture (Fig. 4.7A), following differentiation NSC34 extend long neurites, which can exceed 200 μm. By immunofluorescence staining, we observed a redistribution of the synaptic vesicle marker synaptobrevin (Fig. 4.7A and B): in non differentiated (ND) cells, it stains mostly the cell body, while after differentiation (Diff) it is concentrated in the neurite terminals. By higher magnification (4.7B), it could be appreciated that synaptobrevin is distributed throughout the whole cell body in ND, with some perinuclear regions more intensely stained. Instead, in differentiated cells the cell body appears dark and positive staining is observed only in neuritis and growth cones. This could reflect the fact that synaptobrevin is first inserted into the endoplasmic reticulum membrane and then transported through the Golgi apparatus to synaptic-like vesicles (Kutay et al., 1995).

Sphingolipids are essential components of neuronal membranes. For this reason, we analyzed the localization of GM1 gangliosides. To assess their distribution, we labeled cells with fluorescent cholera toxin, a drug that specifically binds GM1 (Fig. 4.8). By fluorescence analysis, we observed a marked difference in the distribution of these lipids in non-differentiated and differentiated cells: in the first case, most of cholera toxin staining is found intracellularly in vesicular structures with only minimal staining on the cell surface. Following differentiation, clear staining of the plasma membrane is observed (Fig. 4.8A).

To better characterize the GM1-positive vesicular compartment, we performed a double staining with cholera toxin and the late endosome-lysosome marker LAMP1 (Lysosome Associated Membrane Protein 1). LAMP1 shows a vesicular localization both in ND and differentiated cells. In some cases, LAMP1 surrounds GM1 vesicles in control cells (Fig. 4.8B). However, following differentiation, LAMP1-vesicles appear smaller and the staining less intense compared to basal conditions and do not follow GM1 redistribution to the plasma membrane. To assess whether GM1 and LAMP1 stain the same compartment in ND cells, we calculated the percentage of GM1 vesicles positive also for LAMP1 by mask analysis (see Material and Methods for details) (Fig. 4.8B and C). We found that approximately 50% of GM1 vesicles are also stained by LAMP1.

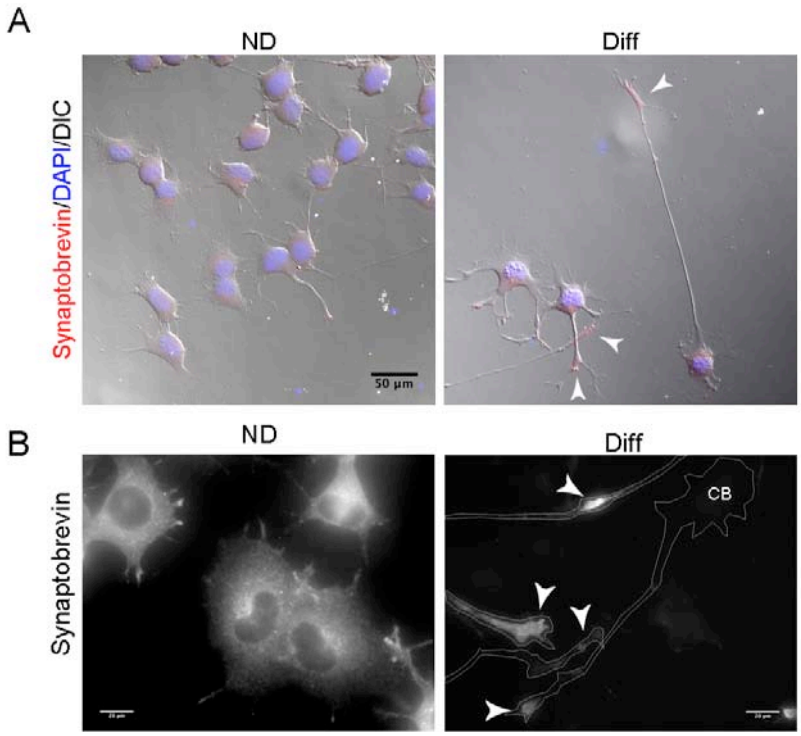

Figure 4.7: Neurite extension and synaptobrevin redistribution following NSC34 differentiation for six days. Panel A shows synaptobrevin immunofluorescence superimposed on DAPI staining (blue) and on the DIC image. The image was acquired with the Zeiss Meta confocal setup. Panel B shows higher magnification wide-field immunofluorescence images, illustrating synaptobrevin redistribution after differentiation. ND: not differentiated; Diff: differentiated. White arrowheads in A and B show synaptobrevin accumulation at neurite terminals. In panel B, cell boundaries are outlined in white in differentiated cells. CB: Cell Body. Scale bars: 50 and 20 µm in A and B, respectively.

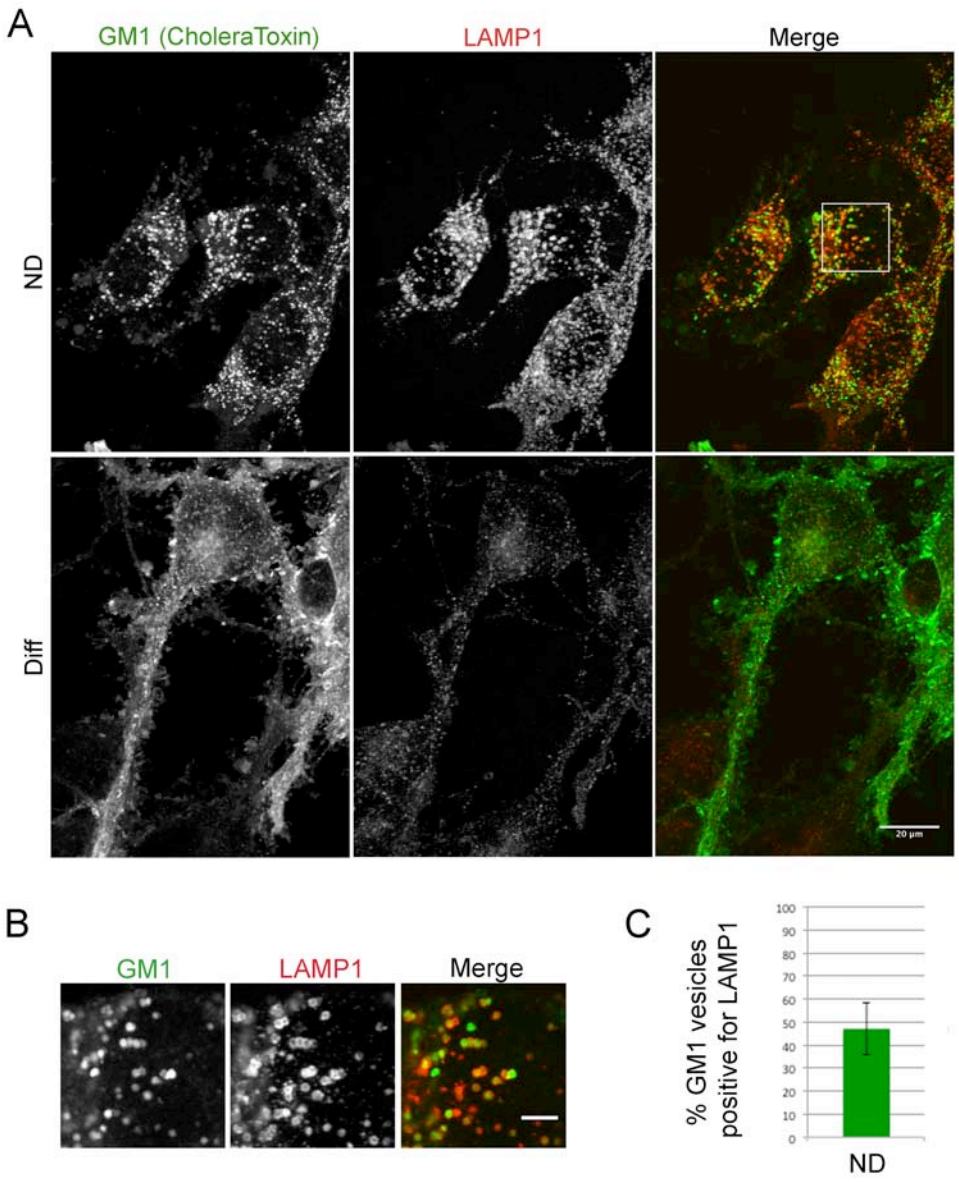

Figure 4.8: Ganglioside GM1 and LAMP1 localization in non-differentiated (ND) and six day differentiated (Diff) NSC34 cells.
A: Representative images of ganglioside GM1 (revealed by fluorescent cholera toxin stainin - green) and LAMP1 (red) in non-differentiated and differentiated cells. Maximun projections of z-stacks are shown. Images were acquired with identical parameters. Scale bar: 20 µm. The boxed area in the ND merge is represented in the enlarged image of panel B. B: single confocal plane (boxed region in panel A) of not differentiated cells stained for ganglioside GM1 (green) and LAMP1 (red). Scale bar: 5 µm. C: quantification with mask analysis of the percentage of GM1 vesicles positive also for LAMP1. Graph shows mean ± SD. 29 cells were analyzed.

(ii). Biochemical analysis

To assess differentiation by biochemistry, we analyzed several neuronal markers by western blot after six days of differentiation. We chose to analyze ChAT (Choline Achetil Transferase) because it is the key enzyme for the synthesis of acetylcholine, the neurotransmitter typical of lower motorneurons, and its increase is specific for motorneuronal differentiation; GAP43 (Growth Associated Protein 43) because it is expressed at high levels in neuronal growth cones during development and axonal regeneration and is therefore considered a general marker of neuronal differentiation; high and low molecular weight neurofilament subunits (NF200 and NF68) as they are intermediate cytoskeletal components typical of neuronal cells and finally the neuronal specific form of Kinesin Heavy Chain (n-KHC).

We observed an increase in GAP43 and in ChAT (Fig. 4.9A and B), but, unexpectedly, we saw a reproducible ~ 50% decrease in NF200 and NF68 levels and in n-KHC (Fig. 4.9C and D).

As the focus of this work is to study VAPB in a motorneuronal disease, we next analyzed the expression of both VAP isoforms following differentiation (Fig. 4.10). Interestingly, both VAPA and VAPB are upregulated. The increase in VAPB levels is higher than that of VAPA: indeed, we observed a 50% increase in VAPA (Fig. 4.10B) and a statistically significant ($p= 0.014$) doubling in VAPB levels (Fig. 4.10D).

(iii). Summary of the results on NSC34 differentiation with retinoic acid

In this section I analyzed the differentiation of NSC34 cells with the method described by Maier. Probably the most striking feature of NSC34 differentiation is the extension of long neurites, but other changes occur as well. By immunofluorescence we showed the redistribution of synaptobrevin, gangliosides GM1 and LAMP1. Moreover, we saw a change in the levels of several neuronal markers, which do not always behave as expected: indeed, while GAP43 and ChAT increase as expected, NF200, NF68 and nKHC decrease. Interestingly, VAPA and B levels also increase following differentiation.

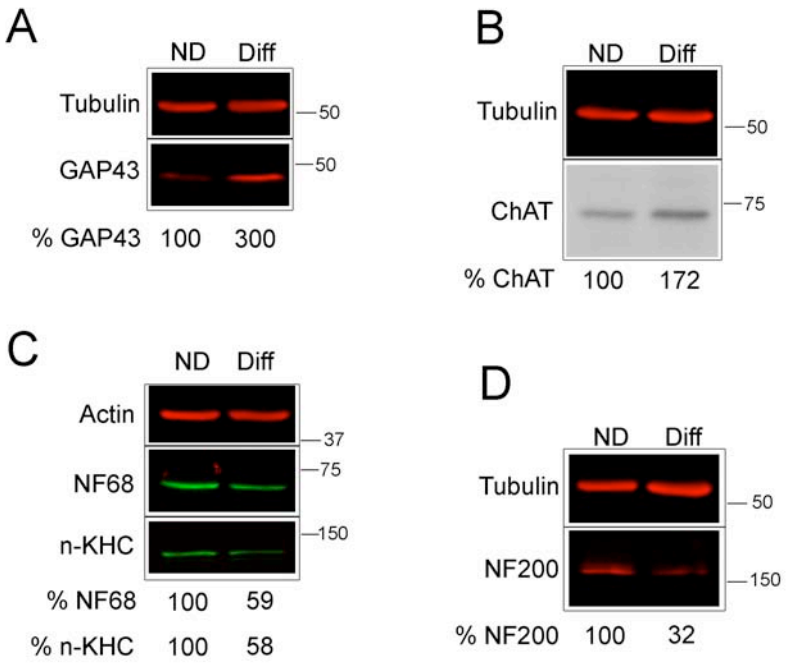

Figure 4.9: Immunoblotting analysis of the indicated neuronal markers in non-differentiated (ND) and six day differentiated (Diff) NSC34 cells.
Except for ChAT, which was revealed by ECL, all blots were acquired with the LiCor Odessey apparatus. Equal amounts of protein (25 μg) were loaded in each lane. The levels of each marker after differentiation, as percentage of the values in non-differentiated cells, are indicated below the lanes. All values were normalized to tubulin or actin, used as loading controls.

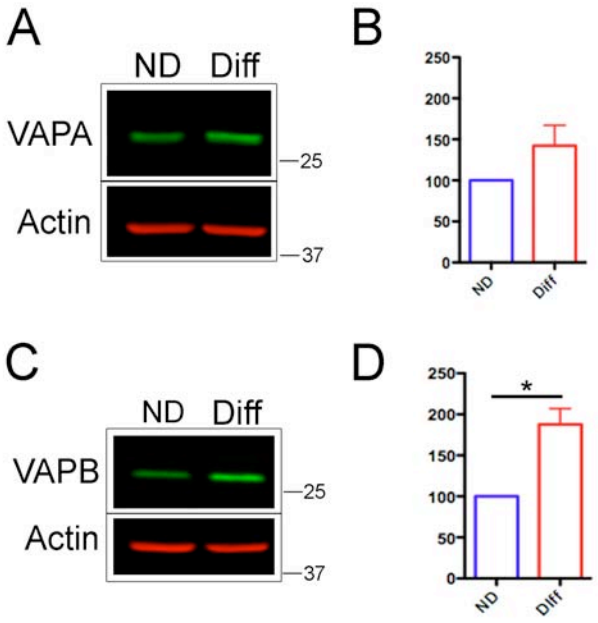

Figure 4.10: VAP protein levels increase following differentiation of NSC34 cells.
Equal amounts of protein (25 μg) deriving from non-differentiated (ND) or six day-differentiated (Diff) cells were loaded in each lane, and analyzed for VAPA (panel A) or VAPB (panel C). The graphs in panels B and D shows means + SEM from two and four independent experiments for VAPA and B, respectively . * p = 0.014

4.2.2. Generation and characterization of VAPB silenced NSC34 clones

(i). Establishment of VAPB-silenced clones

For the establishment of stable silenced VAPB cell lines we decided to use the pSUPER.neo.GFP plasmid, that enables the production of an shRNA which is processed into a mature and active siRNA. Downregulation efficiency and target specificity are essential characteristics of siRNAs to be considered when planning a silencing experiment. For this reason, before producing pSUPER.neo.GFP plasmids, we transiently silenced NSC34 with different siRNAs (Fig. 4.11). We used a mixture of 3 siRNAs (see Materials and Methods for sequences) from Invitrogen that together have a high silencing power. In parallel, we tested each siRNA by itself. All three siRNA were able to downregulate VAPB when compared to the sample treated with a scrambled oligonucleotide duplex. However, siRNA 2 had the poorest downregulating efficiency and was therefore excluded from the following steps. To check specificity of the siRNA, we assessed levels of VAPA, which were unaffected in all conditions.

We cloned siRNA 1 and siRNA 3 into pSUPER.neo.GFP vectors and stabily transfected them in NSC34. Unfortunately, no positive clones were obtained from pSUPER.neo.GFP(siRNA1) transfected cells (data not shown).

From pSUPER.neo.GFP(siRNA3) transfected cells we obtained two positive clones: #1 and #6 (termed shRNA-VAPB clones). As control, we transfected cells with pSUPER.neo.GFP empty vector (termed vector-only clones) and obtained three clones: #11, #14 and #16 (Fig. 4.12). Clone #14 showed slow growth and was therefore excluded from further experiments.

Our two shRNA-VAPB clones showed different levels of downregulation: specifically, #1 and #6 had VAPB levels reduced by ~90 and ~50% respectively. Thus, the #6 clone could be considered a model for haploinsufficiency, and we continued our experiments with both the lines.

As observed in the experiments performed with siRNAs, VAPA levels were unaffected by VAPB silencing (Fig. 4.12A). pSUPER.neo.GFP plasmid codes also for a soluble GFP, whose expression was present in all stable clones as assessed both by biochemical and immunofluorescence analysis . However, GFP levels were not homogeneous when comparing different clones: #1 and #11 had higher GFP expression compared to #6 and #16. Of note, VAPB silencing and GFP expression seemed to correlate: #1 had strong VAPB downregulation and high GFP expression, while #6 mild VAPB downregulation and low GFP expression. This could indicate that in #1 more plasmid copies were stably inserted or that the insertion involved a more actively transcribed site in the chromatin. As indicated by immunofluorescence analysis, clones were homogeneous as more than 90% of the cells express GFP (Fig. 4.12B).

Downregulation of VAPB in clones #1 and #6 was stable over time: reduced levels of VAPB are observed after several weeks in culture (data not shown).

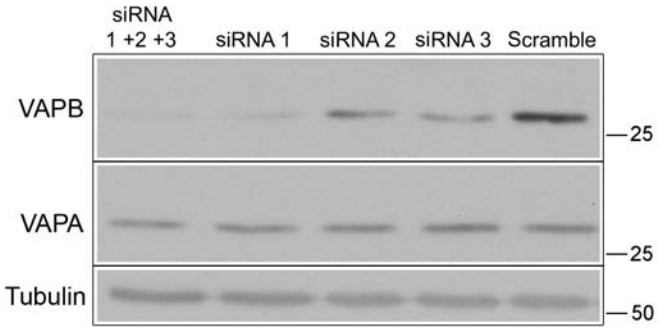

Figure 4.11: transient VAPB silencing in NSC34 cells.
Immunoblotting analysis of NSC34 lysates following 48h transient siRNA silencing. Cells were treated with a mix of 3 VAPB-targeting siRNA, with each one individually or with a control duplex oligonucleotide (scramble), as indicated. VAPB and VAPA levels were assessed by immunoblotting. Tubulin was used as loading control. Equal amounts (25 μg) of proteins were loaded.

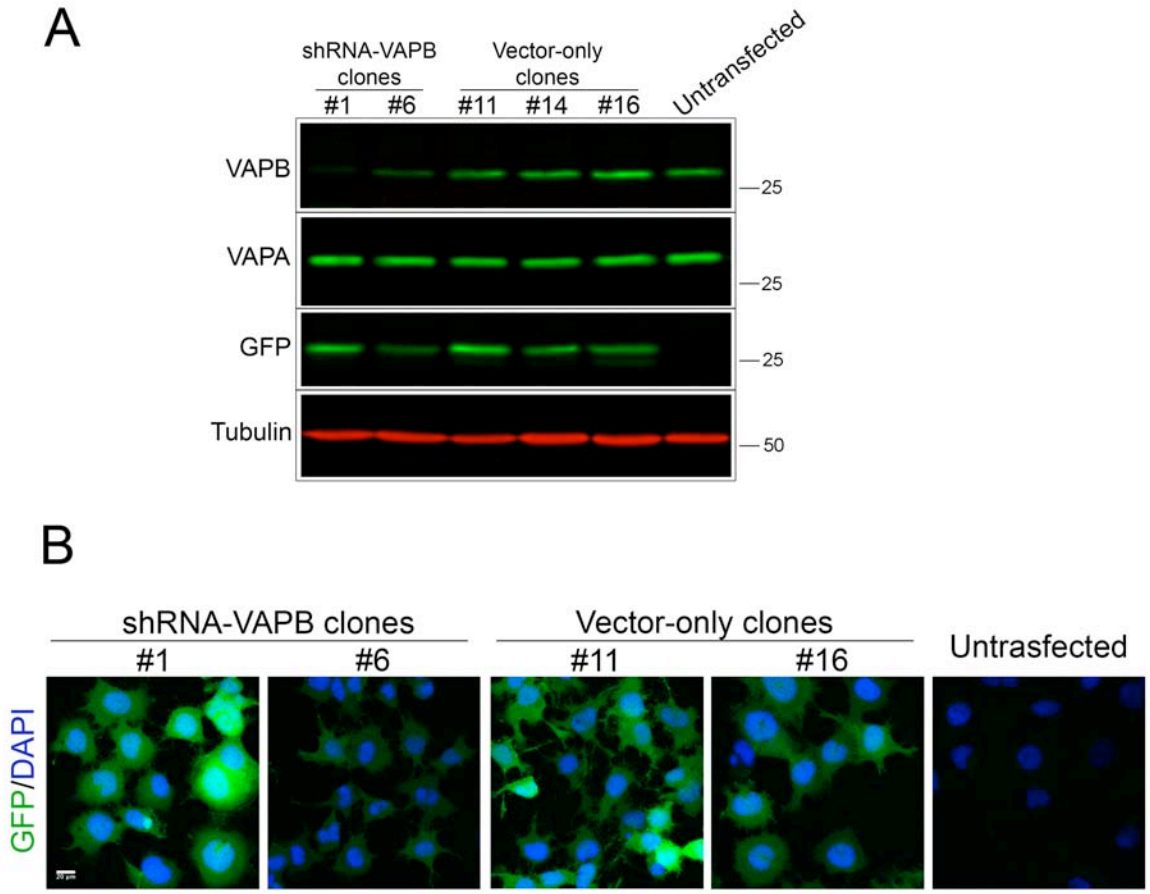

Figure 4.12: establishment of stable VAPB-downregulated NSC34 cell lines.
A: immunoblotting analysis of lysates from positive NSC34-clones. shRNA-VAPB clones were obtained after stable transfection with pSUPER.neo.GFP encoding a VAPB targeting shRNA; vector-only clones were obtained after stable transfection with empty pSUPER.neo.GFP; untrasfected cells were included to show specificity of GFP staining. Equal amounts (25 μg) of proteins were loaded in each lane. B: immunofluorescence staining of soluble GFP expressed by stable clones transfected with pSUPER.neo.GFP vectors. Untransfected cells were included to show specificity of the staining. Nuclei were counterstained with DAPI. Images were acquired with identical parameters. Scale bar: 20 μm.

(ii). Differentiation of VAPB-silenced NSC34

Since we observed an increase in VAPB expression following differentiation with retinoic acid (Section 4.2.1, Fig. 3.10), we sought to understand whether the downregulation of VAPB could alter NSC34 differentiation. To perform this experiment, all stable clones were treated with differentiating medium for six days and next subjected to immunofluorescence or western blot analysis.

From phase contrast images we saw that both VAPB-silenced and control clones extended long neurites (Fig. 4.13), suggesting that no major defects in NSC34 differentiation were present following VAPB downregulation (however, see the section on neurite extension below).

We next analyzed different neuronal markers by western blot. As observed in the previous section, some neuronal markers increase following differentiation, while others unexpectedly decrease. ChAT levels increased in all clones with the exception of the control #16 (Fig. 4.14B). Levels of GAP43 were also higher, even thought basal (non differentiated) expression vary among different clones (Fig. 4.14C). In line with our previous observations, all clones showed a decrease in neurofilaments NF200 and NF68 (Fig. 4.14B and C). Finally we analyzed VAPB levels (Fig. 4.14A). As expected, in both downregulated clones VAPB expression didn't increase. The control clone #16 showed an increase in VAPB expression as previously observed in non transfected cells. Strangely, VAPB levels in clone #11 were stable.

Taken together, these results indicate that VAPB downregulation has no appreciable effect on the alterations of the levels of the analyzed neuronal markers occurring during differentiation.

4.2.3. Effect of VAPB silencing on PI4P, on ceramide transport and on neurite extension of NSC34 cells

(i) Analysis of PI4P levels in Golgi

As summarized in the Introduction, an important function of VAPB is its involvement in lipid transport at membrane contact sites between the ER and the Golgi. VAPs are responsible for the ER-docking of lipid transfer proteins (LTP), which can also associate with the Golgi by binding the phosphoinositide PI4P. Therefore, PI4P and the VAPs work in concert to ensure correct localization of different LTPs. PI4P levels on the Golgi are precisely regulated by the LTP themselves: OSBP, a VAP-binding protein, back-transfers PI4P to the ER where is quickly converted to PI by the phosphatase Sac1, whose function is stimulated by VAP. Alterations in LTP localization and Sac1 activity following VAP depletion might thus cause altered levels of PI4P.

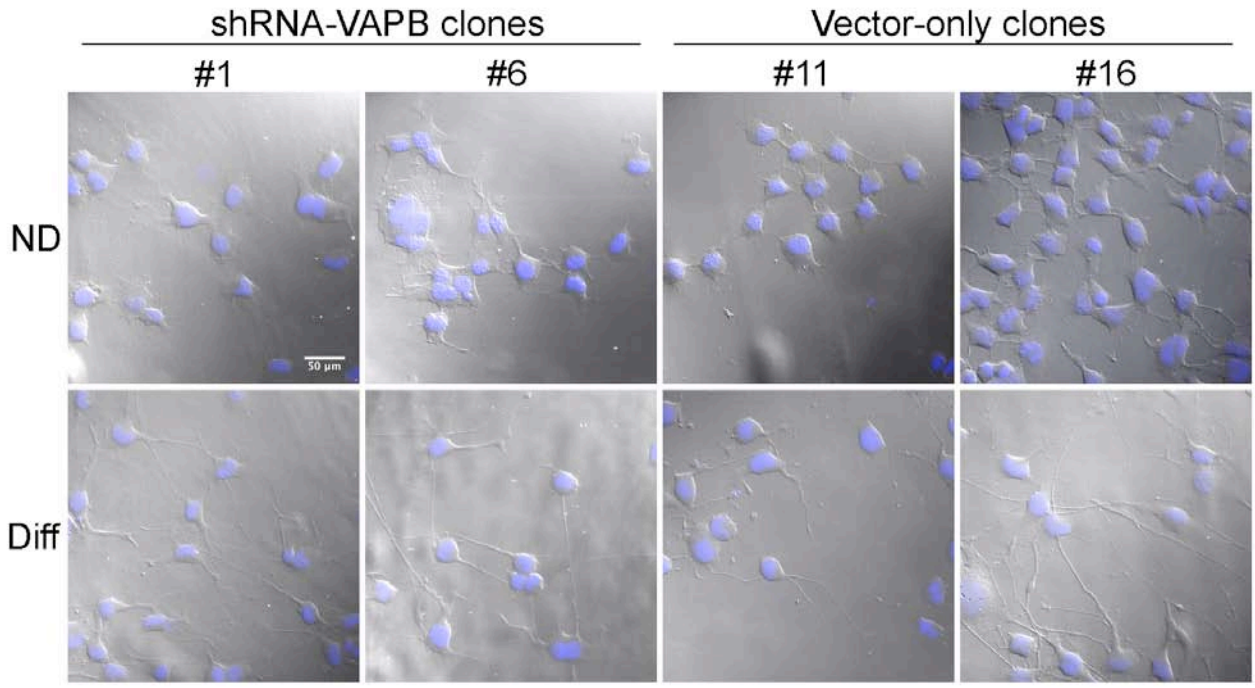

Figure 4.13: shRNA-VAPB clones extend neurites following differentiation.
Cells were differentiated for 6 days (Diff) or maintained in normal growth medium (ND) before fixing and staining. The phase contrast image shows whole cell morphology while DAPI counterstains nuclei. Scale bar: 50 µm.

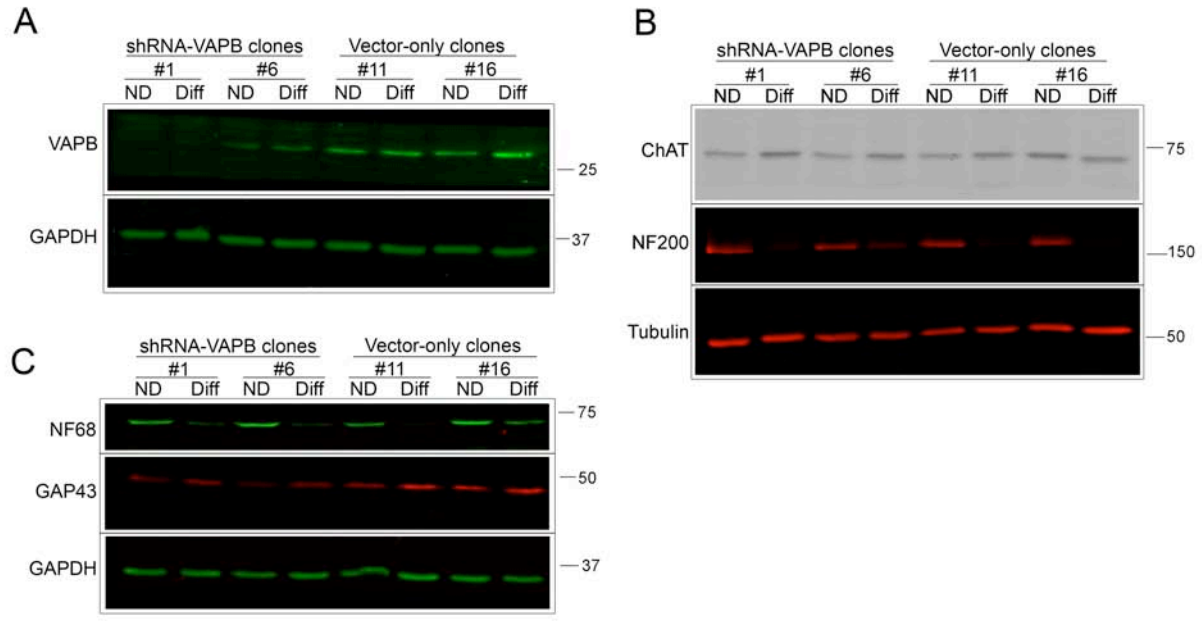

Figure 4.14: Immunoblotting analysis of shRNA-VAPB clone differentiation.
Cells were differentiated for 6 days (Diff) or maintained in normal growth medium (ND) before collection and lysis. Equal amounts (25 µg) of proteins were loaded for analysis of VAPB (A), ChAT and NF200 (B), NF68 and GAP43 (C). GAPDH or tubulin were used as loading controls.

To assess this possibility, we analyzed PI4P content in the Golgi apparatus by immunofluorescence using a protocol that specifically maintains Golgi lipid composition (see Materials and Methods). As can be observed in Fig 4.16, we saw an increase in PI4P in the shRNA-clone #1, which has a strong VAPB downregulation. Instead, shRNA-clone #6, where VAPB is only mildly downregulated, behaved similarly to the control clones. The increase in PI4P content was already present in not differentiated cells and was maintained after differentiation (Fig. 4.15A).

We can conclude that strong, but not mild, VAPB downregulation can affect PI4P levels in the Golgi apparatus.

(ii). Analysis of ceramide transport

Ceramide is synthetized in the ER but needs to be transported to the Golgi to be metabolized into complex sphingolipids. Two pathways exist for ceramide transport: a vesicular, CERT-independent and a CERT-dependent pathway. CERT is a LTP that needs binding to VAPs and PI4P to correctly localize at ER-Golgi membrane contact sites to perform its task.

To understand whether VAPB downregulation might alter ceramide flux to the Golgi, we performed analysis of ceramide transport by looking at localization of the fluorescent ceramide analogue Bodipy-FL-Ceramide (Toth et al., 2006). This molecule exhibits fluorescence in the 488 channel, so we first checked if this signal was covered by the soluble GFP expressed by stable clones. Fortunately, we found that the GFP signal is extremely weak compared to that of Bodipy-FL-Ceramide (Fig. 4.16C): in samples that did not received ceramide, the GFP fluorescence could not be appreciated when images were acquired with the same parameters used for ceramide-treated cells. The weak GFP signal could be seen only after digital enhancement of the 488 channel.

Uptake of Bodipy-FL-Ceramide was performed on ice, in order to allow its accumulation in the ER and prevent its transport. Indeed, at the end of the incubation on ice the fluorescence signal was discernable on the ER and on the plasma membrane, the latter presumably due to Bodipy-FL-Ceramide bound to the cell surface before penetration into the cytosol. After a short ten min incubation at 37°C, Bodipy-FL-Ceramide accumulated in the Golgi (Fig. 4.16A).

To perform the experiment, we first differentiated cells for six days and then compared one shRNA-VAPB with one control clone. We chose to analyze clone #1 as it has a strong VAPB downregulation and was therefore more likely to reveal a defect. As readout, we assessed the percentage of cells with visible ceramide accumulation in the Golgi region. VAPB-downregulated and control cells showed the same percentage of ceramide accumulation in the Golgi (Fig 4.16B).

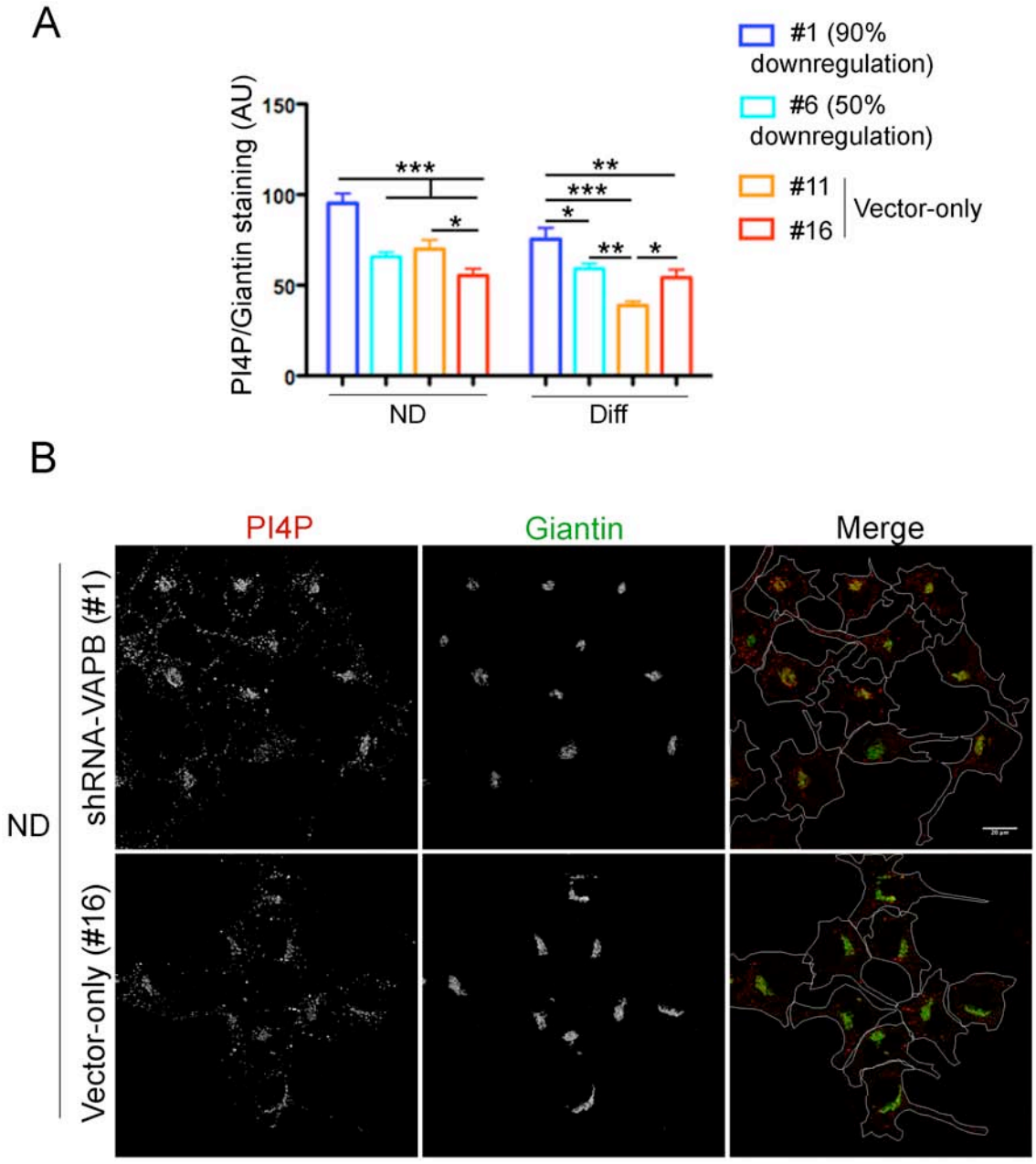

Figure 4.15: PI4P accumulates in the Golgi apparatus of VAPB- silenced cells.
A: quantification of PI4P staining normalized to giantin in Golgi apparatus in shRNA-VAPB and vector-only clones. ND: not differentiated; Diff: differentiated. Cells were differentiated for 6 days before fixing and staining. Non-differentiated cells were maintained in normal growth media. For each sample, 35-50 cells were analyzed. Graph shows mean ± SEM. * p<0,05; ** p<0,01; *** p<0,001 by two way ANOVA (Graphpad Prism) B: representative images of clone #1 and #16 stained with PI4P (red) and giantin (green). Maximum intensity projections of z-stacks are shown. Cell boundaries are outlined in white in the merge image. Scale bar: 20 μm.

We can therefore conclude that with this methodology we could not detect any alterations in ceramide transport in VAPB-downregulated cells. A potential CERT-defect may be masked by the vesicular transport of ceramide, as the two pathways could not be distinguished by this technique.

(iii). Analysis of neurite extensions

VAP proteins are involved in the extension of neurites thanks to their binding to protrudin (see Introduction). As illustrated in Section 4.2.2, we assessed that VAPB-downregulated clones extend long neurites following differentiation with retinoic acid for six days (Fig. 4.13), indicating that VAPB silencing does not completely prevent neutite extension. However, we wanted to perform a more precise analysis to check the presence of subtle defects that could not be appreciated by a qualitative experiment.

To this end, we quantitatively analyzed neurite length in shRNA-VAPB, vector-only clones and untransfected cells. We chose to differentiate them both for six and three days, in order to analyze also an intermediate time point. We performed the immunofluorescence analysis by staining cells for tubulin, which allowed a clear visualization of both cell body and neurites. As readout, we assessed the percentage of cells with at least one neurite longer than 100 μm. As can be observed in Fig. 4.17, both shRNA-VAPB clones had a lower percentage of cells with neurites longer than 100 μm and this situation was present both at three and six days of differentiation.

This experiment shows that both mild and strong VAPB downregulation cause a reduction in neurite extension during NSC34 differentiation.

4.2.4 Summary of the results regarding VAPB-downregulated NSC34

In this chapter I analyzed the results obtained with VAPB-downregulated NSC34. After first describing the generation of such cells, I checked that they can be differentiated following retinoic acid treatment and next used them for experiments regarding lipid transport and neurite extension. Regarding lipid transport, I assessed that 90% VAPB downregulation increased the amount of the phosphoinositide PI4P in the Golgi, but it apparently did not alter the transport of ceramide from the ER to the Golgi. Finally, we obtained very interesting results regarding neurite extension, where both mild and strong VAPB downregulation were able to reduce the development of protrusions.

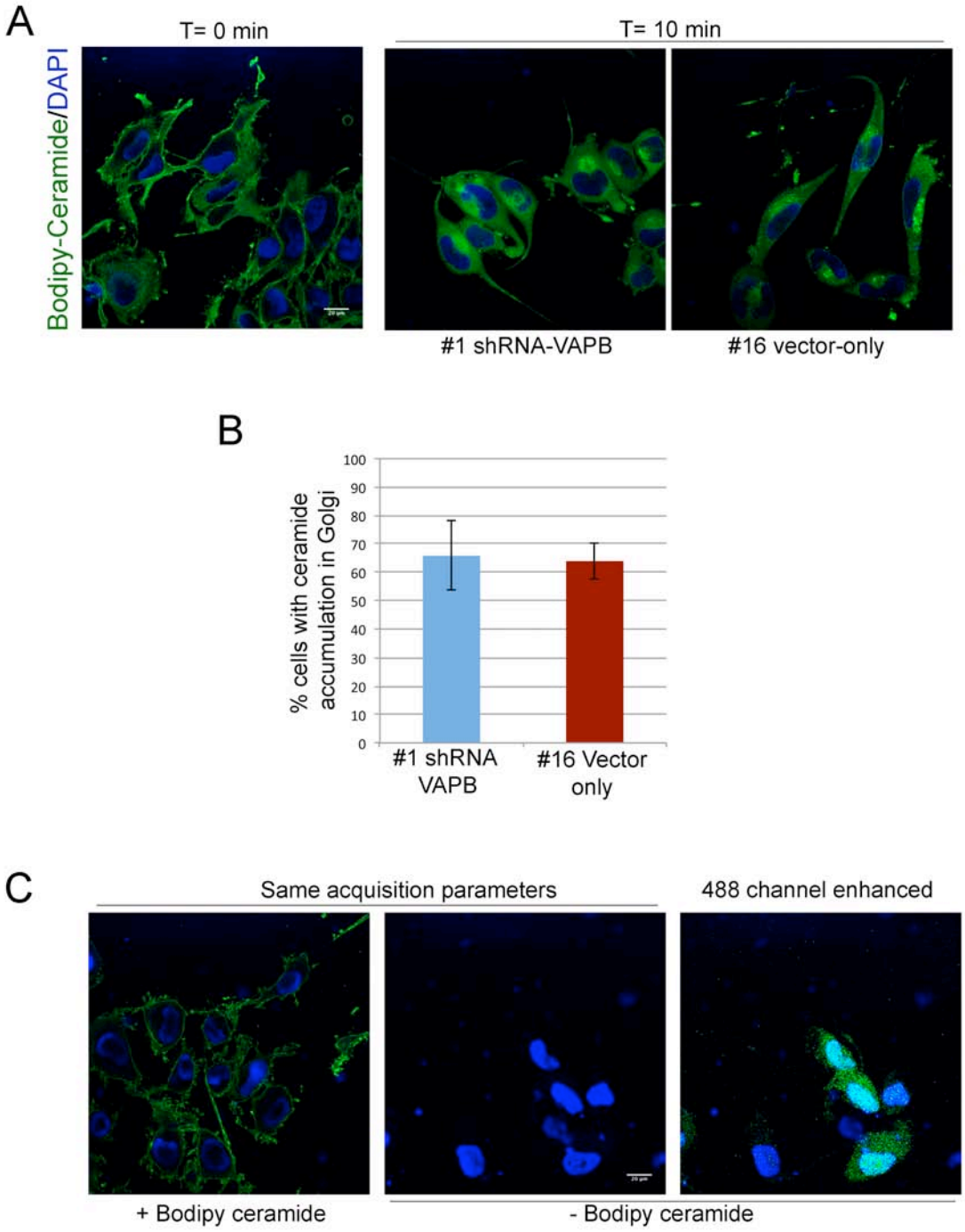

Figure 4.16: ceramide transport is not delayed in a shRNA-VAPB clone.
Analysis of Bodipy-Ceramide transport performed with shRNA-VAPB clone #1 and vector-only clone #16. A: representative immunofluorescence images of ceramide transport. After loading with Bodipy-ceramide, cells where either fixed immediately (time=0) or after a 10 minute incubation to allow ceramide trafficking. Cells are stained with Bodipy-Ceramide (green) and DAPI (blue). Scale bar: 20 µm. B: quantification of the percentage of cells with visible ceramide accumulation in the Golgi. Graph shows mean ± SD from three independent experiments. Approximately 120-150 cells were counted for each condition. No significant difference was obtained following Student's t Test (Excel). C: immunofluorescence analysis of the 488 channel of cells treated or untreated with Bodipy-Ceramide. Middle and right panel show the same field of untreated cells (the right one was digitally enhanced to show GFP staining). Scale bar: 20 µm.

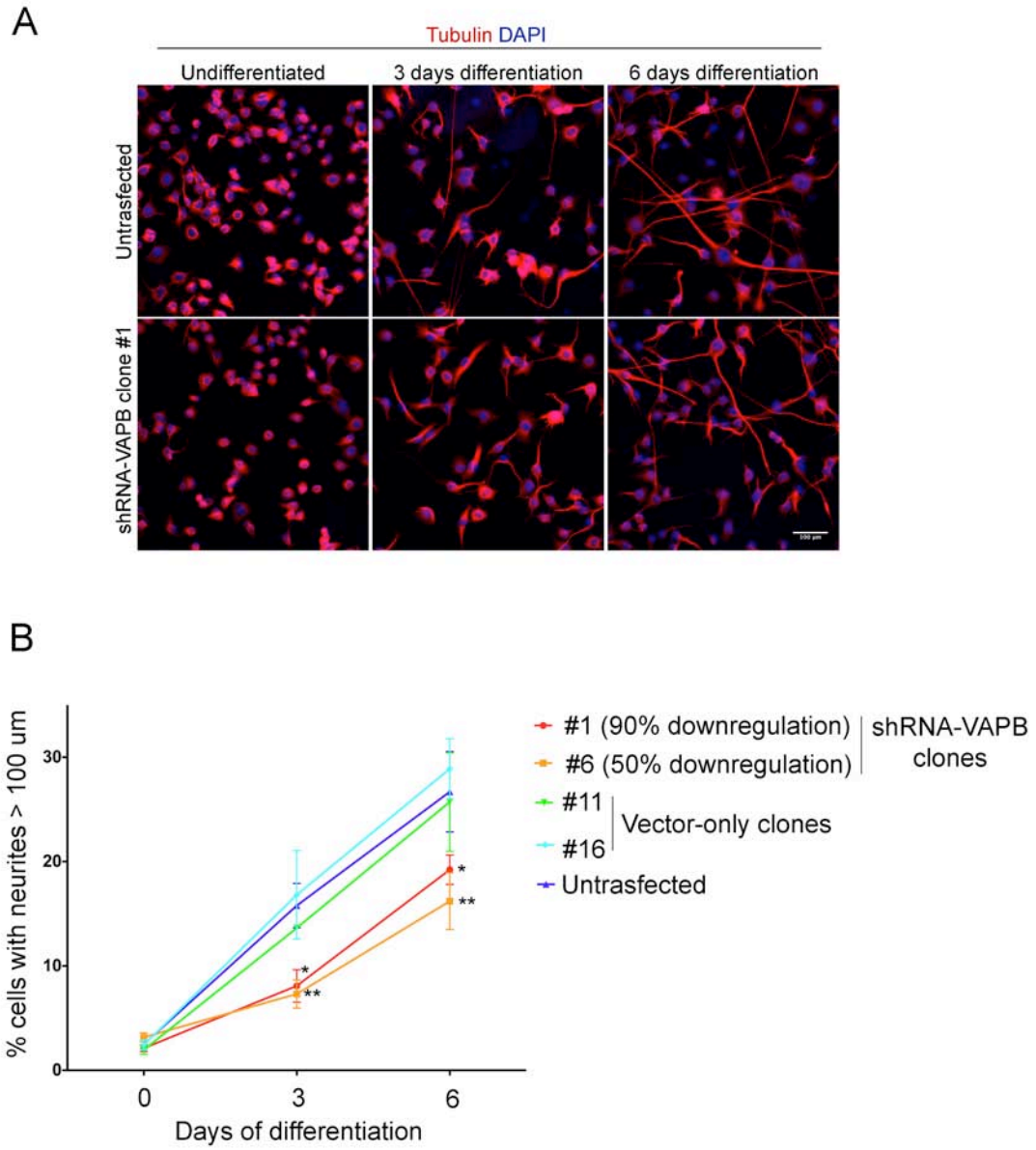

Figure 4.17: VAPB-downregulated clones show reduced neurite extension.
A: representative immunofluorescence images of untransfected and shRNA-VAPB clone #1 cells in basal conditions and after three and six days of differentiation. Cells were stained with tubulin (red) and DAPI (blue). Scale bar: 100 µm. B: quantification of the percentage of cells with a least one neurite longer than 100 µm. Graph shows mean ± SEM from three independent experiments. For each condition, 5-7 images, comprising approximately 250-350 cells, were acquired at low magnification (10x objective) and the cells were manually classified according to neurite length. * p<0,05; ** p<0,01 obtained using two-way ANOVA (Graphpad Prism).

5. Discussion

Among the identified ALS-linked genes, the one coding for *VAPB* is rare. However, the observation that VAPB levels are decreased in sporadic ALS patients and in mutant SOD1 transgenic mice is consistent with a more general role of the VAPs in motor neuron pathophysiology (Anagnostou et al., 2010) (Teuling et al., 2007). Thus, the clarification of the cellular effects of the mutant gene could bring important insights into the molecular pathogenesis of ALS.

The published studies with cell and animal models that have addressed the pathogenic mechanism of mutant VAPB have suggested that various mechanisms may be at play, but have left many questions unanswered. Notably, it has not been clear whether the loss of one wt VAPB allele is in itself sufficient to cause motorneuronal degeneration (haploinsufficiency effect), or whether the expression of the mutant protein is required for pathogenesis. In my thesis, I have addressed this problem by using two complementary cell models: HeLa and NSC34 cell lines expressing P56S-VAPB at moderate levels, and NSC34 cells strongly or partially silenced for VAPB expression. I discuss these two parts of my thesis in separate sections.

5.1. Lack of effect of P56S-VAPB expression on proteostasis and protein transport.

As explained in the Introduction, the expression of P56S-VAPB from one allele could be pathogenic (and thereby transmitted by dominant inheritance) by two different mechanisms: a toxic gain of function or a dominant negative mechanism, by which wt VAPB, VAPA and/or other interacting partners would be sequestered into inclusions by mutant VAPB. Regardless of the mechanism, the question is whether expression of the mutant protein is or is not a necessary ingredient of P56S-VAPB-linked fALS. The results on this question have been so far contradictory, depending on whether cellular or animal model studies are considered.

A number of cellular studies have demonstrated sequestration of the VAPs and of other interacting proteins into P56S-VAPB aggregates (Teuling et al., 2007), with consequent interference in fundamental processes, such as intracellular transport (Prosser et al., 2008), as well as a general interference in proteostasis (Moumen et al., 2011). On the other hand, transgenic mouse models on a wt VAPB genetic background have failed to recapitulate the human disease (see the Introduction for a more detailed description of the mouse models). There are two possible explanations for the discrepancy between the cell and mouse studies: (i) in the cell studies P56S-VAPB was heavily overexpressed, so that the observed effects would not be relevant to cells in which the mutant protein is the product of a single allele; or (ii) the mouse, possibly because of its short life span, cannot provide a suitable model for ALS8,

implying that P56S-VAPB expression *is* harmful to motor neurons, but that the mouse doesn't give us the time to appreciate the incurred damage.

To re-investigate the effects of P56S-VAPB when expressed chronically at moderate levels, we turned to cell lines expressing mutant VAPB under the control of a Tet-repressible promoter. In Doxycycline-free medium, these cells express P56S-VAPB at levels only 2-3 fold higher than the endogenous protein (Fasana et al., 2010) (Papiani et al., 2012) and reach this steady state condition gradually over a period of several days after removal of the antibiotic from the medium. Using these cells, my laboratory previously demonstrated that P56S-VAPB is unstable in comparison to the wt protein, and that its degradation is mediated by the proteasome and involves the participation of a key ERAD player, the AAA ATPase p97 (Papiani et al., 2012). In the first part of my thesis research, I continued the investigation on the mechanism of degradation of P56S-VAPB inclusions as well as on their possible toxic effects on the cells.

First, I confirmed that under basal conditions mutant VAPB inclusions are cleared by the proteasome, both in HeLa and in the model motoneuronal NSC34 cell line; in addition, I showed that autophagy, when stimulated, can further enhance degradation of the mutant protein. Thus, the inclusions can be degraded by both major degradative pathways of the cell; these results predict that, under conditions in which the cell potentiates autophagy, mutant VAPB inclusions will not become overrepresented in comparison to other compartments targeted by autophagy.

I next investigated whether P56S-VAPB inclusions interfere with two fundamental processes: (i) protein degradation mediated by the proteasome and by autophagy; and (ii) protein transport through the secretory pathway.

Moumen reported that transient overexpression of either wild-type or mutant VAPB results in an increase of polyubiquitinated proteins and stabilization of three different proteasomal substrates, among which the classical ERAD substrate CD3δ (Moumen et al., 2011). However, in HeLa Tet-Off cells, clearance of CD3δ, whose degradative pathway shares with the one of P56S-VAPB the involvement both of the proteasome and of p97, was unaffected by the expression of the mutant protein.

Autophagic dysfunction has been described in ALS, and is currently thought to be a major player in ALS pathogenesis (reviewed in (Chen et al., 2012), (Navone et al., 2015)). However, the effect of P56S-VAPB inclusions on autophagic flow had not yet been investigated. I found that autophagy, stimulated either pharmacologically or by starvation, was unaffected by P56S-VAPB expression. Hence, it appears that cells can adjust the capacity of their degradative machinery to cope with moderate levels of mutant VAPB without consequent disturbances in proteostasis.

As summarized in the Introduction, a fundamental process in which the VAPs are implicated is intracellular transport through the secretory pathway, but contrasting results have been reported on the effect of P56S-VAPB expression on this process. In CHO cells, (Prosser et al., 2008) found a strong interference of overexpressed P56S-VAPB (and also of overexpressed wt VAPA) with VSVG transport, whereas no delay of the transport of the same secretory membrane cargo was detected by Teuling et al. in

primary hippocampal neuronal cultures (Teuling et al., 2007). With the HeLa Tet-Off cells, I found that neither transport of VSVG from the ER to the Golgi nor its export to the cell surface were altered by the presence of P56S-VAPB inclusions. I conclude that cells can maintain secretory pathway function in the presence of P56S-VAPB inclusions, notwithstanding their close physical proximity to the Golgi apparatus demonstrated here. Of course, I cannot exclude at present that other cargoes and other cell types may be more sensitive to the presence of P56S-VAPB inclusions. Further studies are required to generalize my findings to other contexts.

The results of the first part of my thesis, showing a lack of interference of moderate levels of P56S-VAPB with basic cellular functions, are consistent with the outcome of analyses of transgenic animals. Furthermore, P56S-VAPB is unstable, as demonstrated by studies carried out previously in my laboratory (Papiani et al., 2012), and this instability likely explains the lack of detectable VAPB inclusions in ALS8 patients' motor neurons generated from iPSCs (Mitne-Neto et al., 2011). In support of the relevance of the *in vitro* studies to the *in vivo* situation, (Aliaga et al., 2013) detected lower levels of mutant than of wild-type protein in the brains of transgenic mouse strains that had comparable levels of mRNA expression. Thus, it is feasible that in the heterozygote -P56S/wt - individual, mutant VAPB inclusions never reach the high levels required for them to exert a damaging effect on motor neurons.

Taking into account my results combined with the above considerations, I decided to investigate ALS8 genesis from a different perspective, i.e., to analyze the effect of reduction of VAPB levels on cellular physiology in the absence of expression of the mutant protein.

5.2. Effect of VAPB downregulation on motorneuronal physiology.

For these studies I chose to work with the motorneuronal-like cell line NSC34. This is a mouse cell line created by fusion of a neuroblastoma line with spinal cord primary motor neurons, and currently represents the best available characterized cell line with motorneuronal characteristics (Cashman et al., 1992). I first analyzed the ability of NSC34 cells to differentiate into cells with more pronounced motorneuronal characteristics, using a recently published protocol (Maier et al., 2013).

Among the observations that I made on the differentiation process, the one regarding GM1 is of particular interest. This glycoshingolipid was found mainly on intracellular vesicles positive for the late endosome/lysosomal marker LAMP1 under basal conditions. Instead, after differentiation, most of the GM1 was seen on the cell surface. A recent study has implicated late endosomes as the carriers of membranes to extending neurites ((Raiborg et al., 2015a) -see also below). Thus, the intracellular GM1 pool in the non differentiated cells may be part of a storage compartment that is recruited during the neurite extension process triggered by differentiation.

A second interesting finding is that the VAPs, especially VAPB, are upregulated during differentiation, suggesting that they play a specific role in motorneuronal differentiation/physiology, and encouraging me to investigate the effect of VAPB downregulation on phenomena in which the VAPs have been implicated. Indeed, it has already been reported that VAPB is upregulated following iPSC

differentiation into motorneurons (Mitne-Neto et al., 2011). I was able to generate two NSC34 clones silenced for VAPB; in one of the clones, VAPB expression was reduced to about 50% of the control cells, providing a model for haploinsufficiency; the other clone had more strongly reduced VAPB levels, approaching homozygous loss of function. I used these two cell lines to investigate the effect of VAPB depletion on (i) ceramide transport, (ii) PI4P levels in the Golgi, and (iii) neurite extension during the differentiation process.

(i). Ceramide transport.

As explained in the Introduction and Results sections of this thesis, the VAPs are involved in ceramide transport from the ER to the Golgi, because of their ability to recruit the ceramide transport protein CERT to the ER (Lev, 2010). A delayed ceramide transport, due to VAPB deficiency, could lead to an imbalance in the sphingolipid composition of the affected cells, with a predicted excess of unprocessed ceramide. Ceramide is known to be neurotoxic and accumulation of ceramide has also been reported in the spinal cord of sALS patients (Cutler et al., 2002).

To investigate the effect of VAPB depletion on ceramide transport, I applied a sensitive microscope assay, in which a fluorescently labeled ceramide is first accumulated in the ER, and then allowed to be transported to the Golgi (Toth et al., 2006). By this assay, I could not detect an effect of near complete VAPB depletion on ceramide transport. To be noted, the assay was effective in revealing a slowdown of ceramide transport in cells transiently overexpressing P56S-VAPB at high levels (results not shown).

The results obtained with the NSC34 clones might seem at variance with those obtained by (Peretti et al., 2008), who demonstrated alterations in CERT localization and sphingomyelin levels in HeLa cells silenced for both VAPA and B. It is possible that in NSC34, VAPA is present in sufficient amounts to guarantee normal CERT-mediated ceramide transport. It is also possible that in these cells, the vesicular route of ceramide transport is the more important one, so that inhibition of LTP-dependent transport is difficult to detect.

(ii). PI4P levels in the Golgi.

As detailed in the Introduction, the VAPs play a crucial role in regulating phosphoinositide levels within the ER-Golgi compartments. The role of the VAPs is intimately connected to the LTP OSBP, whose function has recently been elucidated (Mesmin et al., 2013). OSBP, which forms a MCS between the ER and the trans Golgi, can bind both sterols and PI4P via its ORP domain. The ORP domain should not be confused with the PH domain which, by binding PI4P, serves to anchor OSBP to the Golgi. Instead the ORP domain is used for transport of both cholesterol and PI4P. At the ER, it picks up cholesterol, because PI4P levels are low; at the trans Golgi, it exchanges cholesterol for PI4P, because its affinity for the phosphoinositide is higher than for sterols, and because PI4P levels are high in the trans Golgi.

Release of PI4P to the ER occurs passively, driven by the concentration gradient of the lipid. The concentration of PI4P is indeed kept low by the activity of the ER phosphatase Sac1. As already mentioned, the VAPs interact with Sac1 and enhance its activity (Forrest et al., 2013). The entire cycle drives export of cholesterol from the ER, using the energy stored in PI4P; in the cycle, the VAPs play a dual role: they provide a docking site for OSBP, and they activate Sac1 to dispose of the back-transported PI4P (see Fig. 5.1).

The predicted consequence of VAP depletion should be interruption of the OSBP cycle with a consequent accumulation of PI4P in the Golgi as a result of both impaired docking of OSBP on the ER and reduced Sac1-mediated dephosphorylation of PI4P that would disrupt its concentration gradient. Very interestingly, in the NSC34 clone with near complete VAPB knockdown, I observed the predicted effect both in non-differentiated and in differentiated cells, indicating that, at variance with the results obtained on ceramide transport, the VAPA pool alone is not sufficient to guarantee phosphoinositide balance. This result reflects what has been observed in *Drosophila*, where DVAP (the homologue of both VAP proteins) downregulation increases PI4P levels (Forrest et al., 2013). Although I did not see an effect in the clone with partial VAPB knockdown, one might speculate that a small degree of PI4P accumulation in the Golgi could also be present in cells expressing wt VAPB from one allele, but be undetected in my assay.

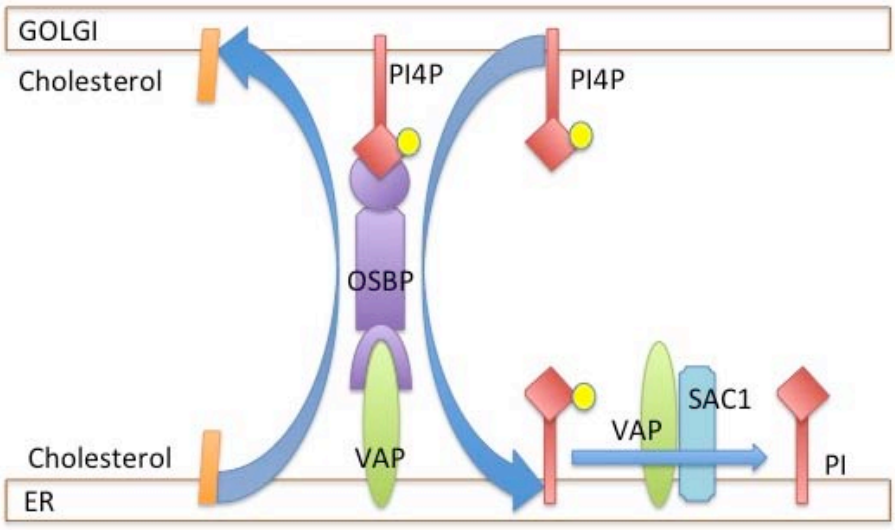

Figure 5.1: Schematic representation of PI4P cycle at ER-Golgi MCS.

An imbalance in PI4P distribution between the Golgi and the ER compartments could have far reaching effects on cellular physiology. Phosphinositides are key molecules in determining compartment identity (Di Paolo and De Camilli, 2006), so an increase in PI4P would alter the Golgi identity kit. There

is a vast number of PI4P interacting proteins that are involved in fundamental cellular processes, like vesicular transport from the Trans Golgi Network. Four-Phosphate-adaptor Protein (FAPP) 1 and 2 are an example of such proteins: they are recruited to the TGN thanks to their binding to both PI4P and the small GTPase Arf1 and regulate Golgi to PM trafficking (Godi et al., 2004). In addition, FAPP2 has a role in intra-Golgi non-vesicular transport of GlucosilCeramide from *cis* to *trans* Golgi, where it is converted into Globosides, a class of complex glycosphingolipids (D'Angelo et al., 2013). Finally, the increase in Golgi PI4P is likely to alter the concentrations of other downstream phosphoinositides, like PI4,5P2 and PI3,4,5,P3.

(iii) Neurite extension during the differentiation process.

Among their many functions, the VAPs have been implicated in neurite extension (see Introduction), so it seemed of great interest to determine whether depletion of VAPB alone would have an effect on this process in a motorneuronal background. As a matter of fact, it has been reported that downregulation of VAPA, but not VAPB, strongly reduces neurite extension in the pheocromocytoma cell line PC12 (Saita et al., 2009). While visual inspection of the differentiated VAPB-silenced cells did not show obvious differences from the control cells, quantitative analysis revealed that fewer silenced than control cells had long neurites (>100 μm) at three and at six days of differentiation. This effect was statistically significant both for the partially and for the near completely silenced clone.

The mechanisms by which the VAPs promote neurite extension could be indirectly related to their roles in protein and lipid transport within the secretory pathway (Kuijpers et al., 2013b). However, recent evidence has uncovered a more direct role of the VAPs in the process, mediated by their interaction with the FFAT-containing protein protrudin (Saita et al., 2009). Protrudin, an ER transmembrane protein, appears to be involved in neurite extension by promoting focal contacts between the ER and late or recycling endosomes; interaction with late endosomes is mediated by its FYVE domain (which binds PI3P, the signature phosphoinositide of late endosomes and lysosomes) and the interaction with Rab7 (Raiborg et al., 2015a) (see Fig. 1.5); the interaction with recycling endosomes would instead be driven by interaction with Rab11 (Shirane and Nakayama, 2006). Protrudin is thought to recruit the microtubule motor KIF5 to the endosomes, permitting their transport to the cell periphery along microtubules. Both recycling and late endosomes would thus provide a source of membrane to be delivered to the growing tips of neurites by exocytosis. My observations on the GM1 distribution in non-differentiated cells fit well with the previously described role of late endosomes in neurite extension (reviewed in (Sann et al., 2009)).

Since protrudin is an ER resident transmembrane protein, the open question is the role of the VAPs in the process of protrudin-dependent neurite extension. Clearly, the VAPs are not required to recruit protrudin to the ER, as is the case for LTPs. The observation that the FFAT sequence of protrudin is required for its activity in neurite extension (Saita et al., 2009) indicates that direct interaction between

the VAPs and protrudin is required. This interaction could result in modulation of protrudin's conformation, making it competent for kinesin recruitment.

Whatever the mechanism by which the VAPs support protrudin function, my observation that depletion of VAPB alone decreases neurite extension in NSC34 cells has implications for motorneuronal cell biology and viability as well as for ALS pathology. As mentioned above, previous studies on VAP function have been carried out by silencing both VAP isoforms (Teuling et al., 2007) (Peretti et al., 2008) or VAPA alone (Saita et al., 2009). My results demonstrate for the first time, an effect of VAPB depletion in the presence of normal levels of VAPA. In other words, VAPB plays a role in neurite extension, whose loss is not compensated by VAPA, a phenomenon which could be explained by insufficient amounts of VAPA in NSC34 cells and/or by a function unique to VAPB in motorneuronal cells, not replaceable by VAPA.

Experiments, in which my NSC34 clones will be transfected with siRNA resistant VAPB or VAPA, are currently being carried out, and may clarify this issue.

A surprising observation of my experiments was that the two NSC34 clones, which have a different degree of VAPB silencing, showed a similar decrease in neurite extension. This finding is somewhat difficult to explain. As neurite extension surely involves more than one mechanism, one might hypothesize that the VAPB-dependent pathway is exquisitely sensitive to VAPB levels, so that a ~50% reduction exerts already the maximum inhibitory effect. Be this as it may, the strong effect seen with clone #6, which has a ~50% reduction in VAPB levels, is consistent with the idea that VAPB haploinsufficiency could trigger motorneuronal degeneration. Indeed, the process of axon and dendrite maintenance is presumably closely related to the one of neurite extension during differentiation (Sann et al., 2009) (Lee et al., 2010). VAPB haploinsufficiency could thus result in insufficient membrane delivery to motorneuronal extensions, a process that could cause muscle denervation and disease onset and progression.

5.3. Conclusions and perspectives

Taken together, the results of my thesis support the hypothesis that ALS8 is caused by VAPB loss of function. I was unable to show any interference of P56S-VAPB inclusions with proteostasis or with the secretory pathway, whereas VAPB silencing did have phenotypic effects in NSC34 cells with regards both to phosphoinositide balance and to neurite extension. The latter observation opens a number of questions that will hopefully be addressed in the future. First, to exclude off-target effects of VAPB silencing, it will be crucial to express siRNA-resistant VAPB in our clones and assess whether the altered phenotype is reversed. I am currently in the process of carrying out these experiments. Second, it will be interesting to unravel the contributions of the two VAP isoforms in neurite extension and phosphoinositide metabolism: will VAPA overexpression in our silenced clones be as effective as VAPB in reversing the phenotype? It would, of course be interesting to generate VAPA silenced NSC34 clones; this could probably be done more easily with CRISPR technology than with shRNA, as done in this

study. It should also be interesting to determine the absolute levels of the two VAP isoforms in NSC34 cells: can the effect of VAPB silencing be explained simply by very low levels of VAPA in these cells? And, finally, since VAPs are partially depleted both in mutant SOD1 mice and in cases of sALS, it should be interesting to investigate whether an increase in VAP levels could partially reverse the pathology caused by other mutations in ALS animal models. A positive result might suggest novel strategies for therapeutic interventions for this fatal disease.

6. Acknowledgments

First, I would like to thank Prof. Alberto Corsini, Prof. Alberto Panerai and Dr. Mariaelvina Sala, for giving me the opportunity to work at the CNR-Institute of Neuroscience, in the Department of Medical Biotechnologies and Translational Medicine of the University of Milano.

I would like to express my sincere gratitude to Dr. Francesca Navone for her constant help, patience and support during my PhD study. I am also extremely grateful to Prof. Nica Borgese: without her lessons, scientific guidance and knowledge this thesis would not have been completed.

I would like to thank Dr. Antonella De Matteis, whose help was unvaluable for the development of part of this research work and who gave me the opportunity to join her laboratory at TIGEM (Pozzuoli, Naples) as a visiting student. Among all members of her lab, I wish to thank especially Dr. Rossella Venditti and Dr. Laura Giaquinto.

I also want to thank all the people working in the laboratory of Prof. Borgese: Sara, Arianna, Bruna and Hugo. Thank you for all the suggestion (and coffee breaks!)

Last but not the least, I would like to thank my family: my parents and my brother Max for supporting me and allowing me to reach this goal.

7. Bibliography

Aliaga, L., C. Lai, J. Yu, N. Chub, H. Shim, L. Sun, C. Xie, W.J. Yang, X. Lin, M.J. O'Donovan, and H. Cai. 2013. Amyotrophic lateral sclerosis-related VAPB P56S mutation differentially affects the function and survival of corticospinal and spinal motor neurons. *Hum Mol Genet*. 22:4293-4305.

Alpy, F., A. Rousseau, Y. Schwab, F. Legueux, I. Stoll, C. Wendling, C. Spiegelhalter, P. Kessler, C. Mathelin, M.C. Rio, T.P. Levine, and C. Tomasetto. 2013. STARD3 or STARD3NL and VAP form a novel molecular tether between late endosomes and the ER. *J Cell Sci*. 126:5500-5512.

Anagnostou, G., M.T. Akbar, P. Paul, C. Angelinetta, T.J. Steiner, and J. de Belleroche. 2010. Vesicle associated membrane protein B (VAPB) is decreased in ALS spinal cord. *Neurobiol Aging*. 31:969-985.

Andersen, P.M., and A. Al-Chalabi. 2011. Clinical genetics of amyotrophic lateral sclerosis: what do we really know? *Nat Rev Neurol*. 7:603-615.

Ash, P.E., K.F. Bieniek, T.F. Gendron, T. Caulfield, W.L. Lin, M. Dejesus-Hernandez, M.M. van Blitterswijk, K. Jansen-West, J.W. Paul, 3rd, R. Rademakers, K.B. Boylan, D.W. Dickson, and L. Petrucelli. 2013. Unconventional translation of C9ORF72 GGGGCC expansion generates insoluble polypeptides specific to c9FTD/ALS. *Neuron*. 77:639-646.

Babetto, E., A. Mangolini, M. Rizzardini, M. Lupi, L. Conforti, P. Rusmini, A. Poletti, and L. Cantoni. 2005. Tetracycline-regulated gene expression in the NSC-34-tTA cell line for investigation of motor neuron diseases. *Brain research. Molecular brain research*. 140:63-72.

Balla, T. 2013. Phosphoinositides: tiny lipids with giant impact on cell regulation. *Physiol Rev*. 93:1019-1137.

Bergmann, J.E. 1989. Using temperature-sensitive mutants of VSV to study membrane protein biogenesis. *Methods Cell Biol*. 32:85-110.

Bernasconi, R., and M. Molinari. 2011. ERAD and ERAD tuning: disposal of cargo and of ERAD regulators from the mammalian ER. *Curr Opin Cell Biol*. 23:176-183.

Blokhuis, A.M., E.J. Groen, M. Koppers, L.H. van den Berg, and R.J. Pasterkamp. 2013. Protein aggregation in amyotrophic lateral sclerosis. *Acta Neuropathol*. 125:777-794.

Brummelkamp, T.R., R. Bernards, and R. Agami. 2002. A system for stable expression of short interfering RNAs in mammalian cells. *Science*. 296:550-553.

Byrne, S., C. Walsh, C. Lynch, P. Bede, M. Elamin, K. Kenna, R. McLaughlin, and O. Hardiman. 2011. Rate of familial amyotrophic lateral sclerosis: a systematic review and meta-analysis. *Journal of neurology, neurosurgery, and psychiatry*. 82:623-627.

Cashman, N.R., H.D. Durham, J.K. Blusztajn, K. Oda, T. Tabira, I.T. Shaw, S. Dahrouge, and J.P. Antel. 1992. Neuroblastoma x spinal cord (NSC) hybrid cell lines resemble developing motor neurons. *Developmental dynamics: an official publication of the American Association of Anatomists*. 194:209-221.

Chen, H.-J., G. Anagnostou, A. Chai, J. Withers, A. Morris, J. Adhikaree, G. Pennetta, and J.S. de Belleroche. 2010. Characterization of the properties of a novel mutation in VAPB in familial amyotrophic lateral sclerosis. *J Biol Chem*. 285:40266-40281.

Chen, S., X. Zhang, L. Song, and W. Le. 2012. Autophagy dysregulation in amyotrophic lateral sclerosis. *Brain Pathol*. 22:110-116.

Chevalier-Larsen, E., and E.L. Holzbaur. 2006. Axonal transport and neurodegenerative disease. *Biochim Biophys Acta*. 1762:1094-1108.

Cutler, R.G., W.A. Pedersen, S. Camandola, J.D. Rothstein, and M.P. Mattson. 2002. Evidence that accumulation of ceramides and cholesterol esters mediates oxidative stress-induced death of motor neurons in amyotrophic lateral sclerosis. *Ann Neurol*. 52:448-457.

D'Angelo, G., T. Uemura, C.C. Chuang, E. Polishchuk, M. Santoro, H. Ohvo-Rekila, T. Sato, G. Di Tullio, A. Varriale, S. D'Auria, T. Daniele, F. Capuani, L. Johannes, P. Mattjus, M. Monti, P. Pucci, R.L. Williams, J.E. Burke, F.M. Platt, A. Harada, and M.A. De Matteis. 2013. Vesicular and non-vesicular transport feed distinct glycosylation pathways in the Golgi. *Nature*. 501:116-120.

Dalva, M.B., M.A. Takasu, M.Z. Lin, S.M. Shamah, L. Hu, N.W. Gale, and M.E. Greenberg. 2000. EphB receptors interact with NMDA receptors and regulate excitatory synapse formation. *Cell*. 103:945-956.

De Vos, K.J., G.b.M. M√≥rotz, R. Stoica, E.L. Tudor, K.-F. Lau, S. Ackerley, A. Warley, C.E. Shaw, and C.C.J. Miller. 2012. VAPB interacts with the mitochondrial protein PTPIP51 to regulate calcium homeostasis. *Hum Mol Genet*. 21:1299-1311.

DeJesus-Hernandez, M., I.R. Mackenzie, B.F. Boeve, A.L. Boxer, M. Baker, N.J. Rutherford, A.M. Nicholson, N.A. Finch, H. Flynn, J. Adamson, N. Kouri, A. Wojtas, P. Sengdy, G.Y. Hsiung, A. Karydas, W.W. Seeley, K.A. Josephs, G. Coppola, D.H. Geschwind, Z.K. Wszolek, H. Feldman, D.S. Knopman, R.C. Petersen, B.L. Miller, D.W. Dickson, K.B. Boylan, N.R. Graff-Radford, and R. Rademakers. 2011. Expanded GGGGCC hexanucleotide repeat in noncoding region of C9ORF72 causes chromosome 9p-linked FTD and ALS. *Neuron*. 72:245-256.

Di Paolo, G., and P. De Camilli. 2006. Phosphoinositides in cell regulation and membrane dynamics. *Nature*. 443:651-657.

Eidels, L., R.L. Proia, and D.A. Hart. 1983. Membrane receptors for bacterial toxins. *Microbiol Rev*. 47:596-620.

Fasana, E., M. Fossati, A. Ruggiano, S. Brambillasca, C.C. Hoogenraad, F. Navone, M. Francolini, and N. Borgese. 2010. A VAPB mutant linked to amyotrophic lateral sclerosis generates a novel form of organized smooth endoplasmic reticulum. *FASEB journal: official publication of the Federation of American Societies for Experimental Biology*. 24:1419-1430.

Ferraiuolo, L., J. Kirby, A.J. Grierson, M. Sendtner, and P.J. Shaw. 2011. Molecular pathways of motor neuron injury in amyotrophic lateral sclerosis. *Nat Rev Neurol*. 7:616-630.

Forrest, S., A. Chai, M. Sanhueza, M. Marescotti, K. Parry, A. Georgiev, V. Sahota, R. Mendez-Castro, and G. Pennetta. 2013. Increased levels of phosphoinositides cause neurodegeneration in a Drosophila model of amyotrophic lateral sclerosis. *Hum Mol Genet*. 22:2689-2704.

Genevini, P., G. Papiani, A. Ruggiano, L. Cantoni, F. Navone, and N. Borgese. 2014. Amyotrophic lateral sclerosis-linked mutant VAPB inclusions do not interfere with protein degradation pathways or intracellular transport in a cultured cell model. *PLoS One*. 9:e113416.

Gkogkas, C., S. Middleton, A.M. Kremer, C. Wardrope, M. Hannah, T.H. Gillingwater, and P. Skehel. 2008. VAPB interacts with and modulates the activity of ATF6. *Hum Mol Genet*. 17:1517-1526.

Godi, A., A. Di Campli, A. Konstantakopoulos, G. Di Tullio, D.R. Alessi, G.S. Kular, T. Daniele, P. Marra, J.M. Lucocq, and M.A. De Matteis. 2004. FAPPs control Golgi-to-cell-surface membrane traffic by binding to ARF and PtdIns(4)P. *Nat Cell Biol*. 6:393-404.

Gonatas, N.K., A. Stieber, and J.O. Gonatas. 2006. Fragmentation of the Golgi apparatus in neurodegenerative diseases and cell death. *J Neurol Sci*. 246:21-30.

Hammond, G.R., G. Schiavo, and R.F. Irvine. 2009. Immunocytochemical techniques reveal multiple, distinct cellular pools of PtdIns4P and PtdIns(4,5)P(2). *Biochem J*. 422:23-35.

Han, S.M., H. El Oussini, J. Scekic-Zahirovic, J. Vibbert, P. Cottee, J.K. Prasain, H.J. Bellen, L. Dupuis, and M.A. Miller. 2013. VAPB/ALS8 MSP ligands regulate striated muscle energy metabolism critical for adult survival in caenorhabditis elegans. *PLoS Genet*. 9:e1003738.

Han, S.M., H. Tsuda, Y. Yang, J. Vibbert, P. Cottee, S.-J. Lee, J. Winek, C. Haueter, H.J. Bellen, and M.A. Miller. 2012. Secreted VAPB/ALS8 major sperm protein domains modulate mitochondrial localization and morphology via growth cone guidance receptors. *Developmental cell*. 22:348-362.

Hanahan, D. 1983. Studies on transformation of Escherichia coli with plasmids. *J Mol Biol*. 166:557-580.

Hetz, C., and B. Mollereau. 2014. Disturbance of endoplasmic reticulum proteostasis in neurodegenerative diseases. *Nat Rev Neurosci*. 15:233-249.

Hetz, C., P. Thielen, S. Matus, M. Nassif, F. Court, R. Kiffin, G. Martinez, A.M. Cuervo, R.H. Brown, and L.H. Glimcher. 2009. XBP-1 deficiency in the nervous system protects against amyotrophic lateral sclerosis by increasing autophagy. *Genes Dev*. 23:2294-2306.

Holthuis, J.C., and A.K. Menon. 2014. Lipid landscapes and pipelines in membrane homeostasis. *Nature*. 510:48-57.

Ince, P.G., J.R. Highley, J. Kirby, S.B. Wharton, H. Takahashi, M.J. Strong, and P.J. Shaw. 2011. Molecular pathology and genetic advances in amyotrophic lateral sclerosis: an emerging molecular pathway and the significance of glial pathology. *Acta Neuropathol*. 122:657-671.

Kabashi, E., H. El Oussini, V. Bercier, F. Gros-Louis, P.N. Valdmanis, J. McDearmid, I.A. Mejier, P.A. Dion, N. Dupre, D. Hollinger, J. Sinniger, S. Dirrig-Grosch, W. Camu, V. Meininger, J.P. Loeffler, F. Rene, P. Drapeau, G.A. Rouleau, and L. Dupuis. 2013. Investigating the contribution of VAPB/ALS8 loss of function in amyotrophic lateral sclerosis. *Hum Mol Genet*. 22:2350-2360.

Kabeya, Y., N. Mizushima, T. Ueno, A. Yamamoto, T. Kirisako, T. Noda, E. Kominami, Y. Ohsumi, and T. Yoshimori. 2000. LC3, a mammalian homologue of yeast Apg8p, is localized in autophagosome membranes after processing. *Embo J*. 19:5720-5728.

Kanekura, K., I. Nishimoto, S. Aiso, and M. Matsuoka. 2006. Characterization of amyotrophic lateral sclerosis-linked P56S mutation of vesicle-associated membrane protein-associated protein B (VAPB/ALS8). *J Biol Chem*. 281:30223-30233.

Kim, S., S.n.S. Leal, D. Ben Halevy, C.u.M. Gomes, and S. Lev. 2010. Structural requirements for VAP-B oligomerization and their implication in amyotrophic lateral sclerosis-associated VAP-B(P56S) neurotoxicity. *J Biol Chem*. 285:13839-13849.

Klionsky, D.J., F.C. Abdalla, H. Abeliovich, R.T. Abraham, A. Acevedo-Arozena, K. Adeli, L. Agholme, M. Agnello, P. Agostinis, J.A. Aguirre-Ghiso, H.J. Ahn, O. Ait-Mohamed, S. Ait-Si-Ali, T. Akematsu, S. Akira, H.M. Al-Younes, M.A. Al-Zeer, M.L. Albert, R.L. Albin, J. Alegre-Abarrategui, M.F. Aleo, M. Alirezaei, A. Almasan, M. Almonte-Becerril, A. Amano, R. Amaravadi, S. Amarnath, A.O. Amer, N. Andrieu-Abadie, V. Anantharam, D.K. Ann, S. Anoopkumar-Dukie, H. Aoki, N. Apostolova, G. Arancia, J.P. Aris, K. Asanuma, N.Y. Asare, H. Ashida, V. Askanas, D.S. Askew, P. Auberger, M. Baba, S.K. Backues, E.H. Baehrecke, B.A. Bahr, X.Y. Bai, Y. Bailly, R. Baiocchi, G. Baldini, W. Balduini, A. Ballabio, B.A. Bamber, E.T. Bampton, G. Banhegyi, C.R. Bartholomew, D.C. Bassham, R.C. Bast, Jr., H. Batoko, B.H. Bay, I. Beau, D.M. Bechet, T.J. Begley, C. Behl, C. Behrends, S. Bekri, B. Bellaire, L.J. Bendall, L. Benetti, L. Berliocchi, H. Bernardi, F. Bernassola, S. Besteiro, I. Bhatia-Kissova, X. Bi, M. Biard-Piechaczyk, J.S. Blum, L.H. Boise, P. Bonaldo, D.L. Boone, B.C. Bornhauser, K.R. Bortoluci, I. Bossis, F. Bost, J.P. Bourquin, P. Boya, M. Boyer-Guittaut, P.V. Bozhkov, N.R. Brady, C. Brancolini, A. Brech, J.E. Brenman, A. Brennand, E.H. Bresnick, P. Brest, D. Bridges, M.L. Bristol, P.S. Brookes, E.J. Brown, J.H. Brumell, et al. 2012. Guidelines for the use and interpretation of assays for monitoring autophagy. *Autophagy*. 8:445-544.

Kruh, J. 1982. Effects of sodium butyrate, a new pharmacological agent, on cells in culture. *Mol Cell Biochem*. 42:65-82.

Kuijpers, M., V. van Dis, E.D. Haasdijk, M. Harterink, K. Vocking, J.A. Post, W. Scheper, C.C. Hoogenraad, and D. Jaarsma. 2013a. Amyotrophic lateral sclerosis (ALS)-associated VAPB-P56S inclusions represent an ER quality control compartment. *Acta Neuropathol Commun*. 1:24.

Kuijpers, M., K.L. Yu, E. Teuling, A. Akhmanova, D. Jaarsma, and C.C. Hoogenraad. 2013b. The ALS8 protein VAPB interacts with the ER-Golgi recycling protein YIF1A and regulates membrane delivery into dendrites. *Embo J*. 32:2056-2072.

Kutay, U., G. Ahnert-Hilger, E. Hartmann, B. Wiedenmann, and T.A. Rapoport. 1995. Transport route for synaptobrevin via a novel pathway of insertion into the endoplasmic reticulum membrane. *Embo J*. 14:217-223.

Larroquette, F., L. Seto, P.L. Gaub, B. Kamal, D. Wallis, R. Lariviere, J. Vallee, R. Robitaille, and H. Tsuda. 2015. Vapb/Amyotrophic lateral sclerosis 8 knock-in mice display slowly

progressive motor behavior defects accompanying ER stress and autophagic response. *Hum Mol Genet*. 24:6515-6529.

Lattante, S., S. Ciura, G.A. Rouleau, and E. Kabashi. 2015. Defining the genetic connection linking amyotrophic lateral sclerosis (ALS) with frontotemporal dementia (FTD). *Trends Genet*. 31:263-273.

Leblond, C.S., H.M. Kaneb, P.A. Dion, and G.A. Rouleau. 2014. Dissection of genetic factors associated with amyotrophic lateral sclerosis. *Exp Neurol*. 262 Pt B:91-101.

Lee, H.W., Y. Kim, K. Han, H. Kim, and E. Kim. 2010. The phosphoinositide 3-phosphatase MTMR2 interacts with PSD-95 and maintains excitatory synapses by modulating endosomal traffic. *J Neurosci*. 30:5508-5518.

Lehman, N.L. 2009. The ubiquitin proteasome system in neuropathology. *Acta Neuropathol*. 118:329-347.

Lev, S. 2010. Non-vesicular lipid transport by lipid-transfer proteins and beyond. *Nat Rev Mol Cell Biol*. 11:739-750.

Lev, S., D. Ben Halevy, D. Peretti, and N. Dahan. 2008. The VAP protein family: from cellular functions to motor neuron disease. *Trends Cell Biol*. 18:282-290.

Lin, M.T., and M.F. Beal. 2006. Mitochondrial dysfunction and oxidative stress in neurodegenerative diseases. *Nature*. 443:787-795.

Lunn, M.R., and C.H. Wang. 2008. Spinal muscular atrophy. *Lancet*. 371:2120-2133.

Magal, E., J.A. Holash, R.J. Toso, D. Chang, R.A. Lindberg, and E.B. Pasquale. 1996. B61, a ligand for the Eck receptor protein-tyrosine kinase, exhibits neurotrophic activity in cultures of rat spinal cord neurons. *J Neurosci Res*. 43:735-744.

Maier, O., J. Bohm, M. Dahm, S. Bruck, C. Beyer, and S. Johann. 2013. Differentiated NSC-34 motoneuron-like cells as experimental model for cholinergic neurodegeneration. *Neurochem Int*. 62:1029-1038.

Matsuzaki, F., M. Shirane, M. Matsumoto, and K.I. Nakayama. 2011. Protrudin serves as an adaptor molecule that connects KIF5 and its cargoes in vesicular transport during process formation. *Mol Biol Cell*. 22:4602-4620.

Matus, S., V. Valenzuela, D.B. Medinas, and C. Hetz. 2013. ER Dysfunction and Protein Folding Stress in ALS. *Int J Cell Biol*. 2013:674751.

Mesmin, B., J. Bigay, J. Moser von Filseck, S. Lacas-Gervais, G. Drin, and B. Antonny. 2013. A four-step cycle driven by PI(4)P hydrolysis directs sterol/PI(4)P exchange by the ER-Golgi tether OSBP. *Cell*. 155:830-843.

Millecamps, S., and J.P. Julien. 2013. Axonal transport deficits and neurodegenerative diseases. *Nat Rev Neurosci*. 14:161-176.

Mitne-Neto, M., M. Machado-Costa, M.C. Marchetto, M.H. Bengtson, C.A. Joazeiro, H. Tsuda, H.J. Bellen, H.C. Silva, A.S. Oliveira, M. Lazar, A.R. Muotri, and M. Zatz. 2011. Downregulation of VAPB expression in motor neurons derived from induced pluripotent stem cells of ALS8 patients. *Hum Mol Genet*. 20:3642-3652.

Morotz, G.M., K.J. De Vos, A. Vagnoni, S. Ackerley, C.E. Shaw, and C.C. Miller. 2012. Amyotrophic lateral sclerosis-associated mutant VAPBP56S perturbs calcium homeostasis to disrupt axonal transport of mitochondria. *Hum Mol Genet*. 21:1979-1988.

Moumen, A., I. Virard, and C. Raoul. 2011. Accumulation of wildtype and ALS-linked mutated VAPB impairs activity of the proteasome. *PLoS One*. 6:e26066.

Nassif, M., S. Matus, K. Castillo, and C. Hetz. 2010. Amyotrophic lateral sclerosis pathogenesis: a journey through the secretory pathway. *Antioxid Redox Signal*. 13:1955-1989.

Navone, F., P. Genevini, and N. Borgese. 2015. Autophagy and Neurodegeneration: Insights from a Cultured Cell Model of ALS. *Cells*. 4:354-386.

Nickel, W. 2010. Pathways of unconventional protein secretion. *Curr Opin Biotechnol*. 21:621-626.

Nishimura, A.L., A. Al-Chalabi, and M. Zatz. 2005. A common founder for amyotrophic lateral sclerosis type 8 (ALS8) in the Brazilian population. *Human genetics*. 118:499-500.

Nishimura, A.L., M. Mitne-Neto, H.C.A. Silva, A.n. Richieri-Costa, S. Middleton, D. Cascio, F. Kok, J.o.R.M. Oliveira, T. Gillingwater, J. Webb, P. Skehel, and M. Zatz. 2004. A mutation in the vesicle-trafficking protein VAPB causes late-onset spinal muscular atrophy and amyotrophic lateral sclerosis. *American journal of human genetics*. 75:822-831.

Ohnishi, T., M. Shirane, Y. Hashimoto, S. Saita, and K.I. Nakayama. 2014. Identification and characterization of a neuron-specific isoform of protrudin. *Genes Cells*. 19:97-111.

Papiani, G., A. Ruggiano, M. Fossati, A. Raimondi, G. Bertoni, M. Francolini, R. Benfante, F. Navone, and N. Borgese. 2012. Restructured Endoplasmic Reticulum, Generated by Mutant, Amyotrophic Lateral Sclerosis-Linked VAPB, is Cleared by the Proteasome. *J Cell Sci*.

Peretti, D., N. Dahan, E. Shimoni, K. Hirschberg, and S. Lev. 2008. Coordinated lipid transfer between the endoplasmic reticulum and the Golgi complex requires the VAP proteins and is essential for Golgi-mediated transport. *Mol Biol Cell*. 19:3871-3884.

Peters, O.M., M. Ghasemi, and R.H. Brown, Jr. 2015. Emerging mechanisms of molecular pathology in ALS. *J Clin Invest*. 125:2548.

Powers, E.T., R.I. Morimoto, A. Dillin, J.W. Kelly, and W.E. Balch. 2009. Biological and chemical approaches to diseases of proteostasis deficiency. *Annu Rev Biochem*. 78:959-991.

Prosser, D.C., D. Tran, P.Y. Gougeon, C. Verly, and J.K. Ngsee. 2008. FFAT rescues VAPA-mediated inhibition of ER-to-Golgi transport and VAPB-mediated ER aggregation. *J Cell Sci*. 121:3052-3061.

Qiu, L., T. Qiao, M. Beers, W. Tan, H. Wang, B. Yang, and Z. Xu. 2013. Widespread aggregation of mutant VAPB associated with ALS does not cause motor neuron degeneration or modulate mutant SOD1 aggregation and toxicity in mice. *Mol Neurodegener*. 8:1.

Raiborg, C., E.M. Wenzel, N.M. Pedersen, H. Olsvik, K.O. Schink, S.W. Schultz, M. Vietri, V. Nisi, C. Bucci, A. Brech, T. Johansen, and H. Stenmark. 2015a. Repeated ER-endosome contacts promote endosome translocation and neurite outgrowth. *Nature*. 520:234-238.

Raiborg, C., E.M. Wenzel, and H. Stenmark. 2015b. ER-endosome contact sites: molecular compositions and functions. *Embo J*. 34:1848-1858.

Raimondi, A., A. Mangolini, M. Rizzardini, S. Tartari, S. Massari, C. Bendotti, M. Francolini, N. Borgese, L. Cantoni, and G. Pietrini. 2006. Cell culture models to investigate the selective vulnerability of motoneuronal mitochondria to familial ALS-linked G93ASOD1. *Eur J Neurosci*. 24:387-399.

Rao, M., W. Song, A. Jiang, Y. Shyr, S. Lev, D. Greenstein, D. Brantley-Sieders, and J. Chen. 2012. VAMP-associated protein B (VAPB) promotes breast tumor growth by modulation of Akt activity. *PLoS One*. 7:e46281.

Ravikumar, B., R. Duden, and D.C. Rubinsztein. 2002. Aggregate-prone proteins with polyglutamine and polyalanine expansions are degraded by autophagy. *Hum Mol Genet*. 11:1107-1117.

Ricard, J., J. Salinas, L. Garcia, and D.J. Liebl. 2006. EphrinB3 regulates cell proliferation and survival in adult neurogenesis. *Mol Cell Neurosci*. 31:713-722.

Robberecht, W., and T. Philips. 2013. The changing scene of amyotrophic lateral sclerosis. *Nat Rev Neurosci*. 14:248-264.

Rocha, N., C. Kuijl, R. van der Kant, L. Janssen, D. Houben, H. Janssen, W. Zwart, and J. Neefjes. 2009. Cholesterol sensor ORP1L contacts the ER protein VAP to control Rab7-RILP-p150 Glued and late endosome positioning. *J Cell Biol*. 185:1209-1225.

Rohrer, J.D., A.M. Isaacs, S. Mizielinska, S. Mead, T. Lashley, S. Wray, K. Sidle, P. Fratta, R.W. Orrell, J. Hardy, J. Holton, T. Revesz, M.N. Rossor, and J.D. Warren. 2015. C9orf72 expansions in frontotemporal dementia and amyotrophic lateral sclerosis. *Lancet Neurol*. 14:291-301.

Ron, D., and P. Walter. 2007. Signal integration in the endoplasmic reticulum unfolded protein response. *Nat Rev Mol Cell Biol*. 8:519-529.

Saita, S., M. Shirane, T. Natume, S. Iemura, and K.I. Nakayama. 2009. Promotion of neurite extension by protrudin requires its interaction with vesicle-associated membrane protein-associated protein. *J Biol Chem*. 284:13766-13777.

Sambrook, and Russel. 2001. Rapid Isolation of yeast DNA. . *In* Molecular Cloning, a Laboratory Manual. Cold Spring Harbor Laboratory Press. 631-632.

Sann, S., Z. Wang, H. Brown, and Y. Jin. 2009. Roles of endosomal trafficking in neurite outgrowth and guidance. *Trends Cell Biol*. 19:317-324.

Saxena, S., E. Cabuy, and P. Caroni. 2009. A role for motoneuron subtype-selective ER stress in disease manifestations of FALS mice. *Nat Neurosci*. 12:627-636.

Shi, J., S. Lua, J.S. Tong, and J. Song. 2010. Elimination of the native structure and solubility of the hVAPB MSP domain by the Pro56Ser mutation that causes amyotrophic lateral sclerosis. *Biochemistry*. 49:3887-3897.

Shirane, M., and K.I. Nakayama. 2006. Protrudin induces neurite formation by directional membrane trafficking. *Science*. 314:818-821.

Skehel, P.A., K.C. Martin, E.R. Kandel, and D. Bartsch. 1995. A VAMP-binding protein from Aplysia required for neurotransmitter release. *Science*. 269:1580-1583.

Smith, B.N., N. Ticozzi, C. Fallini, A.S. Gkazi, S. Topp, K.P. Kenna, E.L. Scotter, J. Kost, P. Keagle, J.W. Miller, D. Calini, C. Vance, E.W. Danielson, C. Troakes, C. Tiloca, S. Al-Sarraj, E.A. Lewis, A. King, C. Colombrita, V. Pensato, B. Castellotti, J. de Belleroche, F. Baas, A.L. ten Asbroek, P.C. Sapp, D. McKenna-Yasek, R.L. McLaughlin, M. Polak, S. Asress, J. Esteban-Perez, J.L. Munoz-Blanco, M. Simpson, W. van Rheenen, F.P. Diekstra, G. Lauria, S. Duga, S. Corti, C. Cereda, L. Corrado, G. Soraru, K.E. Morrison, K.L. Williams, G.A. Nicholson, I.P. Blair, P.A. Dion, C.S. Leblond, G.A. Rouleau, O. Hardiman, J.H. Veldink, L.H. van den Berg, A. Al-Chalabi, H. Pall, P.J. Shaw, M.R. Turner, K. Talbot, F. Taroni, A. Garcia-Redondo, Z. Wu, J.D. Glass, C. Gellera, A. Ratti, R.H. Brown, Jr., V. Silani, C.E. Shaw, and J.E. Landers. 2014. Exome-wide rare variant analysis identifies TUBA4A mutations associated with familial ALS. *Neuron*. 84:324-331.

Stifani, N. 2014. Motor neurons and the generation of spinal motor neuron diversity. *Front Cell Neurosci*. 8:293.

Stoica, R., K.J. De Vos, S. Paillusson, S. Mueller, R.M. Sancho, K.F. Lau, G. Vizcay-Barrena, W.L. Lin, Y.F. Xu, J. Lewis, D.W. Dickson, L. Petrucelli, J.C. Mitchell, C.E. Shaw, and C.C. Miller. 2014. ER-mitochondria associations are regulated by the VAPB-PTPIP51 interaction and are disrupted by ALS/FTD-associated TDP-43. *Nat Commun*. 5:3996.

Suzuki, H., K. Kanekura, T.P. Levine, K. Kohno, V.M. Olkkonen, S. Aiso, and M. Matsuoka. 2009. ALS-linked P56S-VAPB, an aggregated loss-of-function mutant of VAPB, predisposes motor neurons to ER stress-related death by inducing aggregation of co-expressed wild-type VAPB. *J Neurochem*. 108:973-985.

Teuling, E., S. Ahmed, E. Haasdijk, J. Demmers, M.O. Steinmetz, A. Akhmanova, D. Jaarsma, and C.C. Hoogenraad. 2007. Motor neuron disease-associated mutant vesicle-associated membrane protein-associated protein (VAP) B recruits wild-type VAPs into endoplasmic reticulum-derived tubular aggregates. *The Journal of neuroscience: the official journal of the Society for Neuroscience*. 27:9801-9815.

Thoreen, C.C., S.A. Kang, J.W. Chang, Q. Liu, J. Zhang, Y. Gao, L.J. Reichling, T. Sim, D.M. Sabatini, and N.S. Gray. 2009. An ATP-competitive mammalian target of rapamycin inhibitor reveals rapamycin-resistant functions of mTORC1. *J Biol Chem*. 284:8023-8032.

Toth, B., A. Balla, H. Ma, Z.A. Knight, K.M. Shokat, and T. Balla. 2006. Phosphatidylinositol 4-kinase IIIbeta regulates the transport of ceramide between the endoplasmic reticulum and Golgi. *J Biol Chem*. 281:36369-36377.

Tsuda, H., S.M. Han, Y. Yang, C. Tong, Y.Q. Lin, K. Mohan, C. Haueter, A. Zoghbi, Y. Harati, J. Kwan, M.A. Miller, and H.J. Bellen. 2008. The amyotrophic lateral sclerosis 8 protein VAPB is cleaved, secreted, and acts as a ligand for Eph receptors. *Cell*. 133:963-977.

Tudor, E.L., C.M. Galtrey, M.S. Perkinton, K.F. Lau, K.J. De Vos, J.C. Mitchell, S. Ackerley, T. Hortobagyi, E. Vamos, P.N. Leigh, C. Klasen, D.M. McLoughlin, C.E. Shaw, and C.C. Miller. 2010. Amyotrophic lateral sclerosis mutant vesicle-associated membrane protein-associated protein-B transgenic mice develop TAR-DNA-binding protein-43 pathology. *Neuroscience*. 167:774-785.

van Blitterswijk, M., M.A. van Es, M. Koppers, W. van Rheenen, J. Medic, H.J. Schelhaas, A.J. van der Kooi, M. de Visser, J.H. Veldink, and L.H. van den Berg. 2012. VAPB and C9orf72 mutations in 1 familial amyotrophic lateral sclerosis patient. *Neurobiol Aging*. 33:2950 e2951-2954.

van Dis, V., M. Kuijpers, E.D. Haasdijk, E. Teuling, S.A. Oakes, C.C. Hoogenraad, and D. Jaarsma. 2014. Golgi fragmentation precedes neuromuscular denervation and is associated with endosome abnormalities in SOD1-ALS mouse motor neurons. *Acta Neuropathol Commun*. 2:38.

Wang, L., B. Popko, and R.P. Roos. 2011. The unfolded protein response in familial amyotrophic lateral sclerosis. *Hum Mol Genet*. 20:1008-1015.

Wijesekera, L.C., and P.N. Leigh. 2009. Amyotrophic lateral sclerosis. *Orphanet journal of rare diseases*. 4:3-3.

Yamaji, T., and K. Hanada. 2015. Sphingolipid metabolism and interorganellar transport: localization of sphingolipid enzymes and lipid transfer proteins. *Traffic*. 16:101-122.

Yang, M., S. Omura, J.S. Bonifacino, and A.M. Weissman. 1998. Novel aspects of degradation of T cell receptor subunits from the endoplasmic reticulum (ER) in T cells: importance of oligosaccharide processing, ubiquitination, and proteasome-dependent removal from ER membranes. *J Exp Med*. 187:835-846.

Zu, T., B. Gibbens, N.S. Doty, M. Gomes-Pereira, A. Huguet, M.D. Stone, J. Margolis, M. Peterson, T.W. Markowski, M.A. Ingram, Z. Nan, C. Forster, W.C. Low, B. Schoser, N.V. Somia, H.B. Clark, S. Schmechel, P.B. Bitterman, G. Gourdon, M.S. Swanson, M. Moseley, and L.P. Ranum. 2011. Non-ATG-initiated translation directed by microsatellite expansions. *Proc Natl Acad Sci U S A*. 108:260-265.